



Tomas Bata University in Zlín
Faculty of Technology

Doctoral Thesis

**Kvantitativní analýza vytvrzovacích mechanismů
materiálů pro lékařské a technické aplikace**

**Real-time Investigation of Curing Mechanisms of Thermoset Resins
for Medical and Technical Applications**

Johannes Steinhaus

Submitted to Tomas Bata University in Zlín

Faculty of Technology

Zlín, April 2015

Doctoral study programme: P2808 Chemistry and Materials Technology
Degree course: 2808V006 Technology of Macromolecular
Substances

Supervisor: Prof. Ing. Berenika Hausnerová, Ph.D.

Consultant: Prof. Dr.-Ing. Bernhard Möglinger

Composition of Commission for the Defence of Dissertation:

Chairperson:

doc. Ing. et Ing. Ivo Kuřitka,
Ph.D. et Ph.D.

Polymer Centre, Faculty of Technology
Tomas Bata University in Zlín
kuritka@ft.utb.cz

Reviewer:

Prof. Dr. rer. nat. Margit Schulze

Department of Natural Sciences
Bonn-Rhein-Sieg University of Applied Sciences
margit.schulze@h-brs.de

Reviewer:

doc. Ing. Věra Kašpárková, CSc.

Department of Fat, Surfactant and Cosmetics Technology,
Faculty of Technology
Tomas Bata University in Zlín
vkašparkova@ft.utb.cz

Member:

prof. Ing. Miloslav Pekař, CSc.

Institute of Physical and Applied Chemistry
Faculty of chemistry
Brno University of Technology
pekar@fch.vutbr.cz

Member:

prof. Ing. Karel Kocman, DrSc.

Department of Production Engineering
Faculty of Technology
Tomas Bata University in Zlín
kocman@ft.utb.cz

Member:

doc. Mgr. Aleš Mráček, Ph.D.

Department of Physics and Materials Engineering
Faculty of Technology
Tomas Bata University in Zlín
mracek@ft.utb.cz

Member:

Ing. Vladimír Pelíšek, Ph.D.

Dura-line CT, s. r. o.
U Pisaku 682; 763 62 Tlumačov
vladimir.pelisek@duraline.com

© Steinhaus, Johannes

Published by Tomas Bata University in Zlín in the Edition Doctoral Thesis
The publication was issued in the year 2015

Key words in Czech: *termoset, kinetika vytvrzování, dielektrická analýza (DEA), DEA viskozita, smyková viskozita, světelné vytvrzování, fotokompozit, 3D rapid prototyping materiál*

Keywords in English: *thermoset resin, curing kinetics, dielectric analysis (DEA), ion viscosity, shear viscosity, visible light-curing, dental composite, 3D printing rapid prototyping material*

ABSTRAKT

Disertační práce řeší využití dielektrické analýzy (DEA) ve studiu kinetiky vytvrzování fotokompozitů pro dentální aplikace a kompozitů pro 3D rapid prototyping (RP). Díky vysokému rozlišení a senzitivitě je DEA vhodná k podchycení jak počáteční fáze síťování (vysoké frekvence), tak i post-vytvrzovacích procesů (nízké frekvence). Ačkoliv je sledování vytvrzovacího procesu pomocí DEA etablovanou metodou v leteckém i automobilovém průmyslu, pro potřeby medicínských aplikací a též aplikací v RP je nutné přizpůsobit experimentální zařízení i vyhodnocovací metody.

Cílem disertační práce je popsat a porozumět vztahu vytvrzovacího procesu ke složení materiálů, jejich viskozitě a procesním podmínkám (teplotě), a v případě fotokompozitů i intenzitě světelného zdroje a hloubce působení záření.

Pozornost je zaměřena především na získání kinetických parametrů; vypočítané hodnoty reakční rychlosti jsou vztaženy k DEA viskozitě. Pro dentální hmoty bylo zjištěno, že počáteční rychlost vytvrzování je přímo úměrná intenzitě použitého světla, a nikoliv její druhé mocnině, jak uvádí mnoho dosavadních prací. Data získaná ze sledování kinetiky vytvrzování pro rychlé (dentální hmoty) i dlouhé (RP materiály) procesy byla využita pro vytvoření teoretických modelů založených na reakční kinetice.

ABSTRACT

In this doctoral thesis the curing process of visible light-curing (VLC) dental composites and 3D printing rapid prototyping (RP) materials are investigated with the focus on dielectric analysis (DEA). This method is able to monitor the curing of resins in an alternating electric fringe field with adjustable frequencies and is often used for cure control of composites manufacturing in the aviation and automotive industry but hardly established in dental science or RP method development. It is capable of investigating very fast initiation and primary curing processes using high frequencies in the kHz-range as well as very slow post-curing processes beyond the glass transition of cured thermosets using frequencies in the low and sub-Hz-range.

The aim of the Thesis is a better understanding of the curing processes with respect to curing parameters such as resin composition, viscosity, temperature, and for light-curing composites also light intensity and irradiation depth.

Due to the nature of both dental and RP systems an application of specific experimental set-up had to be designed allowing for the generation of reproducible and valid results. Subsequently, different evaluation methods were developed to characterize the curing behavior of both material types.

A special focus was paid to the determination of kinetic parameters from DEA measurements. Reaction rates of the curing of the corresponding thermosets were calculated and applied to the ion viscosity curves measured by DEA to evaluate reaction kinetic parameters. For the dental composites it could be clearly shown that the initial curing rate is directly proportional to light intensity and not to its square root as proposed by many others authors. A good description of the curing behaviour of 3DP RP materials was also achieved assuming a reaction order smaller than one. This data provides the base for the kinetic modeling of polymerization and curing processes proposed within the Thesis.

ABSTRACT IN GERMAN

Thema dieser Doktorarbeit ist die Untersuchung des Härtungsprozesses von lichthärtenden (VLC) Dentalkompositen sowie 3D Printing (3DP) Rapid Prototyping (RP) Materialien mittels Dielektrischer Analyse (DEA). Diese Methode ermöglicht es, das Härtungsverhalten von Harzen im elektrischen Wechselfeld einer Kammelektrode zu verfolgen, wobei ein großer Frequenzbereich zur Verfügung steht. Sie ist weit verbreitet in der Kontrolle von Härtungsprozessen in der Luftfahrt sowie der Automobilindustrie, jedoch findet sie in zahnmedizinischen Einsatzgebieten oder in der RP-Methodenentwicklung nur selten Anwendung. Wegen ihrer hohen zeitlichen Auflösung und Messempfindlichkeit können mithilfe der DEA sowohl sehr schnell ablaufende Initiierungs- und Primärhärtungsprozesse im kHz-Bereich, als auch sehr langsam ablaufende Nachhärtungs- und Alterungsprozesse oberhalb des Glasübergangs gehärteter Duroplaste im sub-Hz-Bereich untersucht werden.

Das Ziel dieser Arbeit ist es den Aushärtungsprozess besser zu verstehen hinsichtlich Parameter, wie Reaktionstemperatur, Harzzusammensetzung und -viskosität sowie bei lichthärtenden Kompositen Lichtintensität und Eindringtiefe.

Da es sich bei den beiden untersuchten Materialklassen (Dental- sowie 3DP RP-Harze) um völlig verschiedene Duroplastsysteme handelt und die DEA Methode sehr empfindlich misst, wurde für jeden Teil dieser Studie ein speziell angepasster Versuchsaufbau erstellt, um reproduzierbar und verlässlich zu messen. Zudem wurden jeweils für beide Duroplastsysteme spezielle Auswertungsmethoden zur Charakterisierung des Härtungsverhaltens entwickelt.

Ein besonderer Augenmerk wurde auf die Auswertung der DEA-Messungen hinsichtlich kinetischer Kennwerte gelegt. Reaktionsraten der Aushärtung der jeweiligen Duroplaste wurden berechnet und dazu verwendet die DEA-Ergebnisse kinetisch auszuwerten. Für die Dentalkomposite konnte klar gezeigt werden, dass sich die anfängliche Härtungsgeschwindigkeit direkt proportional zur eingestrahlt Lichtintensität verhält und nicht quadratisch, wie teilweise in der Literatur beschrieben. Ferner wurde unter der Berücksichtigung einer Reaktionsordnung kleiner als eins eine gute Beschreibung des Härtungsverhaltens des 3DP RP Materials erzielt. Diese Ergebnisse bilden die Grundlage für eine kinetische Modellierung von Polymerisations- und Härtungsprozessen die in dieser Arbeit vorgestellt werden.

CONTENTS

Abstrakt.....	4
Abstract.....	5
Abstract in German.....	6
CONTENTS	7
List of Papers	9
1. State of the art.....	10
1.1 Materials.....	10
1.1.1 Visible light-curing dental composites	10
1.1.2 3D printing rapid prototyping materials	15
1.2 Material properties and application requirements.....	17
1.2.1 Dental resin composites properties and application requirements	17
1.2.2 3D printing RP material properties and application requirements	17
1.3 Initiation process of polymerization and cross-linking.....	20
1.3.1 Light initiation (dental resin composites)	20
1.3.2 Chemical initiation (RP material)	21
1.4 Polymerization process	22
1.4.1 Polymerization process of VLC resin composites	22
1.4.2 Polymerization process of 3D RP-material.....	24
1.5 Modeling of the polymerization and curing processes	25
1.5.1 Theory	25
1.5.2 Possible methods to determine curing kinetics parameters	27
1.6 Effect of light intensity on chemical structure of VLC resin composite	31
1.7 DEA monitoring of curing processes.....	32
1.7.1 Measurement method.....	32
1.7.2 Sensor systems	33
1.7.3 DEA Curve and ion viscosity evaluation.....	34
1.8 DEA vs. Rheometry of VLC resins and composites.....	35
2. Methodology and purpose of the work	38
3. Discussion of the Results	40
3.1 DEA characterization of thermoset resins curing	40

3.1.1	Curing behavior of VLC dental composites	40
3.1.2	Evaluation of curing behavior of 3DP RP-resins	53
3.2	Evaluation of DEA curing curves of VLC dental composites using	
	reaction kinetics.....	60
3.2.1	Reaction kinetics based modeling of the VLC process of dental resins.	60
3.2.2	Kinetics Evaluation of DEA measurement curves	62
3.2.3	Extended model with time dependent initiator concentration	66
3.3	DEA kinetics evaluation of 3DP RP-resins	70
3.3.1	Reaction kinetics based Modeling of the 3DP RP-resin curing	70
3.4	Correlation of ion viscosity (DEA) with shear viscosity (Rheometer).....	73
3.4.1	Investigations of pure dental resins.....	73
3.4.2	Investigations of filled dental composites.....	75
4.	Conclusions	79
5.	Contribution to the science and practice	81
	Acknowledgement.....	82
	References.....	83
	Abbreviations.....	88
	Symbols	90
	GREEK Symbols.....	93
	Publications, Posters and Presentations.....	95
	Curriculum Vitae	97
	Papers I – V	98

LIST OF PAPERS

The following papers are included in the presented doctoral thesis:

P-I Dielectric analysis of depth dependent curing behaviour of dental resin composites.

Steinhaus J, Moeginger B, Grossgarten M, Rosentritt M, Hausnerova B.
Dental Materials 2014, vol. 30, no. 6, 679-687.

P-II Curing kinetics of visible light curing dental resin composites investigated by dielectric analysis (DEA).

Steinhaus J, Hausnerova B, Haenel T, Grossgarten M, Moeginger B.
Dental Materials 2014, vol. 30, no. 3, 372-380.

P-III Time-Resolved Study of the Photo-Curing Process of Dental Resins with the NMR-MOUSE.

Netto A M, Steinhaus J, Hausnerova B, Moeginger B, Blümich B.
Applied Magnetic Resonance 2013, vol. 44, no. 9, 1027-1039.

P-IV Characterizing the Auto-curing Behaviour of Rapid Prototyping Materials for 3D-Printing via DEA.

Steinhaus J, Hausnerova B, Moeginger B, Harrach M, Guenther D, Moegele F. *Polymer Engineering & Science*, accepted March 2015.

P-V Correlation of shear viscosity and dielectric ion viscosity of dental resins – Effects of composition, temperature and filler content. Steinhaus J, Hausnerova B, Haenel T, Selig D, Duvenbeck F, Moeginger B. *Submitted to Dental Materials*, March 2015.

1. STATE OF THE ART

1.1 Materials

1.1.1 Visible light-curing dental composites

Visible light curing (VLC) composites for dental restorations consists of an organic light-curable resin matrix, inorganic solid filler powder and small amounts of functional additives. Application fields for these materials vary from class I to class VI cavity restorations of the posterior and anterior teeth (Fig. 1.1) [1]. VLC composites have a paste-like consistency in order to either fill tooth cavities without any remaining gaps as well as to model and reshape the tooth silhouette (Fig. 1.2). After properly filling a prepared tooth cavity the composite is irradiated and cured with a light-curing unit (LCU) emitting a blue spectrum of approximately 400-500 nm. Due to attenuation effects inside the composite properly light-cured bulky fillings should be subdivided in layers of maximum 2 mm thickness [2, 3].

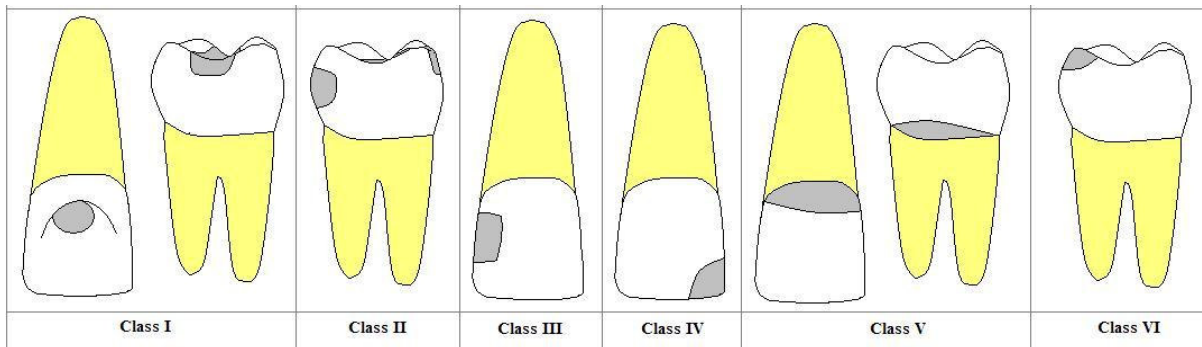


Fig. 1.1: Classifications of different kinds of dental restorations according to Greene Vardiman Black [1].

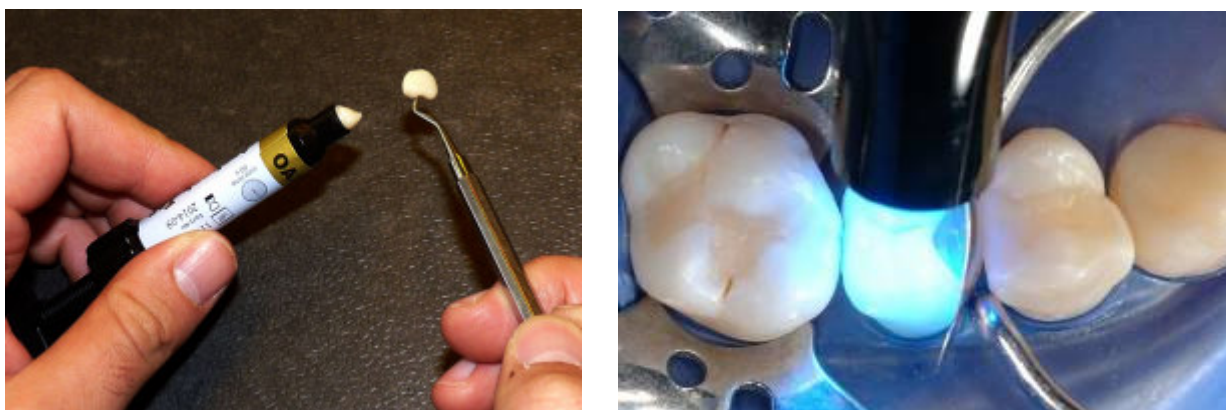


Fig. 1.2: Appearance and handling of a packable dental VLC-composite (left). Light-curing after dentists application in the tooth (right, Voco GmbH).

Table 1.1: Overview over the most commonly applied VLC composite dental filling materials in Europe in 2012. The information is taken from the manufacturers handling information, material data and safety sheets MDS as well as from direct contact with the manufacturers.

Product Name	Producer	Filler content (wt-%)	Monomers	Initiator system
Arabesk Top	VOCO	76.5	Bis-GMA, UDMA, TEGDMA	CQ/DABE
Grandio	VOCO	87	Bis-GMA, TEGDMA	CQ/DABE
Grandio Flow	VOCO	80	Bis-GMA, TEGDMA, HEMA	CQ/DABE
GrandioSO	VOCO	89	Bis-GMA, Bis-EMA, TEGDMA	CQ/DABE
GrandioSO Flow	VOCO	82	Bis-GMA, Bis-EMA, TEGDMA, HEDMA	CQ/DABE
Charisma Opal	Heraeus Kulzer	77	Bis-GMA, TEGDMA	CQ/DABE
Venus Diamond	Heraeus Kulzer	81	TCD-DI-HEA, UDMA	CQ/DABE
Venus Diamond Flow	Heraeus Kulzer	65	UDMA, ethoxylated bisphenol A dimethacrylate	CQ/DABE
Venus Pearl	Heraeus Kulzer	76	TCD-DI-HEA, UDMA	CQ/DABE
Venus Flow	Heraeus Kulzer	62	Bis-GMA, TEGDMA	CQ/DABE
Heliomolar	Ivoclar Vivadent	66.7	Bis-GMA, UDMA, decandioldimethacrylate	CQ/DABE
Tetric EvoCeram	Ivoclar Vivadent	75-76	Bis-GMA, UDMA, ethoxylated Bis-EMA	CQ/DABE
Tetric EvoFlow	Ivoclar Vivadent	57.5	Bis-GMA, UDMA, decandioldimethacrylate	CQ/DABE/APO
Tetric	Ivoclar Vivadent	82	Bis-GMA, UDMA, TEGDMA	CQ/DABE
IPS Empress Direct	Ivoclar Vivadent	75-79	Bis-GMA, UDMA, propoxylated Bis-GMA	CQ/DABE
Tetric Bulkfill	Ivoclar Vivadent	79-81	Bis-GMA, UDMA, ethoxylated Bis-GMA	CQ/DABE/Ge
Quixfil	Dentsply	85.5	UDMA, TEGDMA, dimethacrylate	CQ/DABE
SDR	Dentsply	65.9	UDMA, TEG-DMA, ethoxylated bisphenol A dimethacrylate	CQ/DABE
Esthet X HD	Dentsply	73.2	-	
Spectrum TPH 3	Dentsply	78	UDMA, TEGDMA, ethoxylated bisphenol A dimethacrylate	CQ/DABE
Ceram X Mono	Dentsply	75	Ormosil	CQ/DABE
Filtek XTE Dentin	3M Espe	78.5	Bis-GMA, TEG-DMA, UDMA, Bis-EMA	CQ/DABE
Filtek XTE Enamel	3M Espe	78.5	Bis-GMA, TEG-DMA, UDMA, Bis-EMA	CQ/DABE
Filtek XTE Flow	3M Espe	65	Bis-GMA, TEG-DMA, Bis-EMA	CQ/DABE
Filtek Z500	3M Espe	78.5	Bis-GMA, TEG-DMA, UDMA, Bis-EMA	CQ/DABE
Filtek Z250	3M Espe	60	Bis-GMA, UDMA, Bis-EMA	CQ/DABE

Table 1.1 gives a rough overview over the most commonly applied VLC composite dental filling materials in Europe in 2012 containing the most property characterizing constituents as monomer types, filler content and initiator/accelerator system.

VLC composite resins

The performance of VLC composites in application as well as the mechanical and ageing properties are significantly influenced by the monomer resins. There is a broad variety of requirements that has to be fulfilled by the resins, e.g. suitable viscosity, curing behavior, non-toxicity, low curing shrinkage, high degree of cure (DC), good optical transparency for high depths of cure (DoC) and sufficient ageing properties [2, 4, 5]. Fig. 1.3 shows the most commonly used resin molecules used for VLC composites production. Bisphenol A glycidyl methacrylate (Bis-GMA) and urethane dimethacrylate (UDMA) represent structural monomers having a comparably high viscosity but low curing shrinkage of 6% reducing the risk of gap-formation at the interface between the filling and the tooth. In order to further reduce the curing shrinkage and attain good mechanical properties, high amounts of glass and ceramic fillers are added to the composites. To achieve high filler contents up to 90 wt-% without losing the processability of the composite the viscosity of the uncured resin matrix must not be too high. Therefore, triethylene glycol dimethacrylate (TEGDMA) as a low viscosity resin is frequently used as a diluent monomer [6, 7].

Dynamic viscosities:

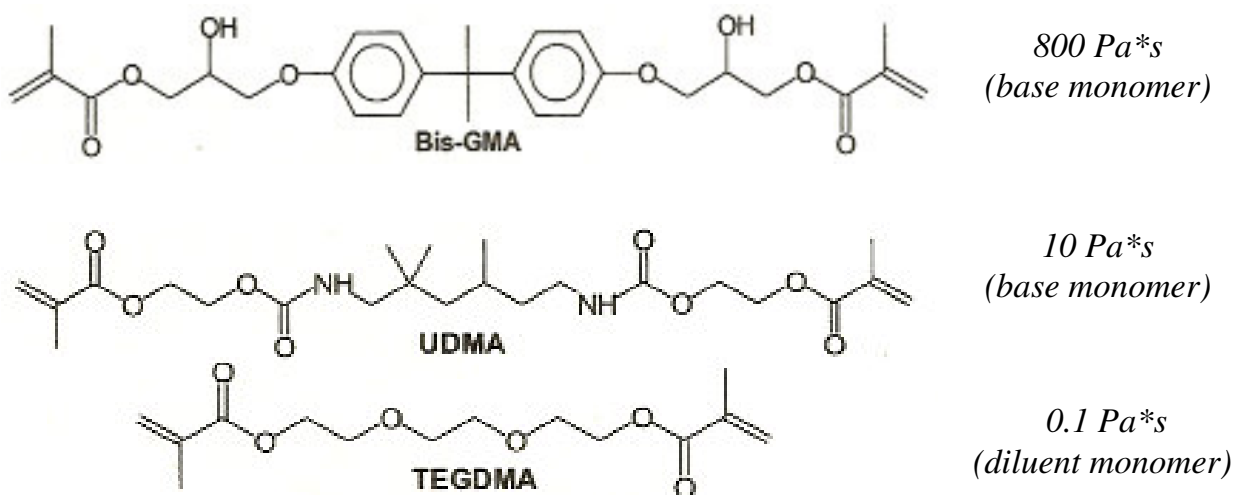


Fig. 1.3: Most frequent used dimethacrylate resin types in dental filling composites. Bis-GMA and UDMA commonly used as base monomer. TEGDMA used as diluent monomer [8, 9].

VLC composite additives

To control the processing properties of VLC composites additives in the total amount of approximately 1 wt-% are added. The most important additive is the photo-initiator-system. Nearly all conventional VLC composites are light-cured with a camphorquinone (CQ)/ ethyl 4-(dimethylamino)benzoate (DABE) System (Table 2.1) [10]. The CQ can be activated with blue light in a range of 400-500 nm forming 2 radicals if reacted with one DABE molecule. The detailed initiation mechanism is presented in chapter 1.3.1.

Due to the fact that the DABE radical is much more reactive it is called accelerator (acceptor) and the CQ is called initiator (donor) [11]. In order to avoid a curing reaction prior to the VLC-process e.g. due to daylight or a surgical light, daylight stabilizers such as butylated hydroxytoluene (BHT) or hydroquinone (HQ) are added to the composite (Fig. 1.4) [2, 3, 5].

Furthermore, in order to mimic different tooth colors and shades pigments are incorporated in the composite. They have a notable impact on the light-curing characteristics like curing rate, DC and DoC [12].

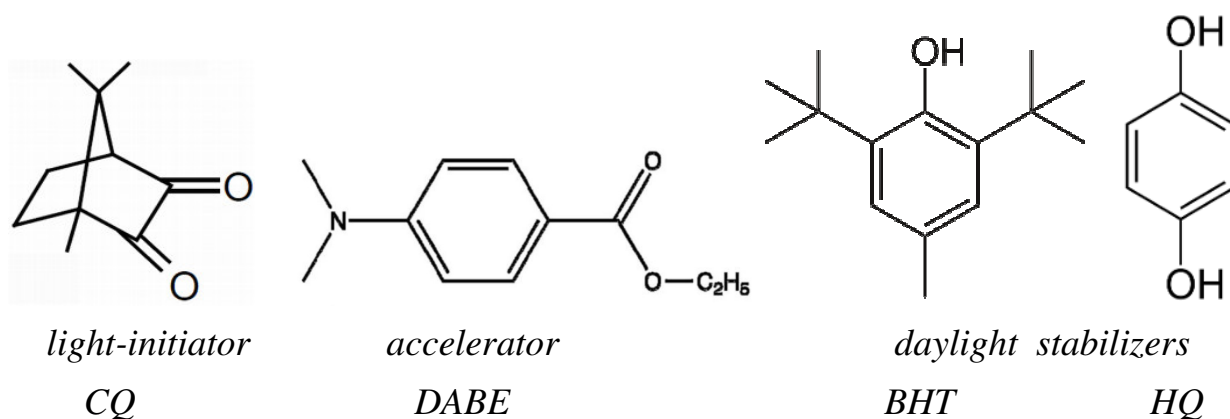


Fig. 1.4: Typical additives used in VLC-composites.

VLC composite fillers

To reach tooth-like mechanical properties (e.g. modulus, strength, abrasion resistance) as well as very low polymerization shrinkage VLC composites are highly filled with glass and ceramic particles in the micro- and sub-micrometer scale up to 90 wt-% (Fig. 1.5). The highest filler contents are achieved with a mixture of nanoparticles (pyrogenous SiO₂) and grinded glass particles in the micrometer scale. These VLC materials are called nano-hybrid composites [2, 13].

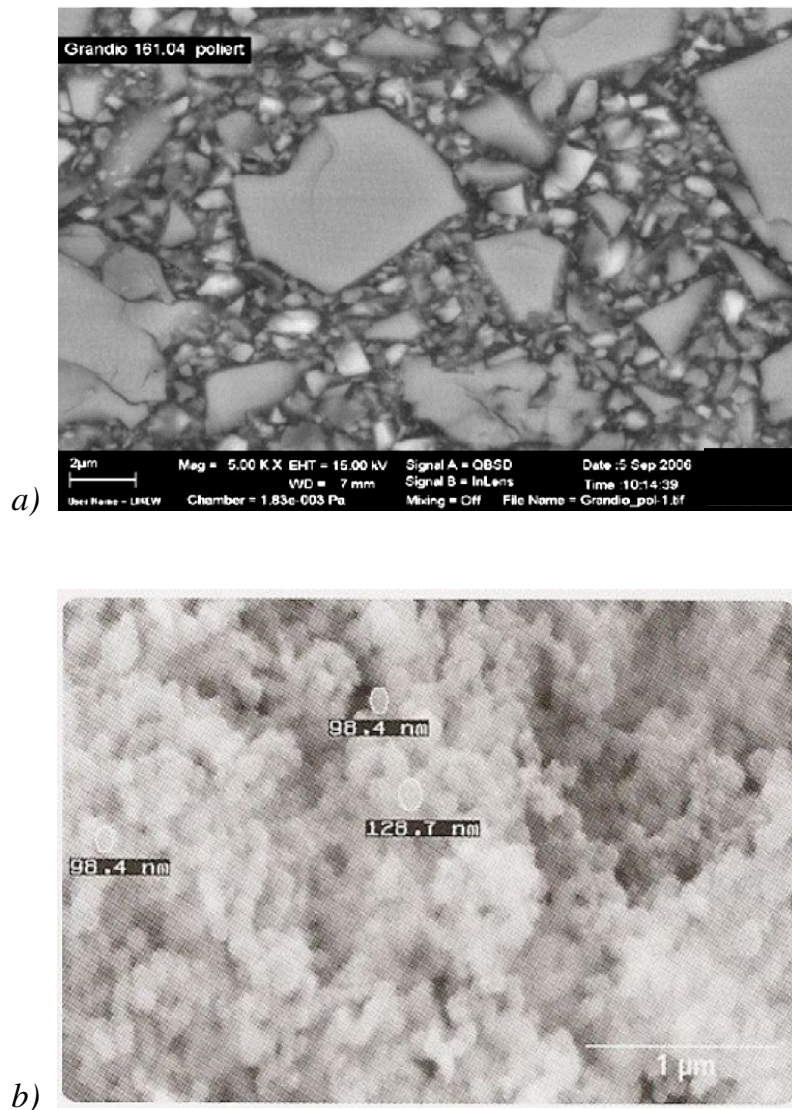


Fig. 1.5: a) SEM picture of a dental nano-hybrid composite (Grandio, Voco GmbH, magnification 5000 \times) [13]. b) SEM picture of pyrogenous SiO₂ particles (Aerosil, Evonik Industries AG, magnification 10000 \times) [2].

1.1.2 3D printing rapid prototyping materials

There are many rapid prototyping (RP) methods (e.g. stereolithography, laser sintering, laminated object manufacturing, fused deposition modeling or 3 dimensional printing (3DP) [14-17]) in order to build up prototypes from 3D CAD-data directly layer by layer without the need of any kind of mould or machining process. The RP material investigated in this work is a polymethyl methacrylate-(PMMA)/ hydroxyethyl methacrylate- (HEMA)/ styrene-system where layers of PMMA powder are selectively printed and thus, polymerized with a HEMA/styrene binder. The ratio of powder:binder in the manufacturing process is approximately 10:1. The principle of the manufacturing process is presented in Fig. 1.6. Detailed information about the polymerization mechanism is given in chapter 1.4.2.

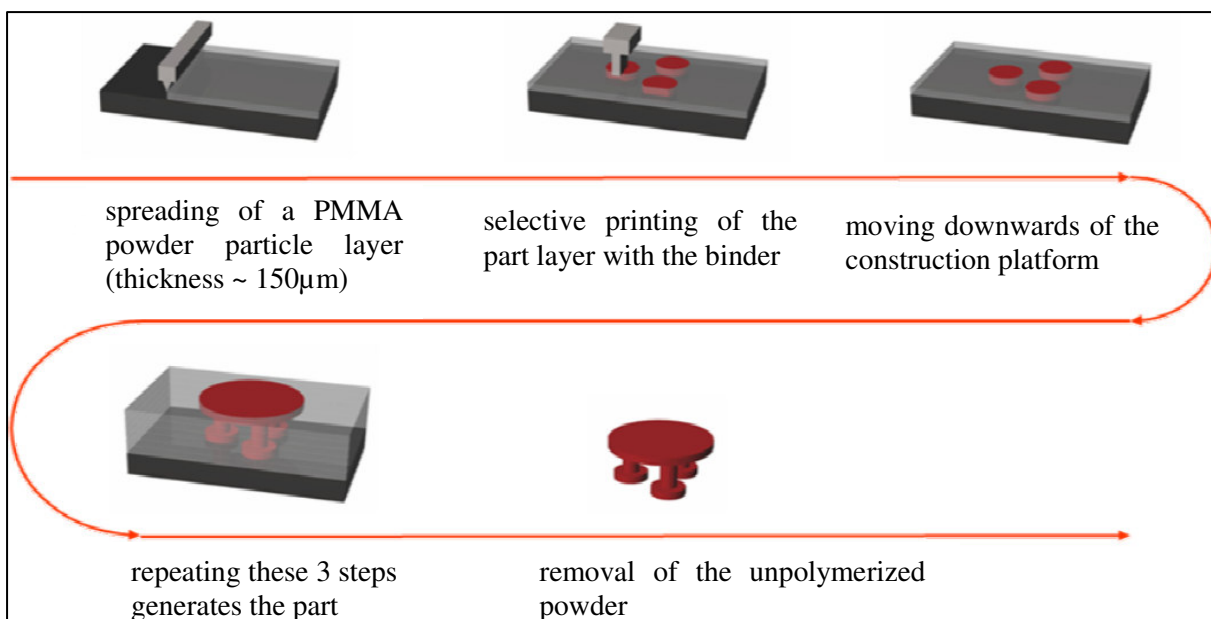


Fig. 1.6: Principle of 3DP RP process (copyright by Voxeljet AG).

PMMA powder

The PMMA-powder represents the main component of the ready-made RP-part. The matrix consists of approximately 90 % PMMA. The powder is composed of PMMA-spheres with diameters in the range of 10-100 μm (Fig. 1.7). To start the polymerization during the printing process it is modified with a dibenzoyl peroxide (BPO). Detailed information about the ready-made RP-part is given in chapter 1.4.2.

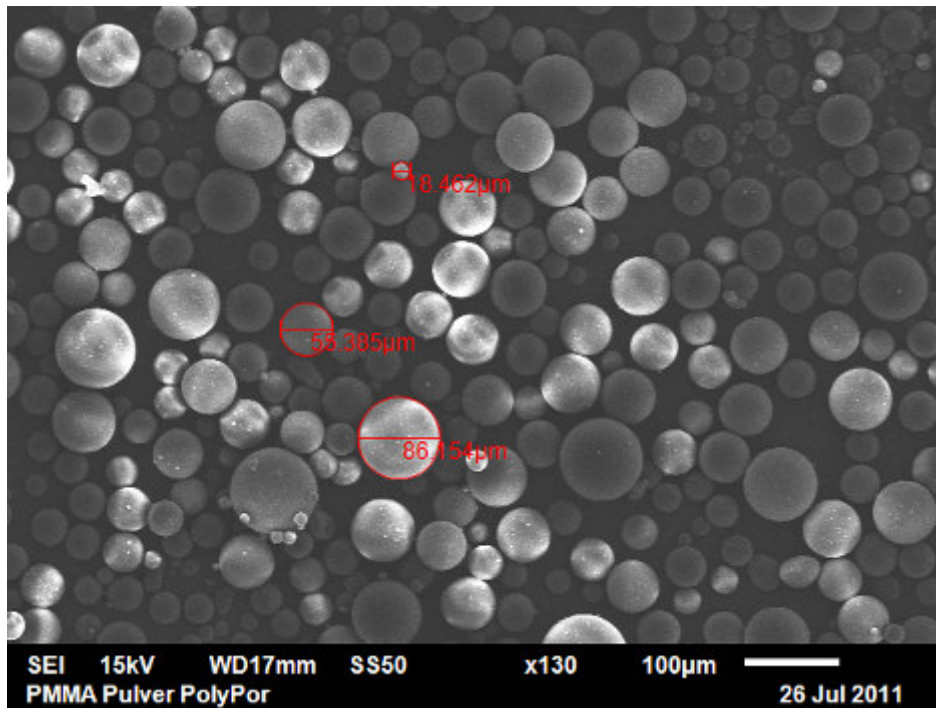


Fig. 1.7: SEM picture of PMMA powder for 3D-Printing (PolyPor powder $<\varnothing 100\mu\text{m}$, Voxeljet AG, magnification 130 \times).

3D printing binder

The binder VXP1 mainly consists of 2 parts styrene and 1 part HEMA (Fig. 1.8) and can be printed with a commonly designed ink-jet printer-head. In order to start the polymerization reaction at temperatures below 40 °C the activator N,N-dimethyl-P-toluidine (DMT) is added allowing for a radical generation together with the peroxide in the PMMA-powder. Details about the initiation mechanism can be found in chapter 1.3.2.

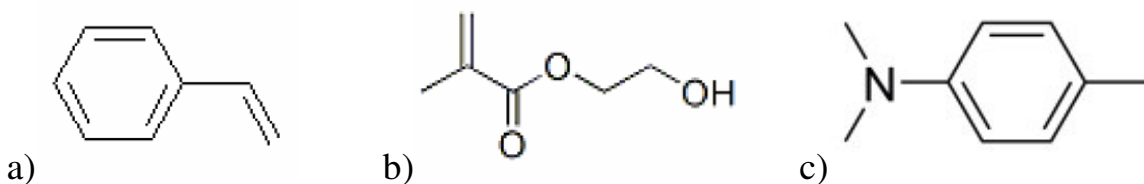


Fig. 1.8: Binder constituents: co-monomers styrene (a) and HEMA (b) and activator N,N-dimethyl-P-toluidine (c).

1.2 Material properties and application requirements

1.2.1 Dental resin composites properties and application requirements

Besides polymerization shrinkage, biocompatibility or wear resistance, one of the most frequent discussed issues in visible light-curing (VLC) composite development and research as well as in photo-chemistry in general is the basic question of how fast and how thick a properly light-cured material can be produced [2, 3, 5, 8, 9, 13]. The requirements of a VLC composite for dental filling application can be divided into the following topics: esthetics, mechanical strength against peak loads, abrasion resistance, low polymerization shrinkage, bond strength, easy applicability, biocompatibility, curing depth, polymerization time, etc. [3, 18, 19] Table 1.2 gives a brief overview over typical material requirements, the failures in application if the requirements are not met, and how the needed properties can be reached.

1.2.2 3D printing RP material properties and application requirements

Rapid prototypes are categorized in design and functional prototypes. Design prototypes give a 3D impression of what the part will look like in the later application. Whereas functional prototypes also have to full-fill functional requirements similar to the application like moving parts, veneers, snap-fit, joints [14-16]. Therefore, the mechanical properties of the RP-material for functional prototypes must not be very different from the material taken for the series parts [20].

The 3D printing (3DP) RP material investigated in this work is mainly used for design prototypes and lost cores in investment casting due to its relatively weak mechanical properties of the porous PMMA-powder-structure. Thus, the main requirements on this material are dimensional precision and short production time. For this purpose the polymerization rate of the powder-binder-system has to be aligned to the printing velocity of the 3DP process in order to avoid warpage of the prototype due to serial polymerization shrinkage of each printed layer [21, 22]. This is done by a delayed polymerization process starting smoothly after several layers of the prototype are printed. The fact that the prototype mainly consists of pre-polymerized PMMA-powder which is not shrinking during the printing is also beneficial to achieve low warpage during the production process. Fig. 1.9 shows an SEM picture of the PMMA powder which is linked by the polymerized binder (left side). The picture was taken from a fragment of a chess tower representing the benefits of a 3DP process having a spiral stair inside (Fig. 1.9, right side). Table 1.3 published by Azari et al. in 2009 gives a rough overview over the main advantages and disadvantages of 3DP systems [17].

Table 1.2: Overview over typical VLC dental material requirements, application failures and how to reach needed properties.

Type of requirement	Possible failures if requirements are not accomplished	How requirements can be reached	Resulting effects (requirements for polymerization process)
---------------------	--	---------------------------------	---

Material processing during the dentists treatment:

good handling and modeling properties	improper modeling of the filling, gap formation	beneficial viscosity of the uncured composite (adjusted resin/filler ratio and type)	change in resin composition influences the polymerization behavior
	composite is starting to cure in the room light	use of daylight stabilizers	delayed polymerization initiation
fast polymerization	incomplete polymerization in the typical light-curing time of 20-40s;	modifying the resin/initiator/accelerator-system, or use of a more powerful LCU	high polymerization shrinkage and stress; build up of internal stress
high DoC	thicker fillings processed in one step may be improperly cured at the bottom	similar refraction indexes of resin and glass filler, or use of a more powerful LCU	higher DC in higher depths → faster polymerization

Kinds of mechanical requirements:

compression strength	fracture of the composite filling or the treated tooth	properly cured resin with good mechanical properties, high filler content, good filler/matrix adhesion	high DC and DoC of the resin
flexural strength	fracture of the composite filling or the treated tooth, or debonding	properly cured resin with good mechanical properties, good filler/matrix adhesion	high DC and DoC of the resin
tensile strength of bondings	tensile debonding, gap formation	properly cured bonding with good mechanical properties, good bonding/filling and bonding/tooth adhesion	-
shear strength of bondings	shear debonding, gap formation	properly cured bonding with good mechanical properties, good bonding/composite and bonding/tooth adhesion	-

Ageing requirements:

no or tooth-like discoloration	filling gets visible in contrast to the tooth	high DC of the composite resin, respectively high chemical resistance	high DC and DoC of the resin
abrasion resistance	abrasion due to chewing or tooth-brushing	properly cured resin with good mechanical properties, good filler/matrix adhesion, small filler particle size	high DC and DoC of the resin

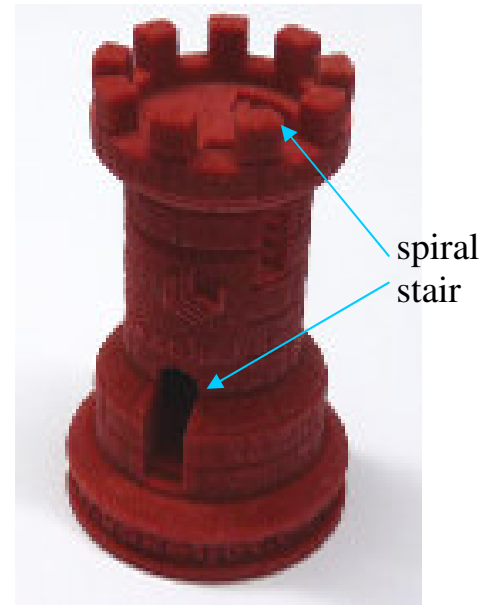
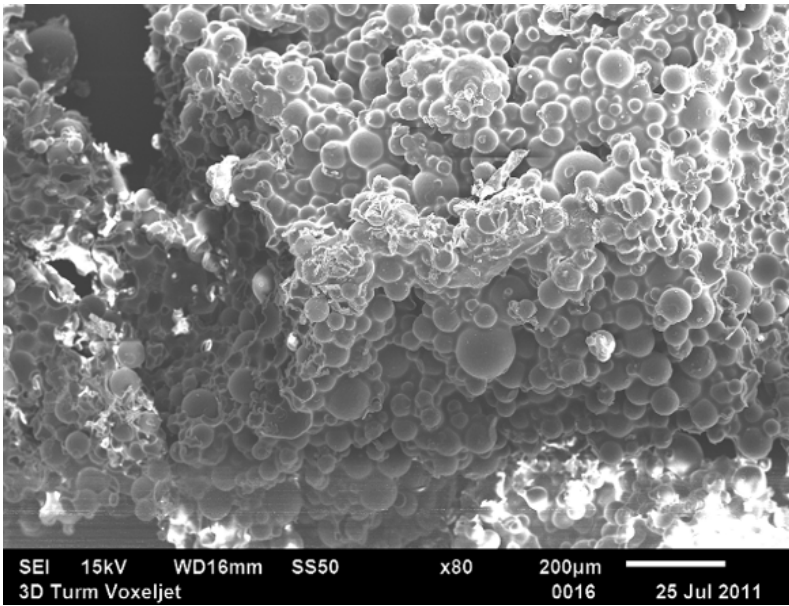


Fig. 1.9: SEM picture of 3DP RP-material, magnification 80× (left), 3DP prototype chess tower with spiral stair inside (right, Voxeljet AG).

Table 1.3: The main advantages and disadvantages of 3DP systems [17].

Advantages	Disadvantages
fast fabrication time	large tolerance (in the range of the powder particle diameter, e.g. 0.1 mm)
low material cost	lower strength models
capability of being colored	rough surface finish
built models can be used for casting purposes directly	
low toxicity	
relative material variety	

1.3 Initiation process of polymerization and cross-linking

1.3.1 Light initiation (dental resin composites)

The light initiation of dental resin composites is realized in most cases by a camphorquinone (CQ)/ethyl 4-(dimethylamino)benzoate (DABE) system. A double bond of the carbonyl group of the CQ is activated with blue light in a wavelength range of 400-500 nm forming an excited singlet state having a half life of nanoseconds [23]. Most of the molecules fall back to the ground state [24] but some are transferred with a certain probability to an excited triplet state having a half life time of about 50 μ s [25]. This excited triplet state may also fall back to the ground state or build other degradation products but again with a certain probability the CQ molecule undergo an ionic exciplex transition with the DABE before forming two radicals by transferring a proton to the CQ (Fig. 1.10) [10, 11, 24]. All possible reaction steps of the CQ/DABE initiation system with their probability factors yielding precise kinetics equations have been presented by Cook in 1991 [24]. Due to the fact that the DABE radical is much more reactive in the VLC-process, and thus reaction rate determining, it is called accelerator, whereas the CQ acts as light initiator [26].

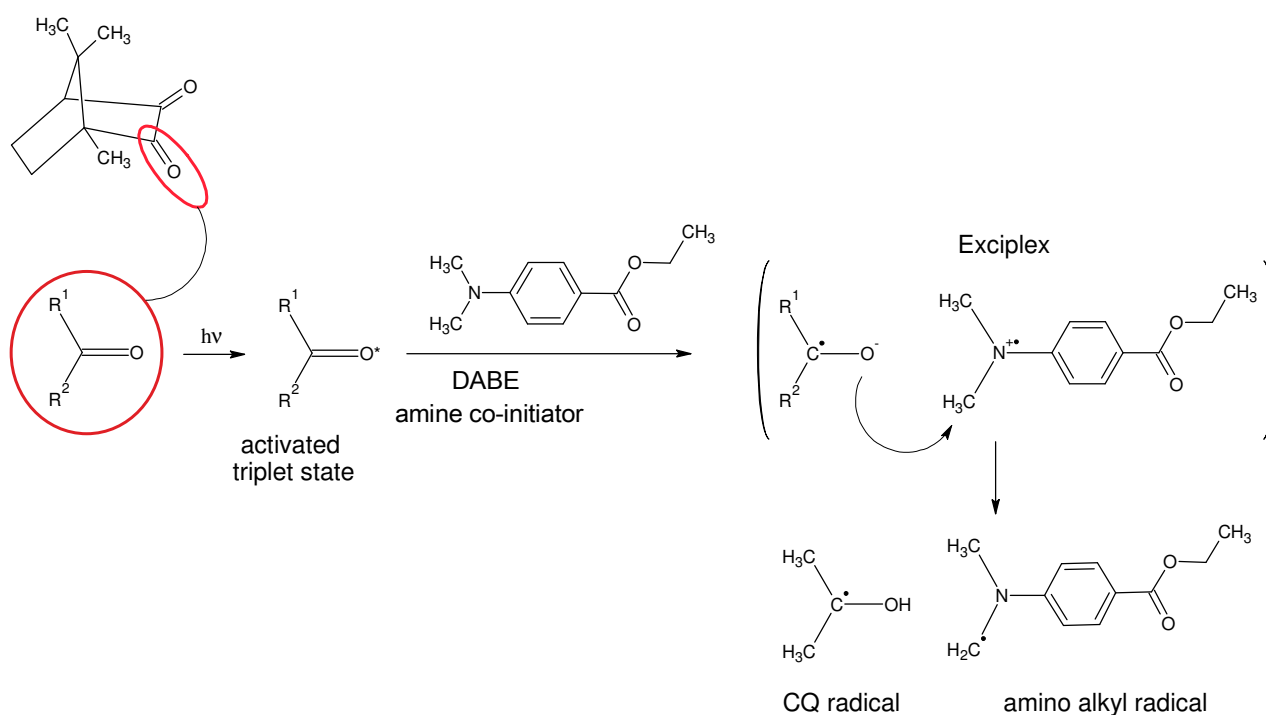


Fig. 1.10: Reaction mechanism of the CQ-ketone light-initiator/DABE-amine co-initiator during light initiation [10, 11]; first step: light absorption and exciplex formation, radical formation: proton transfer from amine to CQ.

1.3.2 Chemical initiation (RP material)

To initiate the polymerization reaction during the RP process at ambient temperature the accelerator N,N-dimethyl-p-toluidine (DMT) is added to the styrene/HEMA-binder. The PMMA-powder containing BPO reacts with the DMT starting the chemical initiation process (Fig. 1.11) [27, 28]. The amine group of the DMT reacts in a first step with the peroxide bond yielding a DMT cation, a benzoate anion and a benzoate radical. In a second step a DMT radical is formed by a proton transfer to the benzoate ion and the benzoate radical decomposes to a phenyl radical under carbon dioxide emission. Both radicals can start the polymerization of the binder in the RP process [29, 30].

N,N-Dimethyl-p-toluidine (DMT)

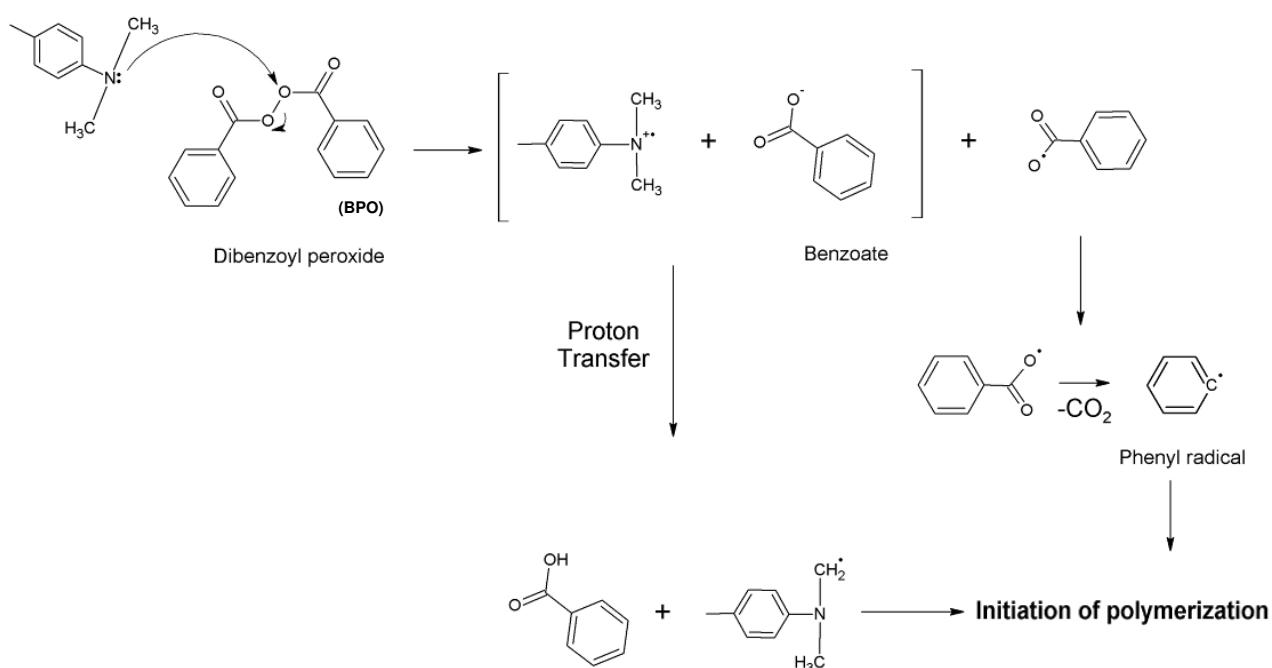


Fig. 1.11: Initiation mechanism of the investigated amine/BPO system for the radical polymerization of styrene and HEMA at room temperature [27, 28].

1.4 Polymerization process

1.4.1 Polymerization process of VLC resin composites

Depending on the different monomer types in the VLC resin composite there are several possibilities of chain propagation and cross-linking during the polymerization process. Assuming a certain mean distance between the homogeneously distributed initiator, this distance determines the length where only linear polymerization can take place. Fig. 1.12 shows the first steps of one possible chain propagation after the polymerization start of a Bis-GMA/ TEGDMA/UDMA resin. It is obvious that after 2-4 polymerization steps the molecular mass is already comparable with that of a small polymer chain. Furthermore, without the presence of a second radical, linear polymerization is the only possible chain propagation but might be negatively effected by steric hindrance after a few propagation steps (Fig. 1.12). Exceeding the mean distance between the homogeneously distributed initiator radicals cross-linking reactions become possible forming a further radical center.

1.4.2 Polymerization process of 3D RP-material

Two species of radicals are formed in the chemical initiation of the RP process. Both the DMT and the phenyl radical (Fig. 1.10) initiate the polymerization by reaction with one of the two binder monomers styrene (M1) or HEMA (M2) (Fig. 1.13, Eq. 1) [31]. Afterwards there are 4 different possible chain propagation steps of the polymerization process (Eq. 2-5). In homo-propagation only one of the two monomers is involved in the chain propagation. Dependent on the particular co-polymerization parameters of the two monomer species also cross-propagation is possible involving both monomers in the chain propagation.

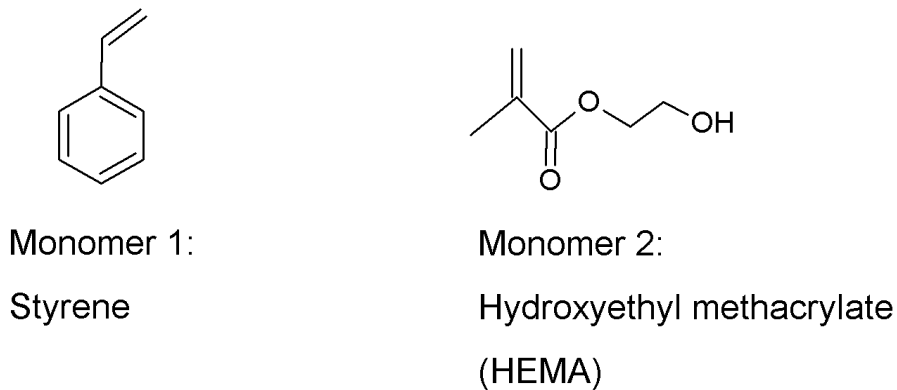
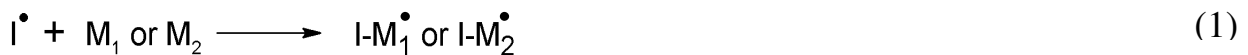
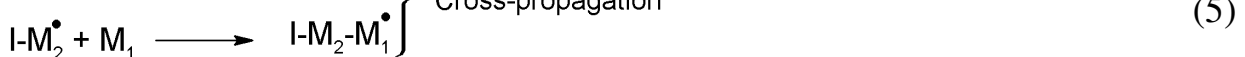
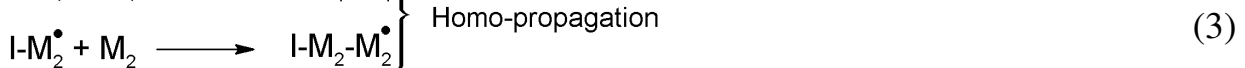


Fig. 1.13: Binder components of a styrene/HEMA co-polymerization.

Initiation of polymerization



Possible chain propagation steps



} Homo-propagation
} Cross-propagation

1.5 Modeling of the polymerization and curing processes

1.5.1 Theory

Taking into account some basic reaction steps (initiation, propagation and termination) of the radical polymerization of thermoset resins allows for the kinetics modeling of the curing process. Eqs. 6-14 show these reaction steps for a photopolymerization [32]. In this initiation process two radicals $R\bullet$ are formed from an excited initiator molecule I (Eq. 6). Then, the radicals react with a monomer M in the first polymerization step (Eq. 7). The rate of initiation R_i is defined as the change of the concentration of $RM_1\bullet$ radicals over time (Eq. 8). Eq. 9 describes the propagation reaction of a linear polymerization with the rate constant k_p yielding the propagation rate R_p together with the monomer and macroradical $M_n\bullet$ concentrations (Eq. 10). A radical polymerization can be chemically stopped by two different kinds of termination reactions [33]. Firstly by recombination of a macroradical with another one (Eq. 11) or a single radical respectively (Eq. 12) and secondly by disproportionation turning two macroradicals into one saturated and one unsaturated inactive polymer chain (Eq. 13). Polymerization also comes to a stop because a lack of monomers. Eq. 14 expresses the rate of termination R_t by introducing the termination rate constant k_t .

Initiation reactions



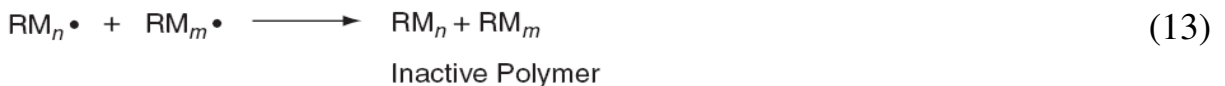
$$R_i = \frac{d[RM_1\bullet]}{dt} \quad (8)$$

Propagation reaction



$$R_p = k_p[M][M_n\bullet] \quad (10)$$

Termination reactions



$$R_t = k_t[M_n\bullet]^2 \quad (14)$$

An overall expression for the polymerization rate R_{poly} is given as [34]:

$$R_{poly} = \frac{k_p}{k_t^{0.5}} [M] \left(\frac{R_i}{2} \right)^{0.5} \quad (15)$$

In the special case of a photo-polymerization the kinetics can be described in the form:

$$R_{poly} = \frac{k_p}{k_t^{0.5}} [M] \left\{ \Phi I_0 (1 - e^{-\gamma [In] l}) \right\}^{0.5} \quad (16)$$

with the quantum yield for initiation Φ , the incident light intensity I_0 , the extinction coefficient γ , the initiator concentration $[In]$ and the layer thickness l .

R_{poly} of a curing reaction typically shows a sharp increase when gelation occurs in the resin matrix followed by a sharp decrease, Fig. 1.14 [25, 35]. This effect known as Trommsdorf-Norrish effect leads to an auto-acceleration as a consequence of a rapid decrease of R_t due to a viscosity increase caused by the growth of polymer molecules. The following sharp decrease of R_{poly} indicates the glass transition of the matrix which decreases the mobility of all radicals drastically. At temperatures below the glass transition every further curing reaction is diffusion controlled [35]. Fig. 1.14 shows this effect on R_{poly} for a linear polymerization of mono-methacrylate monomers and a cross-linking polymerization of dimethacrylate monomers [25, 34]. The typical shape of curve (b) can be found in nearly all the literature described curing kinetics investigations described in chapter 1.5.2.

Describing an investigated polymerization process with mathematical formulas makes it possible to extract reaction kinetics parameters from fitted measurement curves as well as to predict the curing behavior of new materials.

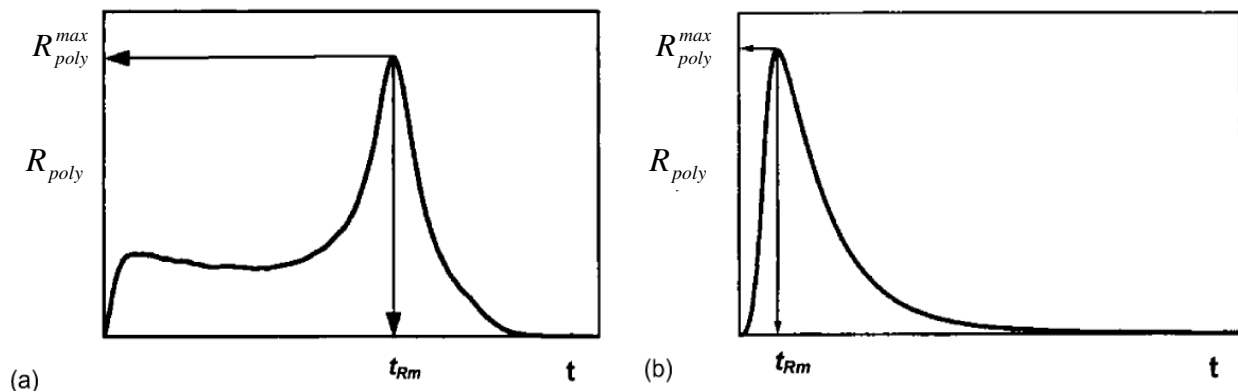


Fig. 1.14: Characteristic curves of the curing kinetics of a linear polymerization of (a) mono-methacrylate and cross-linking of (b) dimethacrylate [25].

1.5.2 Possible methods to determine curing kinetics parameters

Differential Scanning Calorimetry (DSC)

During a curing process the same amount of heat is generated by each polymerization and cross-linking step. Thus, the rate of heat generation correlates with the rate of polymerization R_{poly} , and the amount of heat integrated over curing time corresponds to the degree of conversion (DC). With the DSC this heat release can be traced over curing time and curing kinetics parameters can be determined [36-38]. Fig. 1.15 shows an example of the heat flow and the integrated heat release over curing time of a photo-curing process. In the plot the heat introduced to the sample by the light-curing unit (LCU) is already subtracted.

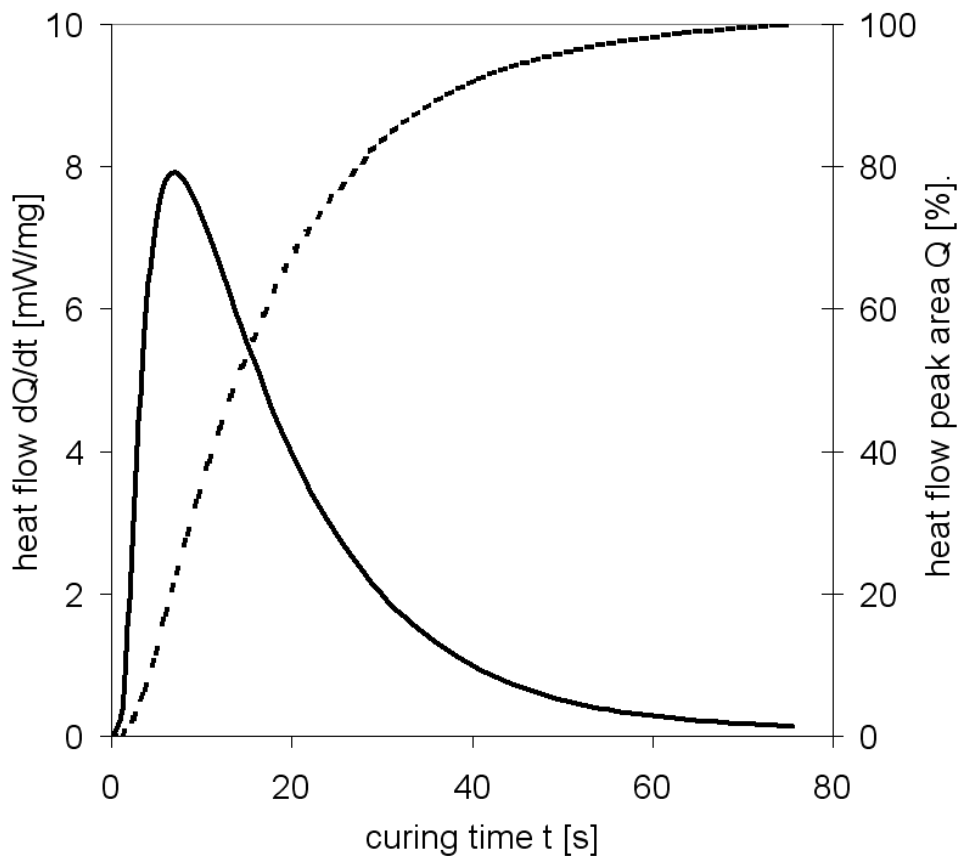


Fig. 1.15: DSC kinetics data of a radical photo-polymerization process; heat flow (solid line) and released curing heat (dashed line).

Fourier Transform Infrared Spectroscopy (FT-IR)

FT-IR in attenuated total reflection (ATR) mode is a widely used method to characterise the curing process of thermoset resins. In the case of acrylic VLC composites the change of the aliphatic C=C double bond band at 1638 cm⁻¹ during the curing process is investigated (Fig. 1.16). The ratio of the peak areas of this band before and after curing is taken to determine the DC (Eq. 17) [39]. Fig. 2.16 shows the change of peak area of the aliphatic C=C band during a light curing process while the aromatic C=C band serving as a reference band remains unchanged. Another kinetics parameter that can be extracted from FT-IR measurements is the change rate of the aliphatic C=C band itself correlating with R_{poly} (Eq. 16) or the change in monomer concentration, respectively. Fig. 1.17 shows R_{poly} and DC over polymerization time [32]. In the literature typical maximum reachable conversion degrees of up to 75 % are reported [5].

$$DC = \left[1 - \left(\frac{(I(1638\text{ cm}^{-1})/I(1608\text{ cm}^{-1}))_{\text{peak area after curing}}}{(I(1638\text{ cm}^{-1})/I(1608\text{ cm}^{-1}))_{\text{peak area before curing}}} \right) \right] * 100\% \quad (17)$$

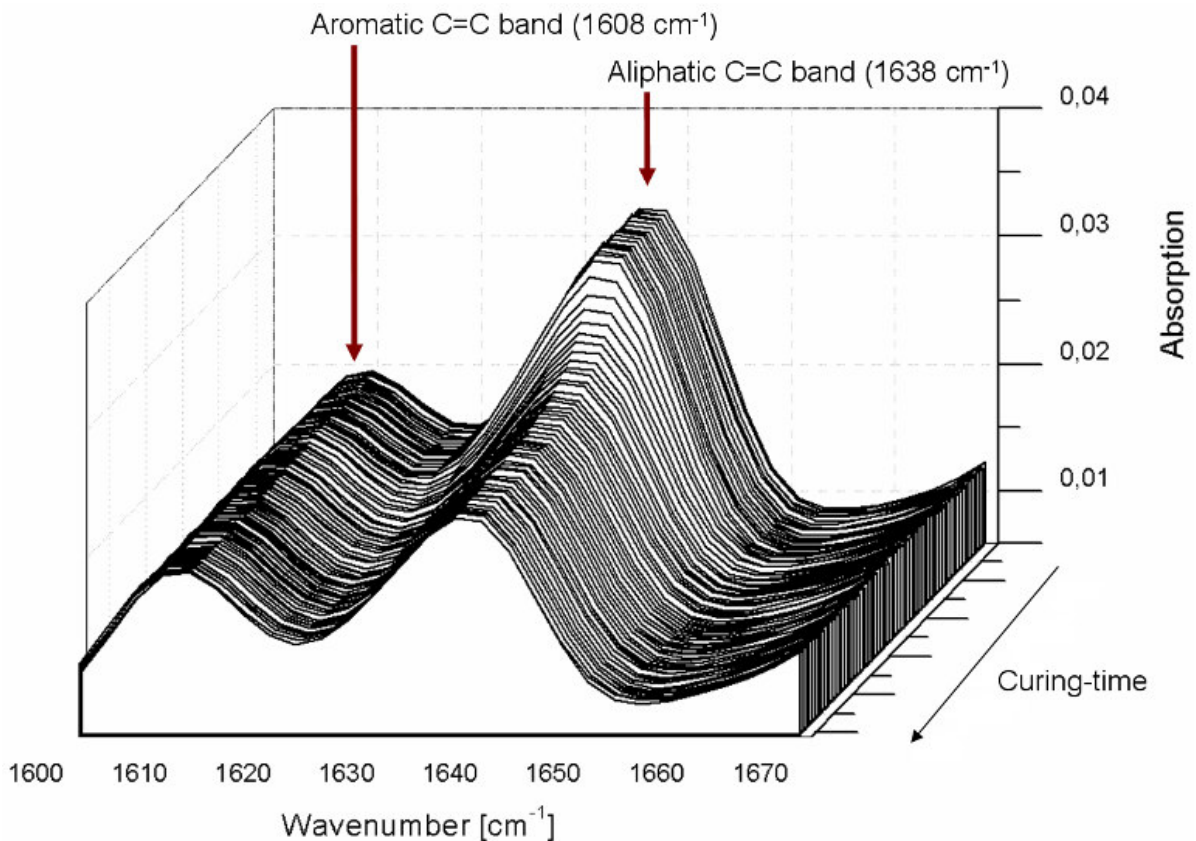


Fig. 1.16: Change of aliphatic C=C band absorption due to decrease of C=C double bonds with curing-time.

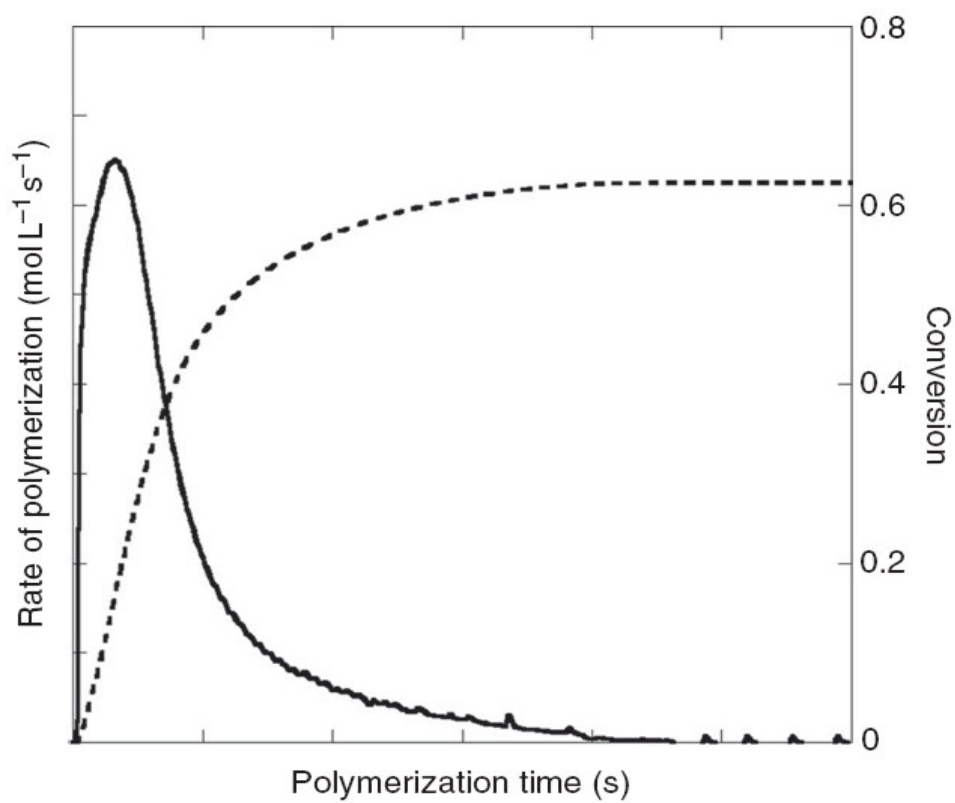


Fig. 1.17: FT-IR kinetics data of a radical photo-polymerization process; rate of polymerization (solid line) and degree of conversion (dashed line) [32].

Shrinkage Measurements (Bonded Disc method)

Transferring a resin monomer into a cured polymer matrix causes a volumetric shrinkage of matter correlating with the number of polymerization and cross-linking reactions respectively. Thus, the relative change in volume $\Delta V/V_0$ can be taken to determine the DC whereas the rate of shrinkage strain $d(\Delta V/V_0)/dt$ corresponds to R_{poly} [40, 41]. In 1991 Watts et al. [40] introduced the Bonded Disc method to investigate the curing kinetics of a photo-polymerization by monitoring the volumetric shrinkage strain over curing time. Fig. 1.18 shows typical kinetics curves obtained by this method [25].

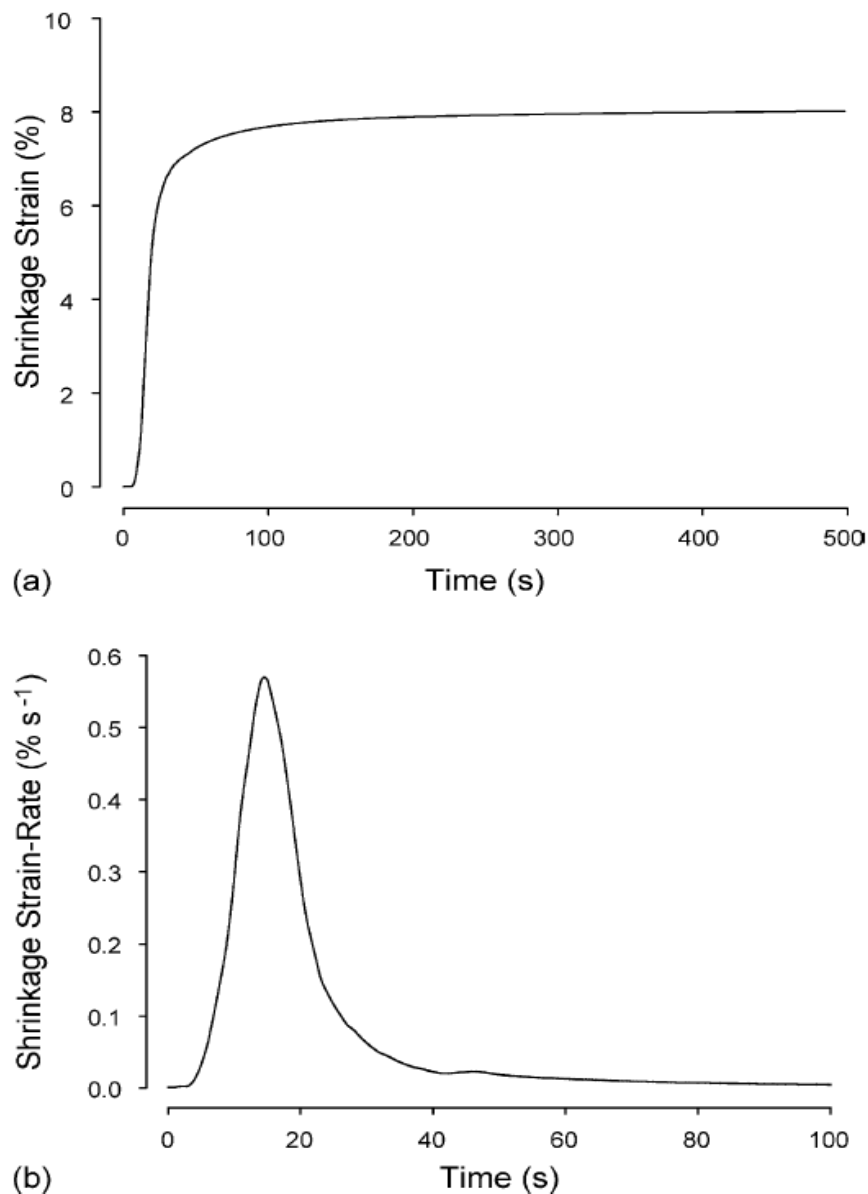


Fig. 1.18: Characteristic shrinkage strain (a) and shrinkage rate (b) curves of the curing kinetics of a dimethacrylate monomer system [25].

1.6 Effect of light intensity on chemical structure of VLC resin composite

The challenge to establish a properly light-cured composite tooth restoration is to affirm that the filling is sufficiently cured at the bottom. Because of this reason the light penetration depth of the composite material is of great clinical relevance for the curing process. Several studies on this topic found an exponential decrease of the initial light intensity I_0 with respect to penetration depth d within the dental filling according to the Lambert-Beer law (Fig. 1.19, left) [2, 3, 5, 10]. Here the decrease is characterized by the attenuation coefficient γ (Eq. 18):

$$I(d) = I_0 e^{-\gamma d} \quad (18)$$

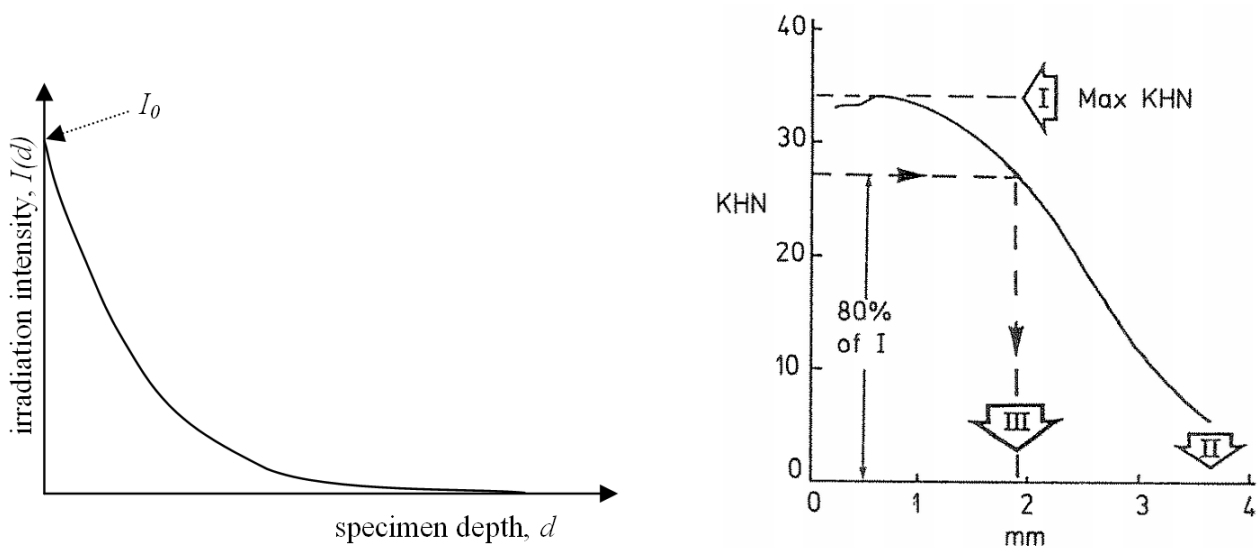


Fig. 1.19: (left) Depth dependent attenuation of the introduced curing light intensity I_0 in the composite specimen according to Eq. 18; (right) depth dependent Knoop hardness according to Watts [5].

As a result a significant change in mechanical properties was found proposing a certain depth of cure (DoC) at which a required minimum degree of cure (DC) is achieved during the light-curing procedure. According to the exponentially decreasing light intensity with penetration depth a similar decrease in radical density can be assumed within the dental filling. Significant changes in the degree of polymerization as well as cross-linking density will be the consequence. Up to now all studies related to DoC measurements have investigated this phenomenon with respect to consequences on the mechanical properties of the dental filling [42]. Fig. 1.19 (right) shows the Knoop hardness (KHN) of a light cured dental composite filling versus specimen depth [5]. In this diagram 3 characteristic values are to be mentioned:

I is the maximum hardness value,

II is the specimen depth at which hardness can still be measured, and

III is the depth at which the hardness value has dropped to 80 % of the maximum value of I.

This 80 % value is typically taken in the literature as the maximum layer thickness for sufficiently cured dental fillings [5]. Nevertheless, none of the studies focused on its cause on the base of differences in the chemical structure. In this PhD project the effect of the light intensity on the structure of VLC composites will be a part of the research.

1.7 DEA monitoring of curing processes

1.7.1 Measurement method

The change of dielectric properties of polymers can be used to investigate the curing process of polymer resins using a dielectric analysis (DEA). Ions (e.g. Cl⁻ ions as impurities) in the resin are forced to move and dipoles are oscillating according to an applied alternating external electrical field in the DEA measurement setup (Fig. 1.20, left). The two effects build up an internal electric field reducing the external one [43]. Due to ion movement and dipole oscillation energy is partly dissipated by internal friction in the polymer resin leading to a phase shift of the induced current (Fig. 1.20, right) [44].

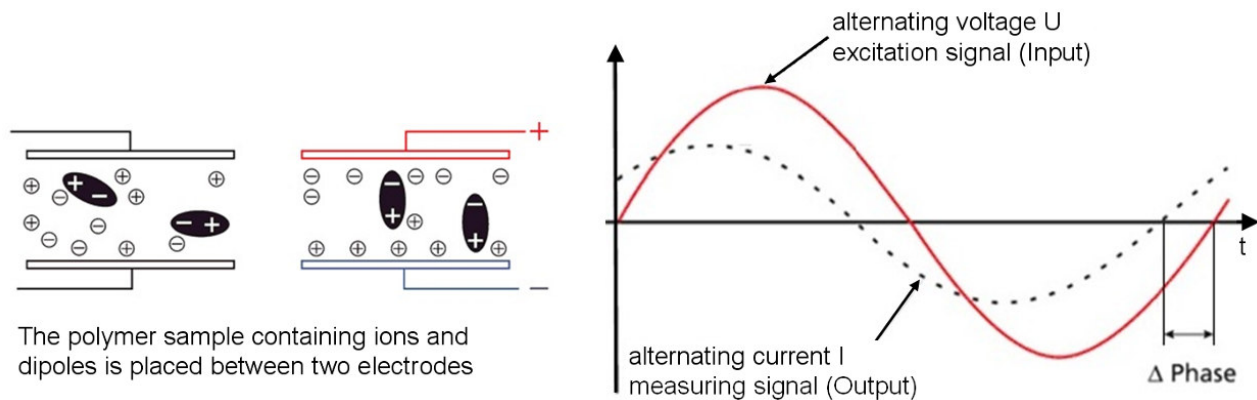


Fig. 1.20: (left) Ion movement and dipole orientation in a capacitor arrangement; (right) phase shift between excitation and measuring signal of a DEA measurement of a viscous resin [45].

As a consequence a complex dielectric constant can be determined depending on the polymer viscosity and the measuring frequency. Over curing time the viscosity changes drastically allowing to characterise the polymerization process precisely with the DEA. In curing monitoring the investigated quantity to trace the curing

process is the ion viscosity η^{ion} . It is depending reciprocally on the ion conductivity σ being proportional to the frequency f , dielectric loss ε'' and the dielectric constant ε_0 (Eq. 19), [45, 46]. Alternatively, according to Zahouly [45] η^{ion} can also be expressed by the reciprocal product of ion mobility $\mu(f)$ times the charge q and the concentration of the mobile ions $[ion]$.

$$\eta^{ion}(f) = \frac{1}{\sigma(f)} = \frac{1}{2\pi f \varepsilon_0 \varepsilon''(f)} = \frac{1}{\mu(f) q [ion]} \quad (19)$$

1.7.2 Sensor systems

The measurement setup of the DEA method differs in some way from the sensor arrangement which is commonly used for dielectric spectroscopy. Instead of a parallel plate capacitor with the specimen between the electrodes, so-called Mini-IDEX DEA sensor has two comb-shaped electrodes arranged intermeshingly over an area of $5 \times 7 \text{ mm}^2$ on a polyimide layer (Fig. 1.21). For a curing measurement the polymer material is placed on the flat sensor surface and the fringe field only interpenetrates the bottom specimen layer instead of the complete bulky specimen [45]. For the investigation of light-curing processes this measurement setup has two advantages. On one hand, the specimen can be easily applied on the IDEX sensor and the curing light can be introduced on the top side. On the other hand, due to the limited penetration depth of the electric field, which is assumed in the range of the electrode distance [45, 47], the curing process can be selectively investigated in different depths simply by varying the specimen thickness [44]. There have already been published real-time curing investigations of VLC composites [48-50] characterizing the curing curves qualitatively. But none of them correlated DEA curing data quantitatively with kinetics models.

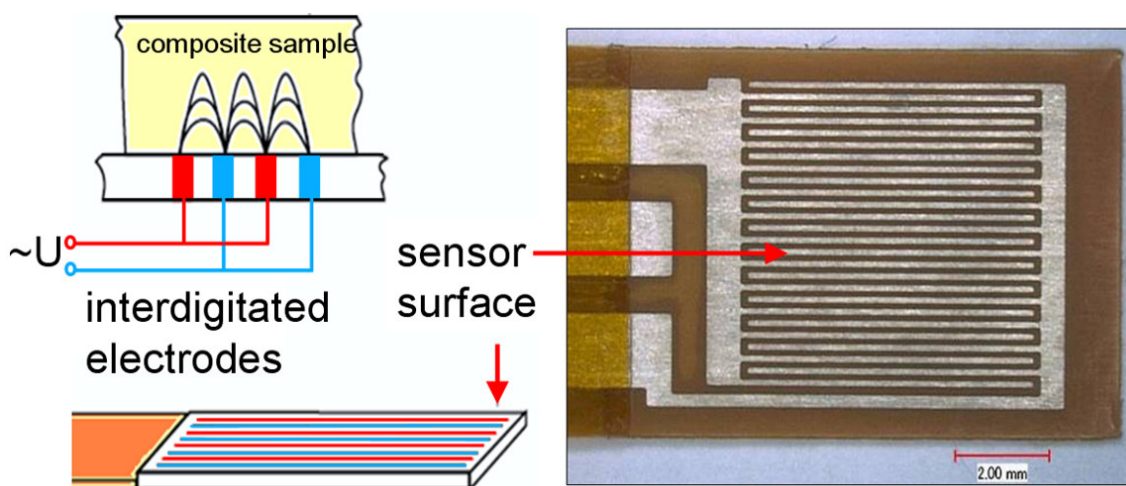


Fig. 1.21: (left) Measuring principle of DEA 231 Epsilon Cure Analyzer [45]; (right) Mini-IDEX sensor, electrode distance: $100\mu\text{m}$, NETZSCH Gerätebau GmbH.

1.7.3 DEA Curve and ion viscosity evaluation

A typical DEA curve tracing the curing behavior of a resin plots the ion viscosity (in logarithmic) versus the curing time. Similarly to shear viscosity, the ion viscosity, which depends reciprocal on the ion mobility, shows a distinctive increase during the curing reaction due to a strong decrease in ion mobility with increasing polymerisation and network density. In the literature only few studies are published on the curing monitoring of polymer resins performed with the DEA. Rosentritt et al. [48] published a study on DEA curing monitoring fast curing VLC composites in 2006. They introduced a method to extract curing parameters characterising the polymerisation state of a tested composite. For this reason the curve minimum, the maximum saturation value, the max slope and the difference between the min-max values have been evaluated (Fig. 1.22).

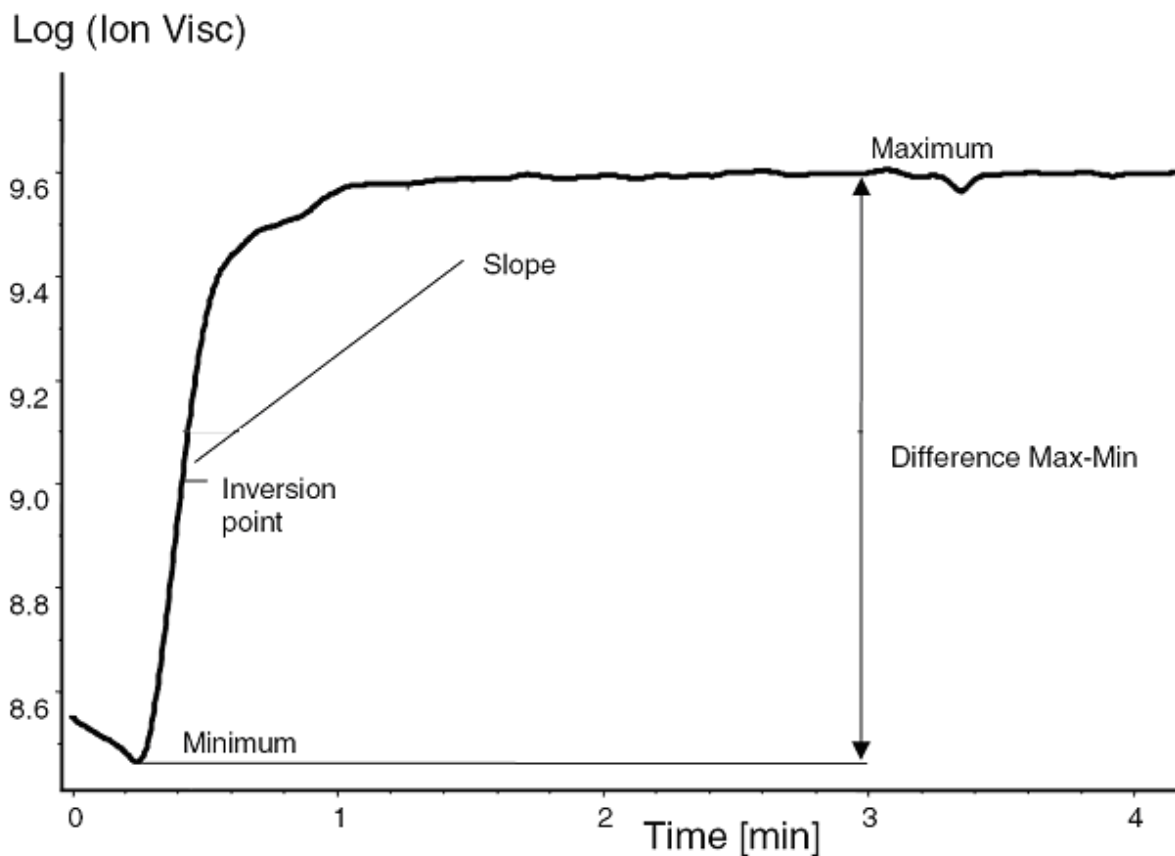


Fig. 1.22: Characteristic DEA curve of the light curing of a VLC dental composite [48].

The min-max value of the ion viscosity was related to the polymerisation progress and network density whereas the slope was related with the polymerization velocity and the conversion rate. They found that the ion viscosity increased about one order of magnitude during the curing process and culminated at a saturation value indicating the polymerization approaching an end. Other studies which have performed DEA real-time curing investigations on epoxy resins found that the

inversion point of the ion viscosity curve closely correlates with the gel point of the curing reaction [51-53]. Rosentritt et al. [48] also stated that the curing reaction did not end directly after the polymerization lamp was shut off. This so-called postcuring phenomenon is also reported in several other studies investigating the curing behavior of VLC composites [49] indicating the potential of the DEA method to characterize curing reactions of polymer resins and composites after passing the glass transition in a state where the curing reaction is diffusion controlled and very slow [35].

1.8 DEA vs. Rheometry of VLC resins and composites

The rheological properties of highly filled resin composites are important for the curing characteristics for two reasons.

Firstly, the viscosity of the pure thermoset resins has a great influence on the curing reaction due to changes of the monomer mobility, and thus their permeability. As shown in Fig. 1.3 the viscosities of typical VLC monomer resins vary from 0.01 up to 800 Pa*s and several studies report the flow behavior of pure resins to be newtonian [54-56]. Table 1.4 shows the viscosity of a monomer blend of Bis-GMA/TEGDMA as a function of mixture ratio and temperature.

Secondly, the flow characteristics of the composites depend not only on a resin composition, but it is strongly affected also by filler type and content. As the composite has to be easily applied in a tooth cavity its flow behavior is of great clinical relevance. In the literature most VLC dental composites are reported to behave both pseudoplasticly [55-57] and thixotropicly [56]. Besides the filler content, filler size, shape and agglomeration have a great influence on the flow properties [2, 58, 59]. Fig. 1.23 shows shear viscosity at a shear rate of 1/s of composites differing with respect to filler content and type. Composites containing mono-disperse pyrogenous SiO₂ nanofiller (see also Fig. 1.5 in chapter 1.1.1) show favorable flow characteristics in comparison to agglomerated nano-particles.

Furthermore, composites with very high filler contents may also exhibit pronounced dilatant properties leading to unfavorable kneading properties and thus, to undesired gap formation at the interface of the tooth restoration which may cause secondary caries.

Rheology of the filled system is relevant for the manufacturing process and for the clinical applicability of VLC dental composites. The viscosity of VLC dental resins and composites can be adjusted by the content of the different monomer types as well as by the filler type. Besides rheological investigation of the uncured composites in steady shear arrangement, the curing process is frequently investigated by dynamic oscillatory rheometry [55-57, 60].

Table 1.4: Shear viscosity of monomers blends of Bis-GMA and TEGDMA at three different temperatures published by Beun and Lee [55, 56].

Bis-GMA/TEGDMA content [%]	Shear viscosity [Pa*s]		
	at 20°C	at 25°C	at 35°C
100 / 0	719	369	52.6
80 / 20	9.20	5.04	1.46
70 / 30	2.29	1.28	0.476
60 / 40	0.550	0.429	0.203
50 / 50	0.201	0.144	0.085
40 / 60	0.087	0.066	0.021
30 / 70		0.035	0.021
20 / 80		0.022	0.014
0 / 100	0.008	0.008	0.007

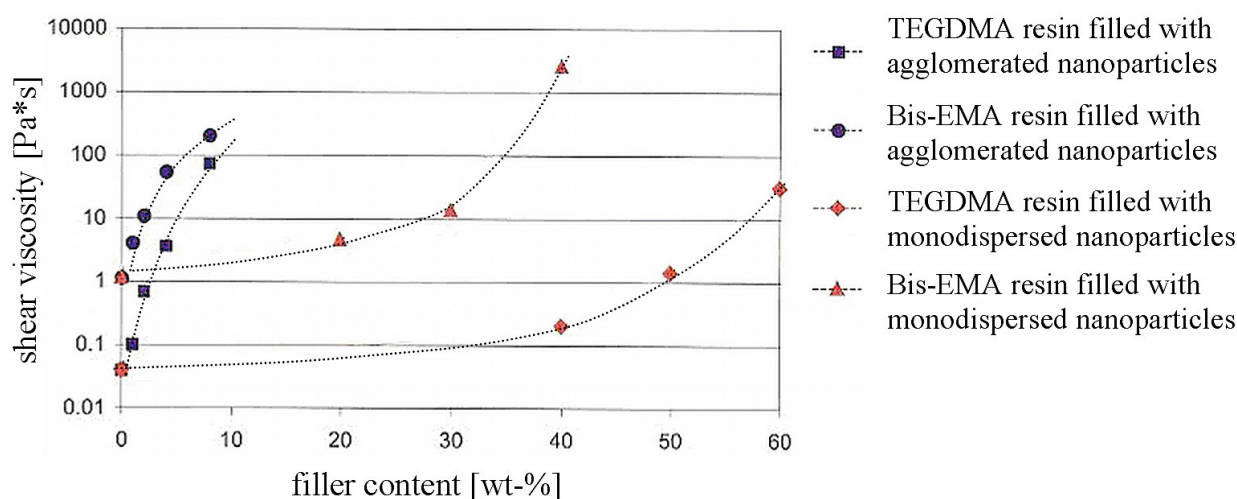


Fig. 1.23: Shear viscosity vs. filler content of experimental composites filled with monodispersed or agglomerated pyrogenous SiO₂ nanoparticles (~ Ø12 nm) [59].

However, after gelation rheometry comes to its resolution limit making it impossible to characterize the curing process for long curing times [57, 60, 61]. In this case the DEA method shows advantages in monitoring the curing of VLC composites. Even at temperatures below the glass transition of the specimen [47, 62, 63]. A direct comparison of a curing process investigated by DEA and rheometry is presented in Fig. 1.24 [47] and provides qualitatively similar results for dynamic viscosity and ion viscosity. This is not surprising as the dynamic viscosity is linked to the ion mobility of the resin according to equation 19. With progressing polymerization and cross-linking during the curing process $\epsilon''(f)$ as well as $\mu(f)$

decrease significantly, whereas η_{ion} increases similar to the dynamic viscosity of a rheologic measurement.

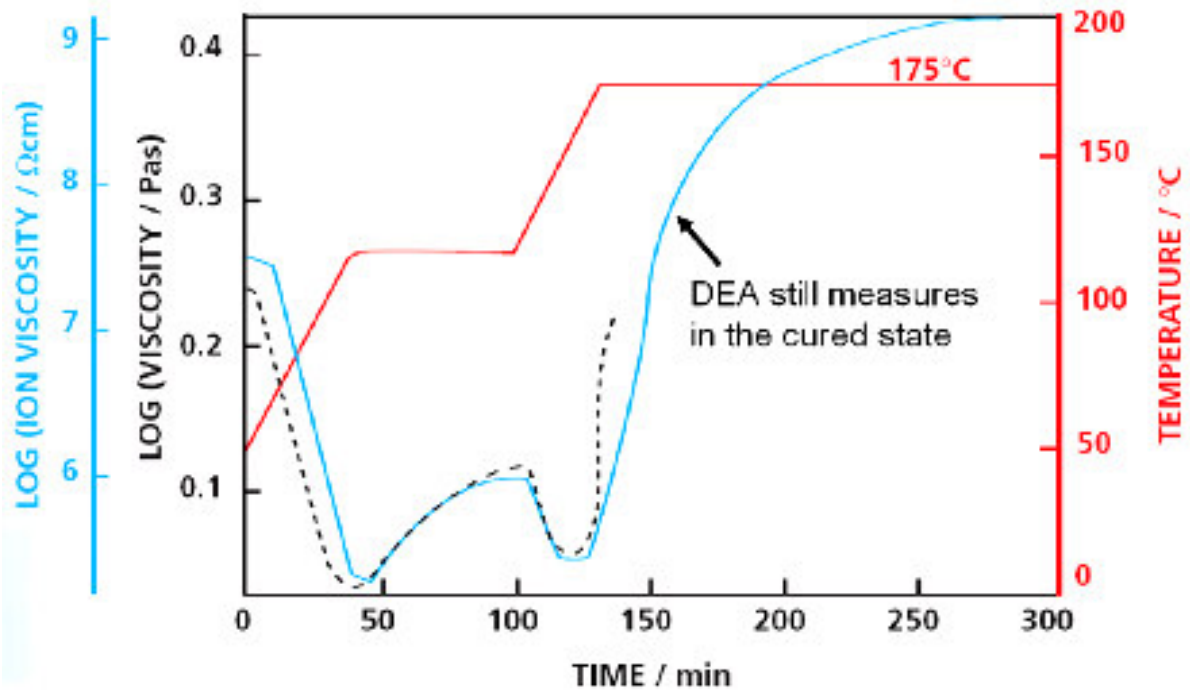


Fig. 1.24: Curing of an epoxy resin during a certain temperature regime (red line): comparison of shear (rheometer, dashed line) and an ion viscosities (DEA, blue line) [47].

2. METHODOLOGY AND PURPOSE OF THE WORK

Besides aviation, automotive and electric industries thermosets play an important role in medical applications and rapid prototyping. Since the important material properties for the later applications are set during the curing process, real-time investigation and characterization of the curing process is the key to successful thermoset product development. The methods employed in this work shall provide information about kinetics parameters as curing rate, gelation point, post-curing kinetics after gelation, degree of conversion (DC) and depth of cure (DoC, in case of light-curing resins) of a polymer network.

Resins to be investigated within this work belong to two fields of application: medical dental applications and rapid prototyping. In principle, the materials belong to 2 classes of resins: photo curing resins (e.g. highly filled visible light-curing (VLC) dental resins substituting the amalgam fillings) and auto cure printing resins. The aim is to provide a methodology to practitioners to optimize and tailor resins in order to shorten the development times and predict/simulate the long-term behavior of the corresponding thermosets.

There are several measurement methods for curing kinetics investigations as differential scanning calorimetry (DSC), Fourier transform infrared spectroscopy (FT-IR) or mechanical methods measuring the shrinkage strain or stress development during the curing process. An important issue is the tracing of the curing process. The curing process depends on composition of the resin, viscosity of the resin, release rate of the curing enthalpy, temperature and filler content. In principle, the total curing process can be divided in the primary curing (generation of the thermoset) and the secondary curing (dark cure and aging of the thermoset).

The curing reaction is to be traced by means of dielectric analysis (DEA). Time dependent ion viscosity serves as an input data for kinetic models. As the compositions of most resins are very complex (resin, inhibitors, stabilizers, fillers etc) the modeling of the curing process has to be performed using a boundary condition free kinetic model besides classical chemical approaches. In the very end the kinetic model is to provide the reaction rate curve to determine the curing time in advance and the change of properties to be expected in the course of time. Table 2.1 gives a brief overview on the performed investigations, scientific goals as well as technical and economic aspects.

Table 2.1: Overview on the planned investigations, scientific goals and technical and economic side goals.

DEA curing investigations of:	Scientific goals:	Technical and economic aspects:
<p>VLC dental resins and composites with respect to:</p> <ul style="list-style-type: none"> - curing depth - resin composition - curing temperature - kinetics modeling 	<p>evaluation of the ability of the DEA for:</p> <ul style="list-style-type: none"> - kinetics investigation and modeling - insights in the depth dependent polymerization structure of a dental filling 	<ul style="list-style-type: none"> - simplification and time reduction of VLC composite development processes with the DEA method - provision of a time and cost efficient investigation method for quality insurance applications
<p>3D printing rapid prototyping resins with respect to:</p> <ul style="list-style-type: none"> - characteristics of the initiation process - the role of the composition on the printing process 	<p>evaluation of the setting process of the investigated 3D printing rapid prototyping system</p>	<p>simplification and time reduction of 3D printing binder development processes with the DEA method</p>

3. DISCUSSION OF THE RESULTS

3.1 DEA characterization of thermoset resins curing

3.1.1 Curing behavior of VLC dental composites

Curing behavior of 6 different light curing dental composites were investigated with dielectric analysis (DEA) using especially redesigned flat sensors with interdigitized electrodes. However, if not stated otherwise, the discussion is based on samples of Arabesk Top material.

DEA of curing reactions - basic curve shape, reproducibility and scattering

The first issue to be considered with DEA method is the reproducibility of the ion viscosity data. Samples taken from the same tube show a good reproducibility during the primary curing phase (Fig. 3.1). This is important as this time range was used to evaluate the reaction constant if the concentration of initiator molecules is known. It should be noted that the measurements carried out on samples from different tubes and/or batches are more scattered.. However, the reason of such a low reproducibility is not attributed to the DEA method accuracy but rather to differences in the materials compositions. As the filler content of these highly filled materials is in the order of 75 to 90 %, fluctuations between two batches may reach ± 3 %. This leads to changes of the resin content between 10 and 30 %, and consequently to differences in the measured initial ion viscosity.

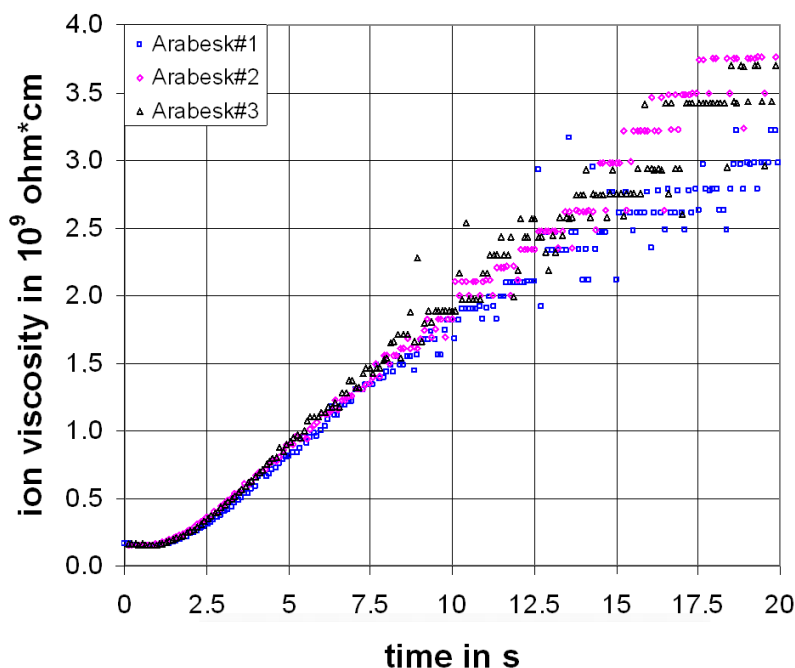


Fig. 3.1: Reproducibility of DEA curing measurements shown for three samples of Arabesk Top [P-II].

Identification of curing stages, investigation of frequency dependency of DEA measurements

From the time dependent DEA curve the following characteristic values can be extracted (Fig. 3.2):

- the constant initial ion viscosity η_0^{ion} of the non-irradiated materials
- the initiation phase with a slight decrease of the ion viscosity
- the linear increase of the ion viscosity indicating the phase of undisturbed chain growth (UCG)
- the degressive increase of the ion viscosity indicating the phase of disturbed chain growth (DCG) slowly approaching the final state
- the final ion viscosity η_{∞}^{ion} of the fully cured materials

The constant initial ion viscosity η_0^{ion} depends mainly on the composition of the resins defining the concentration of ions. It was found that the measured initial ion viscosities change between 3 and 10 % within the same batch depending on the material. Larger changes were found between different batches of the same material. This means that the DEA is able to indicate changes of the raw materials as well as changes in the composition of the produced dental filling materials.

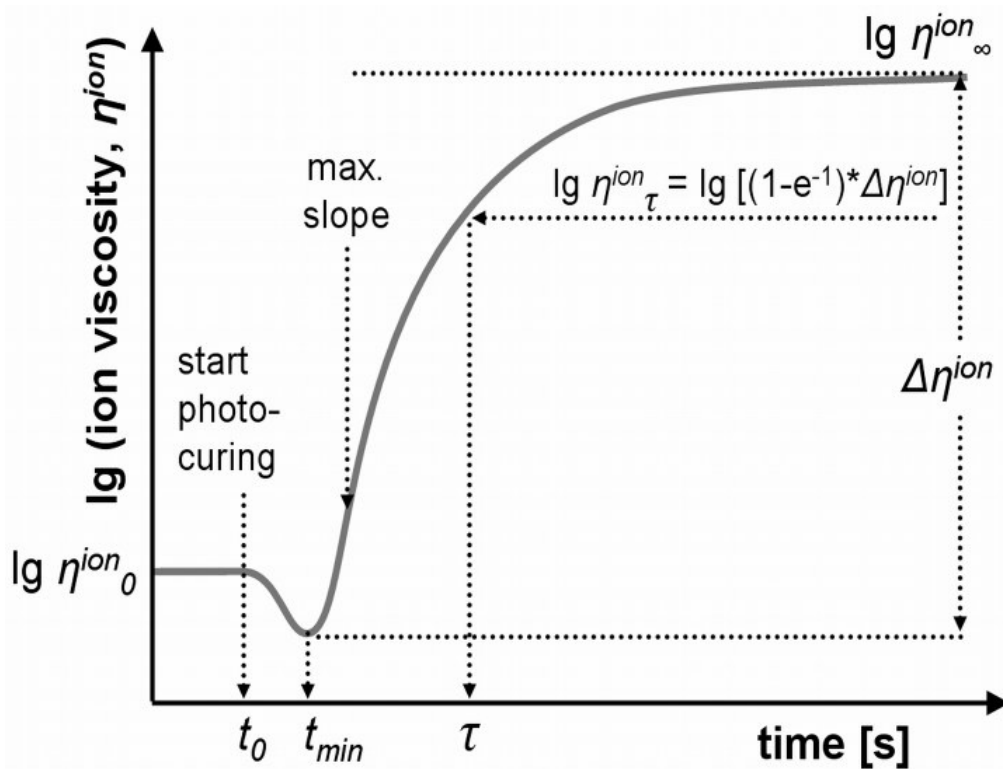


Fig. 3.2: Schematic ion viscosity curing curve of a VLC dental composite in the logarithmic scale with characteristic points.

Depth dependent curing behavior [P-I]

The time dependent ion viscosities during the irradiation of 40 s for different specimen layer depths (from 0.5 to 2.0 mm in 0.5 mm steps to avoid figure crowding) for Arabesk Top dental resin are shown in Fig. 3.3 (further measurement results can be found in paper I [P-I]). The curves were evaluated with respect to characteristic ion viscosity values: initial ion viscosity, slope in the linear range, and average ion viscosity between 37 and 40 s (Table 3.1). The composite exhibits a material specific initial ion viscosity η_0^{ion} of typically $(180 \pm 15) \text{ M}\Omega \cdot \text{cm}$ in the uncured state (Table 3.1). At the beginning of the irradiation there is a depth dependent decrease of the ion viscosity between 8-35 % for Arabesk Top (Fig. 3.3 a). In the initiation phase (Fig. 3.3, b) the ion viscosity drop is more pronounced with increasing depth in the specimen and it lasts longer to reach the initial value again (\rightarrow initiation time). With increasing depth the initiation phase is extended. In a depth of 2 mm it lasts about five times longer than in a depth of 0.5 mm. As the curing time of VLC composites is an important parameter for the clinical application [3, 64-65] the initiation time before the start of the polymerization is an important quantity characterizing the reactivity of such resins and composites.

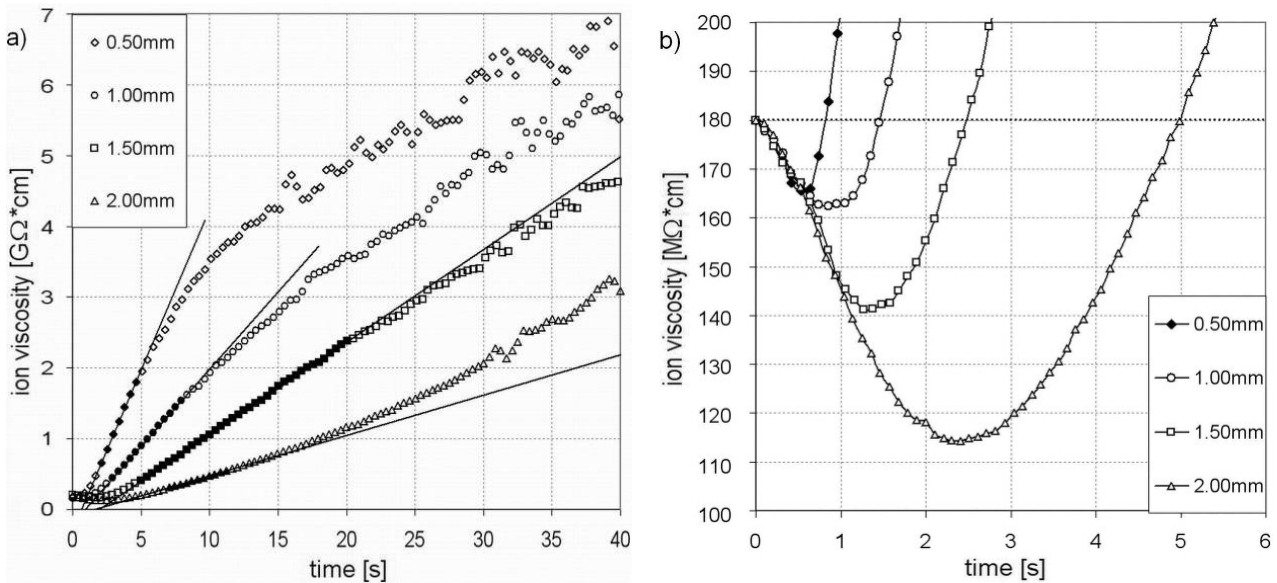


Fig. 3.3: Depth dependent ion viscosity curves of Arabesk Top during light-curing for 40s (the range of linear time dependency is highlighted with full symbols) (a), and in the initiation phase between 0 and 6s (b) [P-I].

The initiation times determined in this study depend on composite type, resin content and the depth within the sample. Generally, these characteristic times are affected by at least three processes:

- (1) Daylight stabilizers and inhibitors, e.g. buthylated hydroxyl toluene, must react in the initiation process prior to the start of polymerization [66].

- (2) Temperature rise in the specimen due to photo-thermal effect and exothermal reactions reducing the resin viscosity, and consequently the ion viscosity [67].
- (3) New ions are temporarily generated during the light initiation process when initiator and accelerator molecules are transferred to radical ions [12, 68] (compare also chapter 1.3). Obviously these ion radicals contribute to the ion viscosity decrease within the initiation phase (different but still a depth dependent mechanism).

Table 3.1: Characteristic ion viscosity values (initial ion viscosity, slope of the linear range and average ion viscosity between 37 to 40 s of irradiation) and times of the initiation process (time of minimum ion viscosity and initiation time) of Arabesk Top in different specimen depths. (n=3, mean values with standard deviations in parenthesis), [P-I].

specimen depth (mm)	0.50	0.75	1.00	1.25	1.50	1.75	2.00
initial ion viscosity, η_0^{ion} (M Ω *cm)	161 (10)	162 (4)	171 (4)	184 (10)	198 (19)	185 (7)	196 (9)
slope of the linear range, $\dot{\eta}_{lin}^{ion}$ (M Ω *cm/s)	460 (33)	295 (46)	218 (9)	164 (10)	131 (13)	66 (6)	58 (6)
average ion viscosity between 37-40s, $\bar{\eta}_{37-40}^{ion}$ (M Ω *cm)	6,780 (310)	6,250 (1,110)	5,790 (1,060)	5,370 (610)	4,610 (650)	3,62 (490)	3,020 (80)
time of minimum ion viscosity, t_{min} (s)	0.53 (0.11)	0.62 (0.01)	0.92 (0.06)	1.20 (0.06)	1.49 (0.06)	1.80 (0.11)	2.48 (0.06)
initiation time, t_{init} (s)	0.83 (0.11)	1.04 (0.01)	1.44 (0.04)	2.10 (0.09)	2.56 (0.16)	4.52 (0.05)	4.99 (0.19)

The starting polymerization increases the ion viscosity [45] and compensates the initiation effects. As a consequence the ion viscosity reaches a minimum. After passing the minimum the ion viscosity increases strongly with a linear behavior during the first polymerization phase (data highlighted with full symbols in Fig. 3.3 a). The ion viscosity increase is found to be depth dependent during the 40 s of irradiation by a factor 15 to 40 for Arabesk Top with respect to the initial ion viscosity η_0^{ion} . The larger the depths in the specimens, the longer the linear ranges of the ion viscosity curves and the curing times, while the slopes of the ion viscosities, $\dot{\eta}_{lin}^{ion}$, decrease correspondingly (Table 3.1). Fitting the depth dependent mean values of $\dot{\eta}_{lin}^{ion}$ with the Lambert-Beer-law yields an attenuation coefficient γ of (1.39 \pm 0.08) mm⁻¹ (R²=0.98) (Fig. 3.4, left). This attenuation coefficient corresponds to an

absorption depth of $d_a=1/\gamma$ of (0.72 ± 0.04) mm, and maximum curing depth $d_0=3*d_a$ of (2.17 ± 0.13) mm.

If the slope of the ion viscosity reflects the polymerization and curing rate, it should exhibit the same depth dependency as the applied light intensity. The depth dependent light intensity fits to the Beer-Lambert law although it is clear that multiple light scattering is not taken into account. The attenuation coefficient of 1.53 mm^{-1} ($R^2=0.99$) is somewhat larger than that found for the slope of the ion viscosity in the linear range of the DEA measurement resulting in a slightly smaller absorption depth of $d_a = 0.65$ mm and maximum curing depth of $d_0 = 1.96$ mm (Fig. 3.4, right). In the light of these results it seems quite reasonable why the maximum increment layer thickness recommended by the manufacturer is 2 mm.

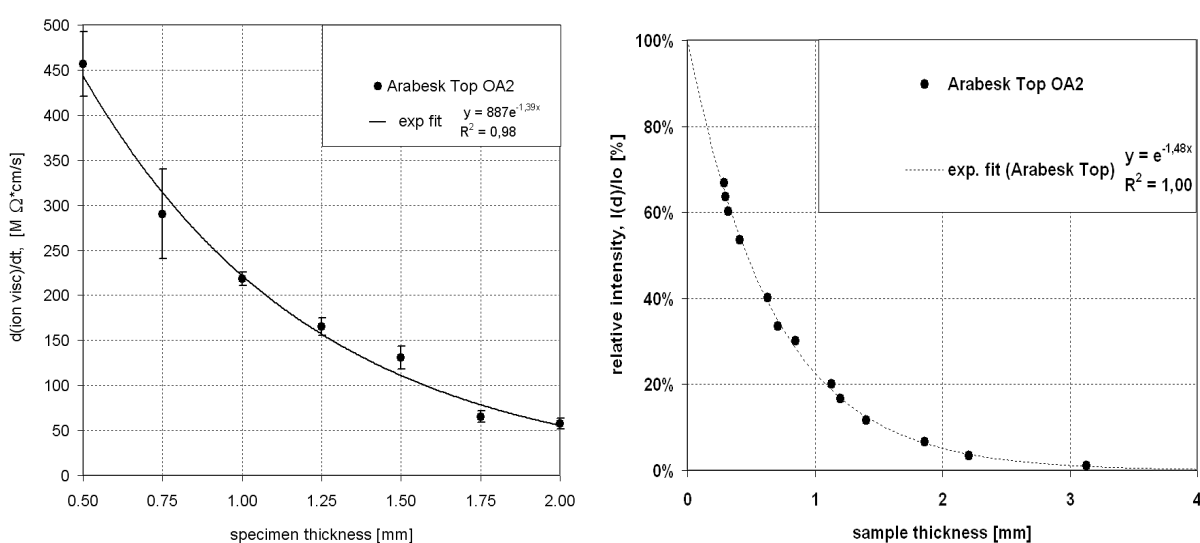


Fig. 3.4: Depth dependent linear slopes of ion viscosity curves of Arabesk Top (left side); depth dependent light intensity absorption (right side); both fitted acc. to Lambert-Beer Law [P-I].

The linear increase of the ion viscosity after the initiation phase allows for insights in the beginning of the polymerization. According to Ferry [69], the viscosity of low molecular weight polymers depends linearly on molecular weight until a critical degree of polymerization is reached. Exceeding this critical molecular weight, the viscosity increases sharply with an exponent of 3.4. Simultaneously, it is the state where the polymerization process slows down due to a significant viscosity increase. Possibly this is also due to beginning gelation and cross-linking, respectively [P-II, 70]. The linear increase of ion viscosity with time indicates the existence of an UCG during the first seconds of the polymerization until the polymer chains reach a length that either allows for cross-linking with neighboring chains or transition to the glassy state (Fig. 3.5, left). For depths up to 1.5 mm the duration of the phase of UCG increases but it is compensated by decreasing reaction rates, which are indicated by decreasing slopes of the ion viscosity. Furthermore, it

supports the kinetics mechanism of the curing process that a remarkable amount of the CQ is “instantaneously” activated in this layer [P-II].

At depths exceeding 1.5 mm the light intensity is attenuated to one tenth or less (Fig. 3.4, right). Therefore, the activation of CQ becomes time dependent. Now the ion viscosity shows an increase after the linear range, indicating an acceleration of the curing process for a certain time interval (Fig. 3.3, curve for 2 mm depth). The change of the principal time dependency of the ion viscosity with depth is shown schematically in Fig. 3.5, right.

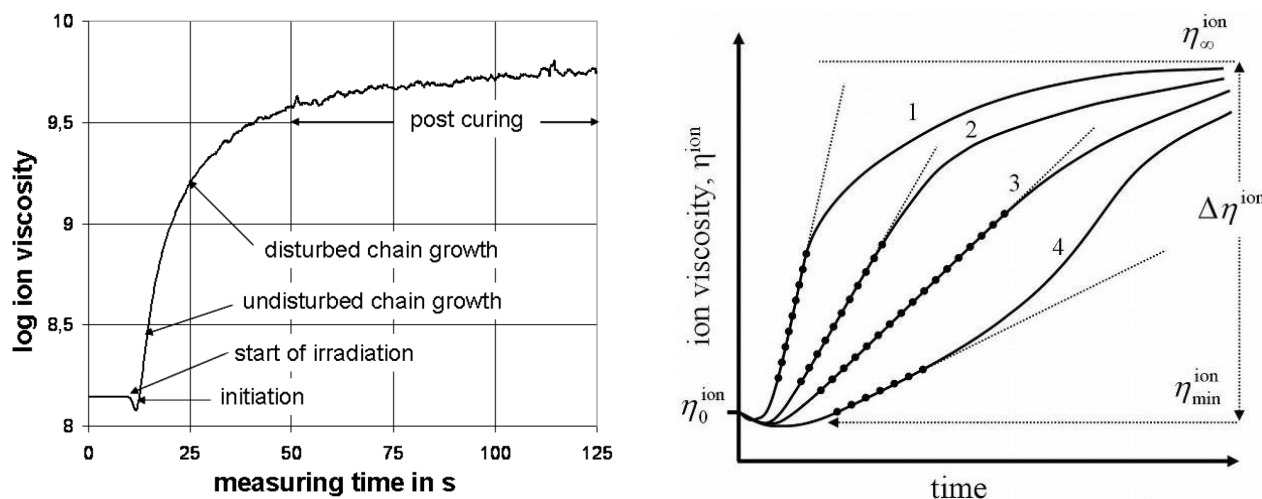


Fig. 3.5: Schematic ion viscosity curve in the logarithmic scale with characteristic ranges (left side) [P-II]; Schematic representation of the ion viscosity curves for increasing depths within the sample - curve #1 is close to the surface, curve #4 is very deep in the sample (right side) [P-I].

How can this changing curing behavior be explained with respect to curing depth? CQ photo initiator and amine accelerator are homogeneously distributed in the resin. Assuming a mean distance between the molecules one can divide the resin into elementary volumes, whose size depends on the concentration of the CQ or amine molecules, respectively. As the light intensity decreases exponentially within the specimen, the concentrations of CQ and amine radicals decrease accordingly. This means that the available resin volume for a single radical consists of more and more CQ elementary volumes with increasing depth. In Fig. 3.6 the depth dependent curing behavior is demonstrated by considering three layers in different depths with different curing kinetics:

The top layer is irradiated with very high light intensity leading to an instantaneous and high concentration of CQ and accelerator ion radicals. The concentration of radicals can be considered to be constant and time independent. The mean distance between them is rather small and only few polymerization steps are necessary to reach the boundaries of the elementary volumes where cross-linking starts.

In the intermediate layer, the light intensity is reduced to the extent where the generation of CQ and amine radicals becomes slightly time dependent, but the initial concentration of radicals is still high. This leads to decreasing reaction rate of the firstly generated radicals, which is compensated by newly generated radicals. Consequently, a linear increase of the ion viscosity in relatively large range of curing time is obtained.

In the bottom layer the light intensity is reduced to less than 10 % of the initial value. The generation rate of radicals is small, and therefore the radical concentration increases with time. The polymerization heat of the ongoing reaction and the heat from the LCU contribute to the temperature increase of the sample. The continuous radical generation together with the temperature increase leads to an enhanced reaction rate. The available volumes of the radicals become much larger than the elementary volumes of CQ and amine molecules. Therefore, the phase of UCG lasts significantly longer on average although there are few radicals generated further. These further radicals together with the immobilization of the long growing chains may be responsible for the observed acceleration of the reaction rate.

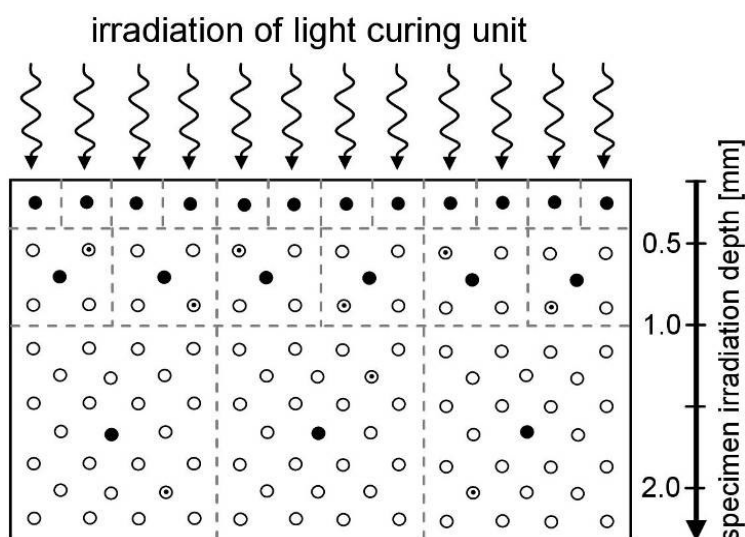


Fig. 3.6: Model of the radical density change with increasing depth in a sample (white spots: initiator molecules, black spots: activated radicals, dotted spots: posterior activated radicals), [P-I].

If polymerization and cross-linking happen according to the model proposed in Fig. 3.6, the molecular structure of the dental resin in the top layer corresponds to a thermoset (as polymerization starts from many radicals with a high reaction rate). Cross-linking already occurs in the early stages of irradiation if neighboring macromolecules begin to interpenetrate. In the bottom layer only few radicals are generated and the macromolecules have to become very long before they can interpenetrate and allow for cross-linking. However, if the length of the macromolecules increases, the molecules pass over into the glassy state. Their

molecular mobility decreases significantly and as a consequence also the reaction rate. This may happen before cross-linking becomes possible. Therefore, the molecular configuration in the bottom layer corresponds rather to a thermoplastic structure.

Depth dependent curing behavior at very low irradiances investigated by NMR-MOUSE [P-III]

The photo-curing reaction of dental resins has been examined with unilateral nuclear magnetic resonance (NMR-MOUSE) allowing for a non-destructive high-resolution measurement of depth profiles as a function of time and space. The NMR signal is sensitive to both the monomer concentration and changes in molecular mobility. The space and time dependence of the NMR signal can be described by the photo-polymerization reaction kinetics together with a heuristic approximation of the temperature dependence.

NMR is used as an analytical tool to study matter in a magnetic field under the impact of radio-frequency (rf) pulses. The samples under study must have a nuclear isotope with angular momentum (spin) different from zero which orients in a magnetic field [71]. In the investigated dental composites hydrogen nuclei with spin $\frac{1}{2}$ were observed by relaxometry.

In a static magnetic field B_0 , the spins get aligned parallel to it. A radio frequency pulse with a magnetic field B_1 perpendicular to B_0 manipulates the nuclear magnetization, and the magnetization response to radio frequency pulses is analyzed. One of the most important NMR phenomena is the echo caused by constructive interference of magnetization components. A spin echo is generated by two rf pulses and observed at the echo time t_E after the first pulse, where t_E is twice the pulse separation. NMR relaxometry concerns the measurement of the NMR relaxation times T_1 and T_2 . The longitudinal relaxation time T_1 specifies the time needed for the magnetization to reach thermal equilibrium. The transverse relaxation time T_2 is the time with which the impulse response decays in a perfectly homogeneous magnetic field and it is determined with the help of spin echoes. When the field is inhomogeneous, the impulse response decays faster with the relaxation time T_{2eff} . Carr et al. [72, 73] proposed a multi-echo method to measure a train of echoes in inhomogeneous fields whose decay traces the decay of the impulse response in homogeneous fields in the absence of translational diffusion. Given the self-diffusion coefficient D , the decay of the magnetization signal $M(t)$ is described by

$$M_{xy}(t) = M_0 e^{-\left(\frac{1}{T_2} + \frac{1}{12} \gamma^2 G^2 t_E^2 D\right)t} = M_0 e^{-\frac{t}{T_{2eff}}} \quad (20)$$

with the time lag between successive echoes t_E , the gyromagnetic ratio characteristic of each isotope γ and the magnetic field gradient G , and magnetization signal in thermodynamical equilibrium M_0 . The characteristic decay constant of a Carr Purcell

Meiboom Gill (CPMG) echo train is called T_{2eff} , and under low absolute values of G , D and t_E , it is well approximated by T_2 .

However, the time resolution of the NMR mouse method is limited to approximately 2 data points per minute. Thus, the light-curing reaction of the dental composite samples had to be stretched over several minutes by reducing the irradiation intensity to 1 % of the commonly used value of 800 mW/cm². Due to a comparably short measurement time window of 25 s, the CPMG decays have no good signal-to-noise ratio as illustrated in Fig. 3.7 (a) for an Arabesk Top composite in a sample depth of 1.2 mm. In fits with exponential decays, the fitting parameters “amplitude” and “relaxation time” show errors exceeding 30 %. Therefore, they could not be used to describe the reaction. On the other hand the echo sum integrated over 25s has a sufficiently good signal-to-noise ratio for that purpose.

Figure 3.7 (b) summarizes the echo sums of the Arabesk Top dental resin composite as a function of time and sample depth. Two different time periods can be discerned in the curing curves separated by their maxima: initiation phase and curing phase. The duration of the initiation phase increases with increasing depth as the light, which initiates the reaction, is more attenuated. The subsequent curing process obeys the following relation for the time-dependent monomer concentration which was derived in paper III according to Kohlrausch [74]:

$$[M](t) = [M]_0 e^{-\frac{2}{3}\left(\frac{t-t_0}{\tau}\right)^{3/2}} \quad (21)$$

with the initial time t_0 , the initial monomer concentration $[M]_0$ and the reaction time constant τ which increases with increasing distance from the light source.

To describe the complete curing curves, two new terms were empirically included in Eq. (21): term 1 accounts for the initiation phase, improving the correlation coefficient R^2 , and term 2 represents an experimental offset C yielding

$$[M](t) = [M]_0 \underbrace{\frac{2}{3}\left(\frac{t-t_0}{\tau}\right)^{3/2}}_{\text{term 1}} e^{\left[\frac{2}{3}\left(\frac{t-t_0}{\tau}\right)^{3/2}\right]} + \underbrace{C}_{\text{term 2}} \quad (22)$$

Differentiation of Eq. (22) provides the time when the NMR signal achieves its maximum value

$$t_{max} = \exp\left(\frac{2}{3}\ln(3/2)\right)\tau + t_0 \quad (23)$$

Figure 3.8 (a) shows examples of fits of the experimental data by Eq.(22) for Arabesk Top at depths of 1.7 and 3.8 mm ($R^2 > 0.98$), where all the parameters were set to be varied. The fits show that a constant value for the initial monomer concentration $[M]_0$ is found for all depths, and the reaction time constants τ depend

exponentially on depth as expected from Eq. (21-23). The offset level increases with increasing depth. The spatial dependence of the maximum signal with the relative error bars is presented in Figure 3.8 (b).

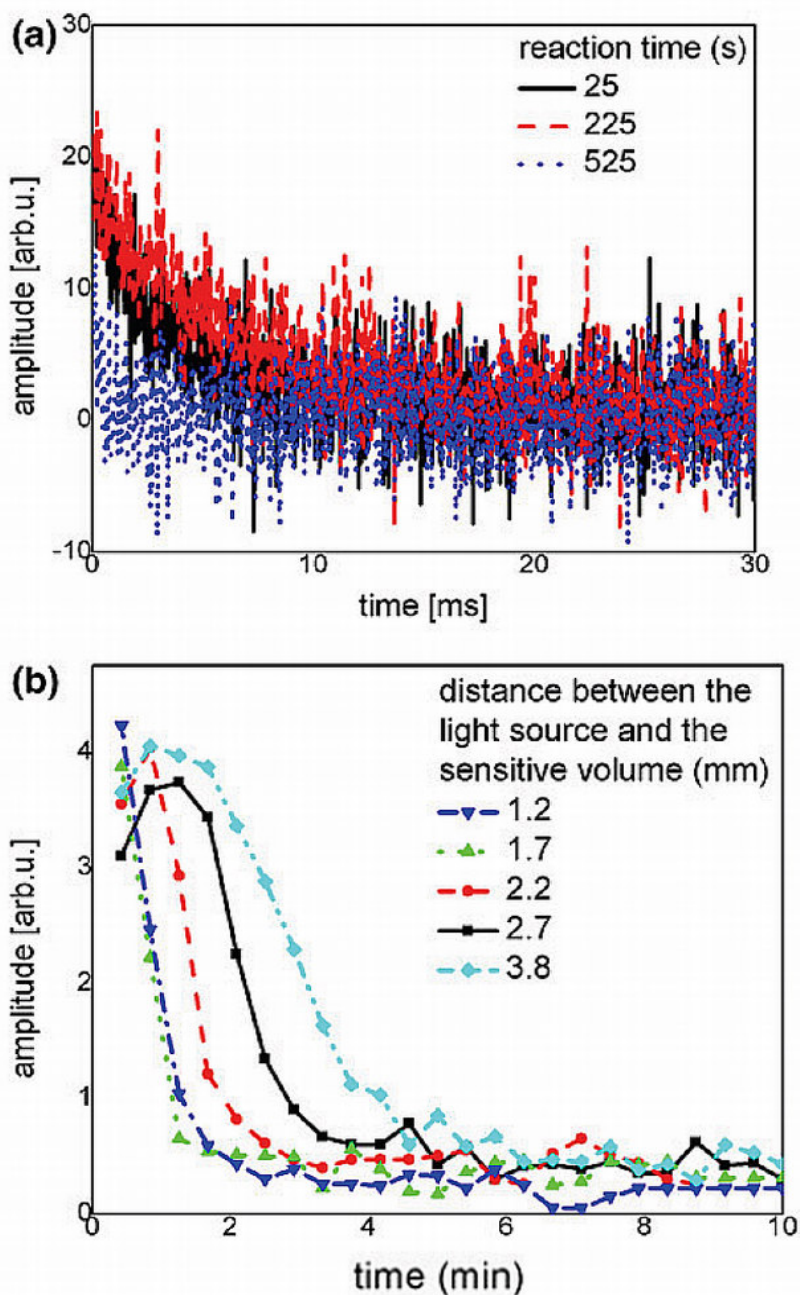


Fig. 3.7: Time dependent CPMG decays of an Arabesk Top composite at 1.2 mm sample depth with unacceptable signal-to-noise ratio (a), Sums of the 64 first echoes in the CPMG detection trains at different sample depths versus curing time by means of single-sided NMR for the Arabesk Top (b) composite sample [P-III].

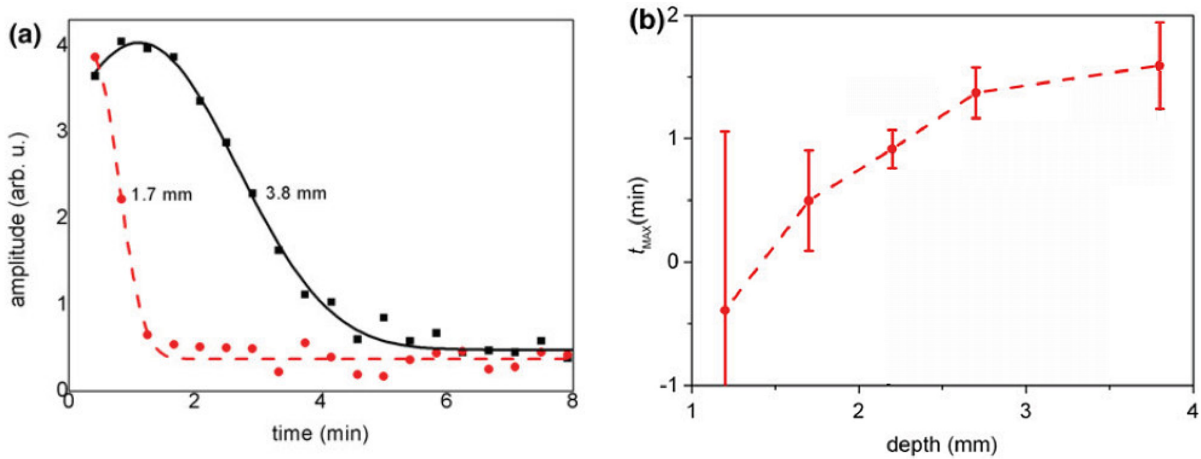


Fig. 3.8: Time dependent CMPG decays of an Arabesk Top composite at 1.7 and 3.8 mm sample depth taken from Fig. 3.7 (b) and fitted acc. to Eq. (22) (a), relation between the signal maximum and sample depth of Arabesk Top (b) [P-III].

Effect of resin composition on curing behavior (unpublished data, not included in Papers I-V)

The effect of the monomer composition on the curing behavior of VLC resins was investigated for four different bisphenol A glycidyl methacrylate (Bis-GMA) / triethylene glycol dimethacrylate (TEGDMA) ratios (Fig. 3.9). Both DEA (Fig. 3.9, left) and FT-IR-measurements (Fig. 3.9, right) show significant differences in the time dependent curing behaviour of the resins with respect to initiation time, curvature and saturation values. BisGMA has an approximately 100,000 times higher shear viscosity than TEGDMA, and thus correspondingly different ion mobility.

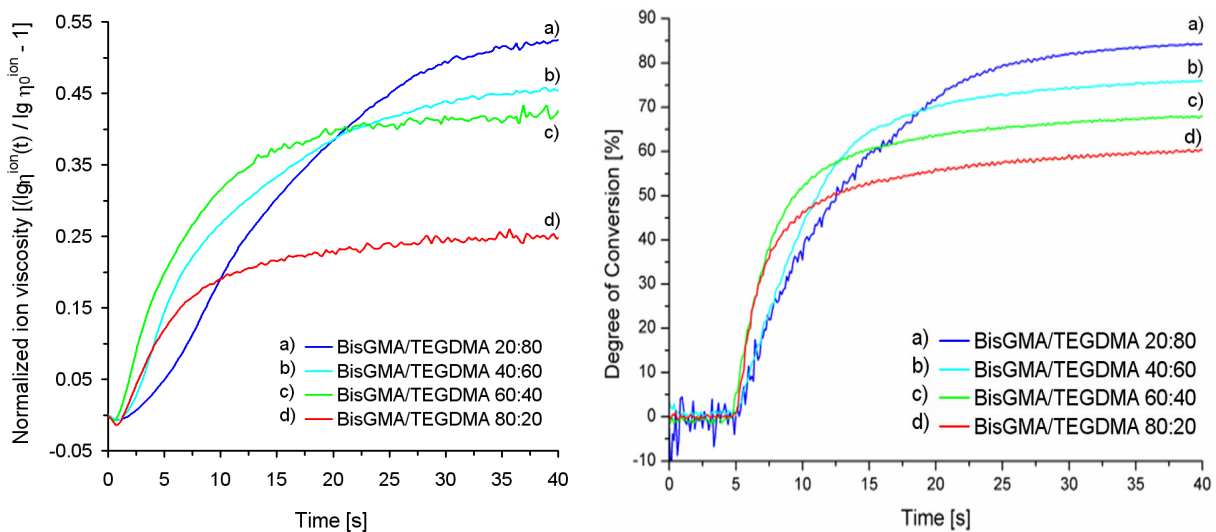


Fig. 3.9: Comparison of normalized DEA curing curves (left) with FT-IR DC-curves (right) of an experimental VLC resins varying in a monomer composition.

Due to the fact that BisGMA has a significantly higher ion concentration than TEGDMA which leads to an offset in ion viscosity (see also chapter 3.4) the lg-DEA curves in Fig. 3.9 (left) are normalized with respect to the initial value. Although the exact influence of the resin composition on the curing kinetics has not been quantified in detail up to now, it is interesting how similar the DEA and DC (Fig. 3.9, right) curves are. In fact both diagrams show the same curing behavior.

The curing reaction of a VLC resin is governed by a photo-initiator-system containing light initiator camphorquinone (CQ) and accelerator ethyl 4-(dimethylamino)benzoate (DABE) which is much more reactive than CQ (\rightarrow polymerization rate determining). Furthermore the VLC resins have to be stabilized to avoid the start of polymerization prior to illumination at ambient light. A typical daylight stabilizer is hydroxytoluene (BHT). The detailed initiation mechanism is presented in chapter 1.3.1.

A dental resin contains different additives such as initiator system and stabilizer to adjust the performance. To investigate the effects of these additives on the curing behaviour the experimental resin Bis-GMA/TEGDMA having a mixture ratio of 60:40 has been prepared containing a) only the photo-initiator CQ, b) CQ + accelerator DABE and c) CQ + DABE + stabilizer BHT. From Fig. 3.10 it can be seen that DABE has a significant accelerating effect on the curing behavior whereas BHT mainly affects the final ion viscosity indicating differences of the reached DC.

Changing the amount of the initiator system CQ/DABE has significant effects on the curing behaviour (Fig. 3.11). The red curve with 1.1 g/kg initiator content shows a significantly slower curing kinetics whereas the increase from 3.3 to 5.5 g/kg leads to almost no further effect (and in fact the content of an initiator in the commercial VLC composites does not exceed the value of 3.3 g/kg CQ).

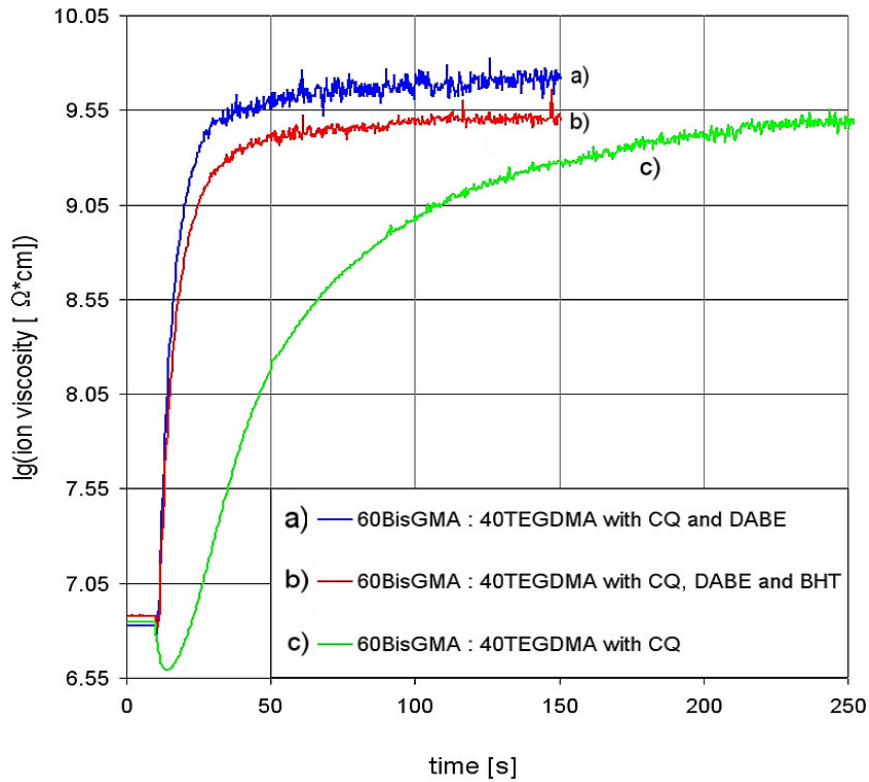


Fig. 3.10: DEA curing curves of an experimental VLC resin with varying composition with respect to initiator (CQ), accelerator (DABE) and stabilizer (BHT) presence

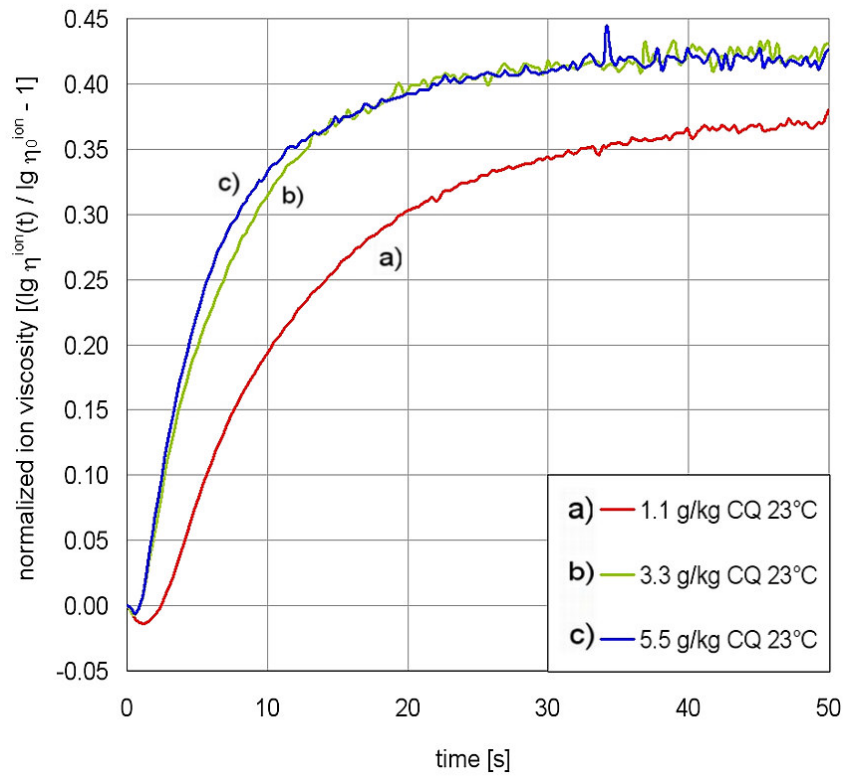


Fig. 3.11: Normalized lg-DEA curing curves of an experimental VLC resin with varying light initiator content.

3.1.2 Evaluation of curing behavior of 3DP RP-resins [P-IV]

The rapid prototyping printing materials used in this study are two component polymer systems consisting of PMMA powder and a liquid binder VXP1 (Voxeljet Technology GmbH). It was tested at two stages - new (VXP1-new) and 6 months old (VXP1-old).

DEA curing measurement – basic curve shape, reproducibility, identification of curing stages and frequency dependency

The ion viscosity of the PMMA powder measured with a frequency of 10 Hz drops from high values in the dry state by 3 to 5 decades in the moment of the addition of a binder. In the case of VXP1-new binder it passes through a minimum and increases slowly for 60 min to values being half a decade below the initial ion viscosity (Fig. 3.12, right).

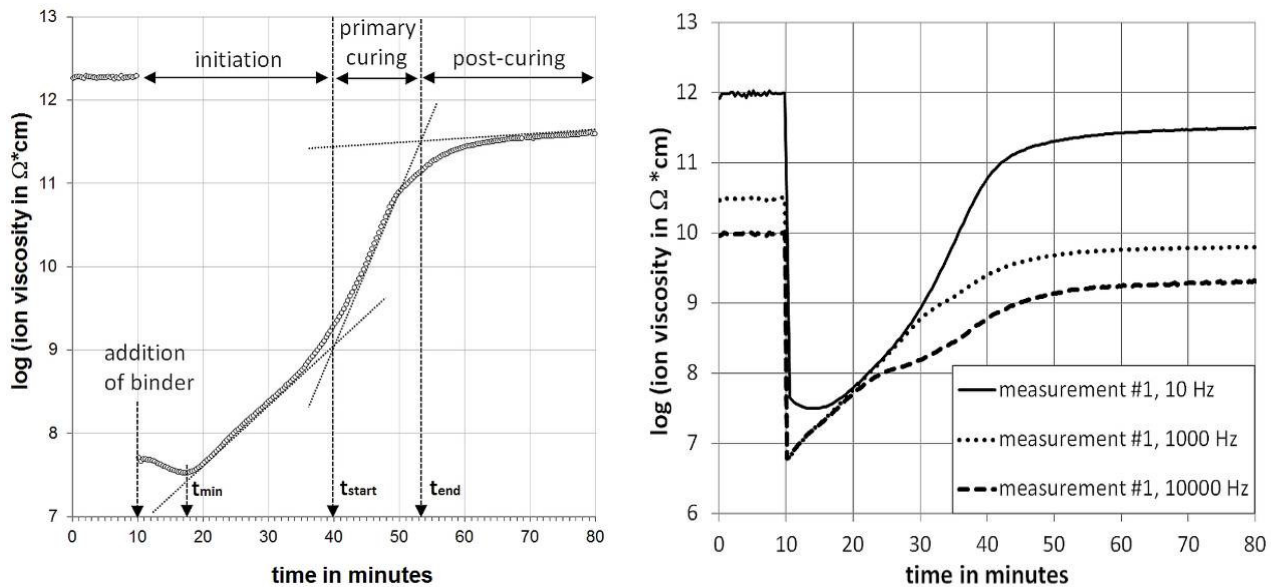


Fig. 3.12: Evaluation of $\log(\text{ion viscosity})$ curves with corresponding curing phases (left). Frequency dependent ion viscosity with binder VXP1-new (right) [P-IV].

Three phases in the curing process can be distinguished in the ion viscosity curves after binder addition: 1st initiation, 2nd primary curing and 3rd post-curing (Fig. 3.12, left). The two steps “initiation” and “primary curing” are better separated for 1,000 and 10,000 Hz. Furthermore, the time dependent ion viscosities depend strongly on the chosen frequency (Fig. 3.12, right), as the ion viscosities before binder addition and at t_{min} , t_{start} and t_{end} exhibit significantly different frequency dependency (Table 3.2). For frequencies of 10 Hz, 1,000 Hz and 10,000 Hz (change by a factor 1,000) the ratios of the ion viscosities (normalized to the 10,000 Hz

value) of the initial and end ion viscosities are similar but change during the initiation and curing phase in a different manner:

- initial ion viscosity η^{ion}_0 decreases in the steps 235 : 5 : 1
- minimum ion viscosity η^{ion}_{min} decreases in steps 5 : 1 : 1
- start ion viscosity η^{ion}_{start} decreases in steps 1.7 : 1.5 : 1
- end ion viscosity at 100 min η^{ion}_{100} decreases in steps 299 : 6 : 1

The time to minimum ion viscosity t_{min} is shifted towards the moment of binder addition with increasing frequency (Table 3.2). Interestingly, the slopes of the log(ion viscosity)-curves coincide well independent of frequency within the linear range of the initiation phase (Fig. 3.12, right).

Table 3.2: Frequency dependent ion viscosities and characteristic times of VXP1-new binder determined by DEA [P-IV].

Parameter	Unit	Frequency		
		10 Hz	1,000 Hz	10,000 Hz
η^{ion}_0	GΩ*cm	1330	28.6	5.7
$\Delta\eta^{ion}_0$		363	2	2.1
η^{ion}_{min}	MΩ*cm	32	6.5	6.3
$\Delta\eta^{ion}_{min}$		1	1.8	1.8
t_{min}^*	min	4.5	0.6	0.4
Δt_{min}		1.7	0.3	0.3
η^{ion}_{start}	MΩ*cm	784	689	457
$\Delta\eta^{ion}_{start}$		339	326	25.9
t_{start}^*	min	23	24.2	24.9
Δt_{start}		4.2	4.1	4.6
η^{ion}_{100}	GΩ*cm	386	7.2	1.3
$\Delta\eta^{ion}_{100}$		57	0.7	0.5
t_{end}^*	min	35.5	38.8	39.1
Δt_{end}		4.2	4.4	4.2
* values corrected with respect to time of binder addition t = 10 min				

Effect of binder components and binder aging on curing behavior

In order to understand the curing process of the commercial binder VXP1 the effects of its constituents HEMA and styrene on the time and frequency dependent ion viscosity was investigated as well as aged VXP1 (Fig. 3.13, left).

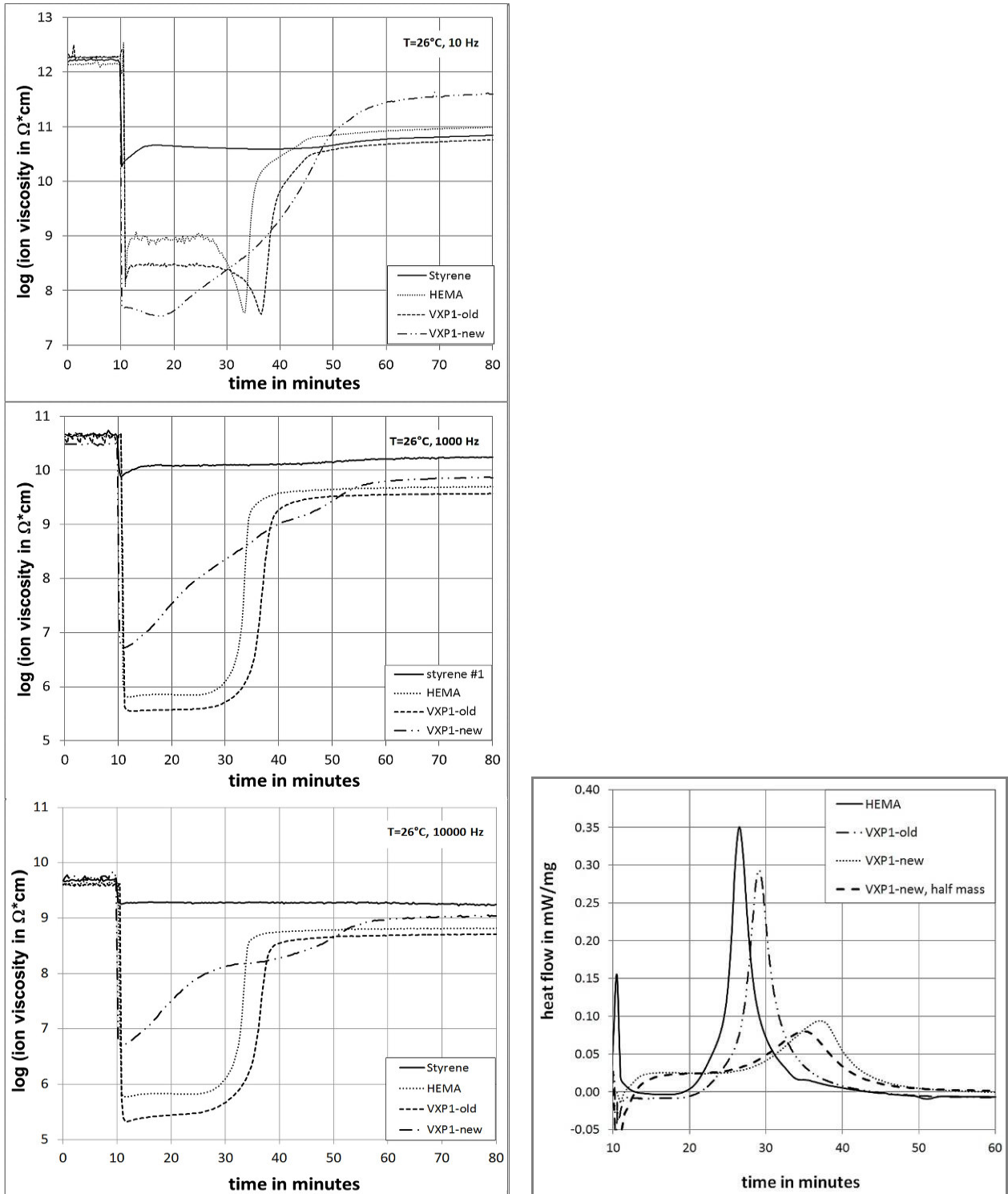


Fig. 3.13: Effect of different binders on ion viscosity of styrene, VXP1-new, HEMA and VXP1-old measured at 10, 1000 and 10000 Hz (left). Corresponding heat flow curves (without styrene) measured with DSC (right) [P-IV].

For all 3 frequencies the ion viscosity curves of new VXP1 show a time dependency differing from those obtained for aged VXP-1 as well as HEMA and styrene. After the sharp drop due to a binder addition it reaches quickly a minimum. Then it increases continuously until reaching the end ion viscosity η^{ion}_{end} . The curing process with new VXP1-binder lasts typically 15 min longer than that for HEMA and VXP1-old (Table 3.3).

The HEMA and VXP1-old binders show a sharp drop with a subsequent plateau during the initiation phase before the primary curing leads to a very sharp increase. Their ion viscosity curves at 10 Hz differ in two features significantly: After remaining constant on the plateau level for 15 min a further decrease occurs before suddenly the primary curing starts. At the end of this sudden increase the slope of the $\log \eta^{ion}(t)$ -curve decreases significantly and remains constant for another 10 min. Therefore, two end times are provided for the ion viscosity curves at 10 Hz in Table 3.3.

The styrene binder shows a small drop after binder addition compared to the other binders and almost no further change of ion viscosity. In the ion viscosity curves at 10 Hz and 1,000 Hz a little step might be identified in the time range from 45 to 50 min after binder addition, however, even after 120 min the samples were soft and uncured.

How can the different curing curves be understood with respect to the different binder types? During the initiation the binder swells the PMMA particles and mobilizes the initiator molecules trapped in the PMMA particles. Initiator-activator reactions generate radicals starting the copolymerization of styrene and HEMA. The initiation lasts a certain time until the ion viscosity has reached the starting ion viscosity η^{ion}_{start} for the investigated PMMA-VXP1 system which was found to be $5 \cdot 10^8 \Omega\text{cm}$ and reached after typically 34 min. It is obvious that VXP1-new binder generates different initiation processes than VXP1-old and HEMA binders exhibiting the ion viscosity plateau for about 20 min. The DSC curve of VXP1 (Fig. 3.13, right) shows a constant exothermal heat flow already after an onset time of 4 min until primary curing starts. This means that chemical reactions take place already after 4 min. The corresponding ion viscosity increases slowly and continuously during this initiation phase. This increase can be explained by both reduction of monomer mobility because of the swelling of the PMMA particles combined with ion diffusion into the particles or a slow and immediately starting polymerization process. Both processes increase the overall viscosity, and thus the corresponding ion viscosity.

After reaching the start time t_{start} the reaction rate of VXP1-new increases significantly as the system transfers to the phase of primary curing (Fig. 3.13, left, 10 Hz, at ~ 40 min). This sudden change can be explained by the Trommsdorf effect [25, 35]. The polymer chains have reached a length which reduces their mobility significantly. The rate of radical annihilation reactions goes to zero and the

polymerization is only determined by the monomer mobility. Due to the polymerization the viscosity of the binder system has reached a level – shown by the relatively high starting ion viscosity η^{ion}_{start} – keeping the polymerization rate moderate during the primary curing phase compared to VXP1-old and HEMA. This benefits twice to the performance of the final RP parts as thermal stresses are kept low and enough relaxation time is given to them.

The curing behavior generated by the pure HEMA binder differs significantly. The ion viscosity remains on a constant but strongly frequency dependent level for 15 min. Then the ion viscosity measured at 10 Hz drops by more than one decade while only small ion viscosity changes are observed at 1,000 Hz and 10,000 Hz. If one associates the ion viscosity at 10 Hz with the long range mobility of ions and the ion viscosity at 1,000 and 10,000 Hz with short range mobility this means that a minimum long range mobility of the monomers is required to start polymerization. The fact that the ion viscosity is increased by almost 3 decades within less than two minutes after passing the minimum at 10 Hz shows that the polymer chain radicals have to be immobilized. This leads immediately to Trommsdorf-like polymerization behavior which is decelerated when the glass temperature of the HEMA styrene copolymer exceeds ambient temperature. Furthermore, it seems that the short range mobility does not depend on frequency as the ion viscosities at 1,000 and 10,000 Hz are similar during the initiation phase.

Table 3.3: Frequency dependent times of cure of the binders HEMA, VXP1-old and VXP1-new determined by DEA. (The VXP1-old measurement was an additional measurement 6 month later. After ageing there was not enough binder left for a multiple determination.) [P-IV]

Binder	Start time t_{start}			End time t_{end}		
	10 Hz	1,000 Hz	10,000 Hz	10 Hz	1,000 Hz	10,000 Hz
	[min]	[min]	[min]	[min]	[min]	[min]
HEMA	23.8	23.6	22.8	25.3/35.5	25.7	26.5
	± 1.1	± 0.3	± 0.8	± 0.9	± 0.9	± 0.8
Styrene	34.5	34.3	n.e.*	48.1	45.6	n.e.*
	± 0.6	± 0.5		± 0.9	± 0.9	
VXP1-old	26.2	24.3	25	28.8/36.2	26.2	27.5
VXP1-new	26.8	27.6	29.6	38.9	42.4	43
	± 3.4	± 3.1	± 2.9	± 3.7	± 4.1	± 3.3
*n.e. = impossible to evaluate						

Further, the behavior of VXP1-old binder can be explained because of the higher volatility of styrene indicated by lower melting and boiling temperatures, lower viscosity, and higher vapor pressure [P-IV]. During storage the VXP1 binder lost styrene due to evaporation and permeation. This leads to an increasing HEMA concentration in the binder containers. As the number of ions in the binder remains constant it causes an increasing ion concentration, and thus decreasing the ion viscosity. Small rests of styrene in the binder reduce its viscosity as styrene has a significant lower viscosity than HEMA decreasing the ion viscosity further. These two effects explain the lower level of the ion viscosity of VXP1-old during the initiation phase. Pure HEMA and VXP1-old binders cure rapidly within 2 min, while the VXP1-new binder requires almost 15 min (Table 3.3).

However, binder systems containing small amount of styrene obviously behave differently to that containing a large amount. Styrene and PMMA have similar solubility parameters [P-IV]. Therefore, mainly styrene is responsible for swelling of the PMMA particles, and the release of initiator molecules. As styrene acts as a softener in PMMA, the glass transition temperature is decreased especially in areas of high styrene concentrations. In the areas where the glass transition temperature approaches ambient temperature, the release of initiator molecules becomes efficient and the curing starts. However, the degree of swelling, and thus the release of initiator molecules depend on the partial concentration of styrene in the binder. If the styrene concentration is low only small amounts of initiator molecules can be released and activated. The result is a rather low rate of curing which may lead to the limited increase of the ion viscosity at 1,000 and 10,000 Hz during the initiation phase. During this phase the HEMA-styrene copolymers have grown to a length that immobilizes their radical ends and primary curing starts in a Trommsdorf-like manner.

The ion viscosity curves of styrene binder show only a small drop with binder addition and no curing reaction. According to Eq. (19) the ion viscosity depends reciprocally on the ion mobility and the concentration of ions. As styrene has a significantly lower viscosity, and thus higher mobility than HEMA, it must be a liquid containing almost no ions. With respect to the behavior of the aged VXP1 binder this means that the lower ion viscosity results from a reduction of the viscosity because of the remaining styrene and as well as an increase of the ion concentration because of the styrene evaporation. HEMA is essential to start the curing process of these binders.

The differences in the curing behavior of both VXP1 and HEMA binders provide a clear picture of the steps occurring within the curing process of this 3DP RP system consisting of initiator containing PMMA powder and activator containing binder. In the moment of addition the binder wets the PMMA particles. Then mainly styrene starts to swell the PMMA particles from the surface and mobilizes the initiator molecules which can now react with the activator molecules of the binder to radicals. This effect is pronounced for high styrene concentrations in the binder as it

leads to a significant decrease of the glass transition temperature of the PMMA due to softening.

At the beginning only few radicals are generated and the curing rate is low. With ongoing radical generation the curing rate slowly increases until the HEMA-styrene chains are immobilized. At this moment the primary curing starts in a Trommsdorf-like manner. The curing rate increases further, and the chains grow until mixture of copolymer and binder reaches its glass transition temperature. Now the curing rate decreases significantly, and the system transfers into the post-curing phase.

Implementation of DEA-curing monitoring for 3DP RP production process

The measurement of ion viscosity allows also for the tracing of the curing process under processing conditions (Fig. 3.14). The drops of ion viscosity are seen after each binder addition taking place typically after every 1.5 min. They are less pronounced as the amount of binder is less than half that of the lab tests. However, the depth sensitivity is limited to the electrode distances meaning that the IDEX sensor sees 1 or 2 processing steps while the TMS sensor sees 5 to 6 processing steps. Thus, the process control of a whole RP part is not possible, but the DEA can be used to compare the measured ion viscosities of the process with a reference curve to document changes.

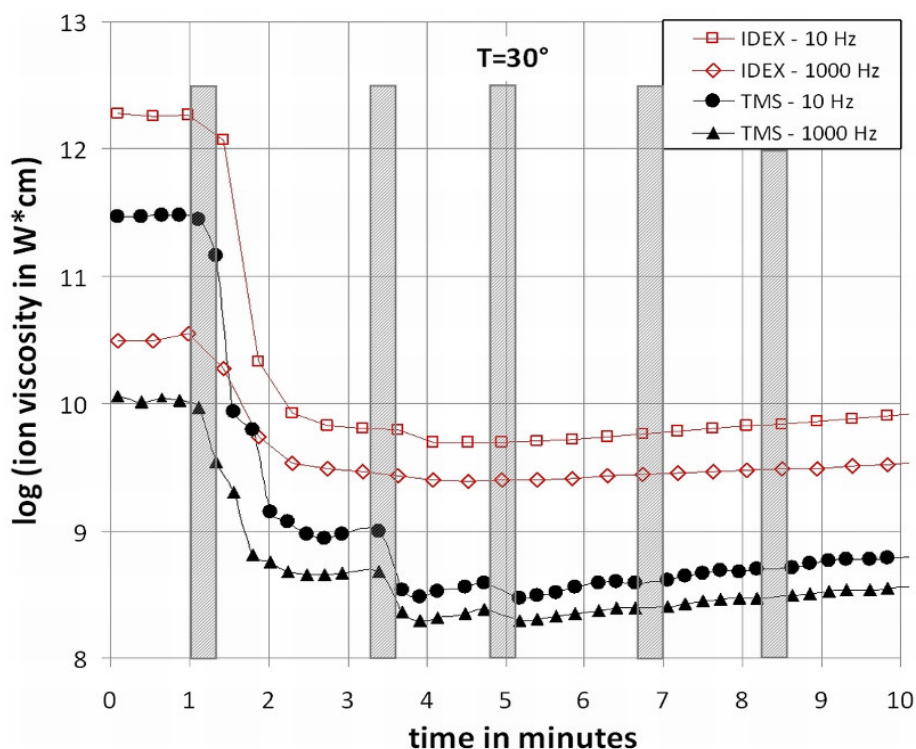


Fig. 3.14: Ion viscosity measured in the RP printing process at frequencies of 10 and 1000 Hz (grey bars indicate the times when a new powder layer is printed with binder) [P-IV].

3.2 Evaluation of DEA curing curves of VLC dental composites using reaction kinetics

3.2.1 Reaction kinetics based modeling of the VLC process of dental resins [P-II]

The viscosity of polymers depends linearly on molecular mass as long as the chain lengths are too short to form entanglements. As the ion viscosity η_{ion} expresses the motion of a charged probe in a viscous surrounding on the molecular level, it has to be proportional to the rheological viscosity η^{rheo} after the initiation phase and to the molecular mass M of the growing chains [77] as long as the material is below M_{crit} :

$$\eta^{ion}(t) \sim \eta^{rheo}(t) \sim M^n(t) \quad (24)$$

with:

η^{ion} ion viscosity

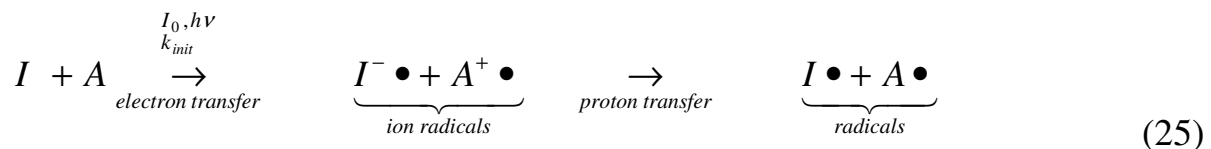
η^{rheo} viscosity of melt or monomer liquid

M molecular mass

n exponent, $n=1$ if $M < M_{crit}$ and $n=3.4$ if $M > M_{crit}$

M_{crit} is the molecular weight which has to be exceeded to account for entanglements.

Due to the irradiation the initiator molecules are partly brought to an excited long living triplet state which starts the initiation reaction by radicalizing the non-light sensitive co-agent molecule:



All possible initiation reactions are described in detail by [24]. For our purpose it is sufficient to assume an instantaneous generation of radicals for the first approximation which only depends on the depth according to absorption and scatter of light. Then the relevant initiation time is very short and can be considered as a reaction delay. Thus, the curing reaction is started either by an amine ion radical $A^+ \bullet$ or an amine radical $A \bullet$, which reacts with neighboring dimethacrylate monomers (DMA) leading to the start reaction:



and the subsequent growth reaction:



with:

k_{start} reaction constant of amine radicals

k_{ucg} reaction constant of undisturbed chain growth (UCG)

As the concentration of activated initiator molecules $c_0^{initiator}$ is small compared to the DMA monomers concentration and time independent due to the high light intensity, the curing reaction is almost completely determined by the reaction constant k_{ucg} . Under this condition the reaction rate is given by a linear differential equation in terms of c^{DMA} :

$$\frac{dc^{DMA}(t)}{dt} = -k_{ucg} * c_0^{initiator}(x) * c^{DMA}(t) \quad (28)$$

with:

c^{DMA} concentration of DMA monomers

$c_0^{initiator}$ concentration of activated initiator molecules.

Solving Eq. (28) yields the time dependent DMA monomer concentration:

$$c^{DMA}(t) = c_0^{DMA} * e^{-k_{ucg} * c_0^{initiator}(x) * t} \quad (29)$$

The time dependent degree of conversion $\alpha(t)$ is:

$$\alpha(t) = \frac{c_0^{DMA} - c^{DMA}(t)}{c_0^{DMA}} = 1 - \frac{c^{DMA}(t)}{c_0^{DMA}} = 1 - e^{-k_{ucg} * c_0^{initiator}(x) * t} \quad (30)$$

With increasing degree of conversion (DC) the molecular mass of the polymer chains grows. On the base of relation (24) together with equation (30) and the corresponding boundary conditions [P-II] one gets:

$$\eta^{ion}(t) = \eta_{\infty}^{ion} - (\eta_{\infty}^{ion} - \eta_{0,init}^{ion}) * e^{-\frac{t-t_{init}}{\tau_{reac}}} \quad (31)$$

with:

η_{∞}^{ion} final ion viscosity
 $\eta_{0,init}^{ion}$ initial ion viscosity
 t_{init} initiation time
 τ_{reac} reaction time constant

which can be expanded for short irradiation times yielding:

$$\eta^{ion}(t - t_{init}) = \eta_{0,init}^{ion} + \underbrace{\Delta\eta_{max}^{ion} * k_{ucg} * C_0^{initiator}(x)}_{\text{slope } B} * (t - t_{init}) \quad (32)$$

This means k_{ucg} and t_{init} can be determined by slope B and the intercept. In the experiment a linear increase of ion viscosity with time is expected after an initiation phase until the glass transition temperature exceeds the temperature of the sample. Then the increase of the ion viscosity should slow down as the mobility of the molecules freezes in and the molecular motion becomes diffusion controlled.

3.2.2 Kinetics Evaluation of DEA measurement curves [P-II]

In order to demonstrate the capability of the DEA to monitor fast curing processes, six light curing dental composites were investigated (Table 3.4).

Table 3.4: Investigated light curing dental composites; composition according to data sheets and safety data sheets

Product name	Producer	Filler content [wt-%]	Monomers	Initiator system
Filtek Supreme XT	3M ESPE	65	Bis-GMA, TEGDMA, Bis-EMA	CQ/DABE
CeramX	Dentsply	76	MMA, modified poly-siloxane, DDDMA resin	CQ/DABE
Dyract Xtra	Dentsply	77	UDMA, TCB resin, TEGDMA	CQ/DABE
SDR	Dentsply	68	UDMA, TEGDMA, Bis-Methacrylate	CQ/DABE
Arabesk	VOCO	77	Bis-GMA, UDMA, TEGDMA	CQ/DABE
Grandio	VOCO	87	Bis-GMA, TEGDMA	CQ/DABE

The direct evaluation of the ion viscosity curves shows that the materials differ significantly with respect to initial ion viscosity η_0^{ion} , final ion viscosity η_{∞}^{ion} and reaction time constant τ_{reac} , while the time to minimum ion viscosity t_{min} is for all materials close to 1 second (Table 3.5). Especially, the final ion viscosities may exhibit large scatter, e.g. for Dyract Xtra it is almost the same as the mean value. Of course, this also affects the corresponding reaction time constant determined from the final ion viscosity according to Eq. (32).

Although all materials are composed in a similar way, the time dependency of the polymerization and curing process differ with respect to initiation time and initial reaction rate (slopes of the corresponding curves) after the initiation phase (Fig. 3.15). Filtek Supreme XT (flowable) exhibits an ion viscosity being significantly lower even in the long time range, whereas Ceram X reaches the state of reduced ion mobility already after 5 seconds.

Immediately after switching on of the light curing unit (LCU) the irradiation excites camphorquinone molecules (CQ) to a triplet state from which they can react with co-initiator molecules – so-called accelerators – generating two ion radicals. The duration of the initiation phase depends on the composition of materials as the resin viscosity defines the mobility of the CQ molecules and the time to generate a reasonable number of ion radicals. The pronunciation of the decrease of ion viscosity is mainly affected by the filler content as it reduces the global ion concentration. Furthermore, these initiator ion radicals start the polymerization process. In the case of CQ, the co-agent radicals (mostly amines) are the rate determining species [10, 24]. This means that there are always two superposing processes – ion radical generation and chain growth – during the initiation phase.

Table 3.5: Direct evaluation of the ion viscosity curves

Material	η_0^{ion}	η_{∞}^{ion}	t_{min}	τ_{reac}
	[10 ⁶ *Ω*cm]	[10 ⁶ *Ω*cm]	[s]	[s]
Filtek Supreme XT	4.06 ± 0.42	1150 ± 150	0.75 ± 0.07	38.4 ± 2.1
Ceram X	910 ± 87	10730 ± 310	0.93 ± 0.15	16.9 ± 6.3
Dyract Xtra	56.4 ± 4.5	11770 ± 9800	0.63 ± 0,06	64.9 ± 45.1
SDR	512 ± 44	7720 ± 2940	0.78 ± 0.16	71.9 ± 44.8
Arabesk Top	171 ± 4	11570 ± 1840	1.05 ± 0.21	53.2 ± 2.8
Grandio	89 ± 6	10450 ± 1920	0.67 ± 0.06	88.4 ± 4.2

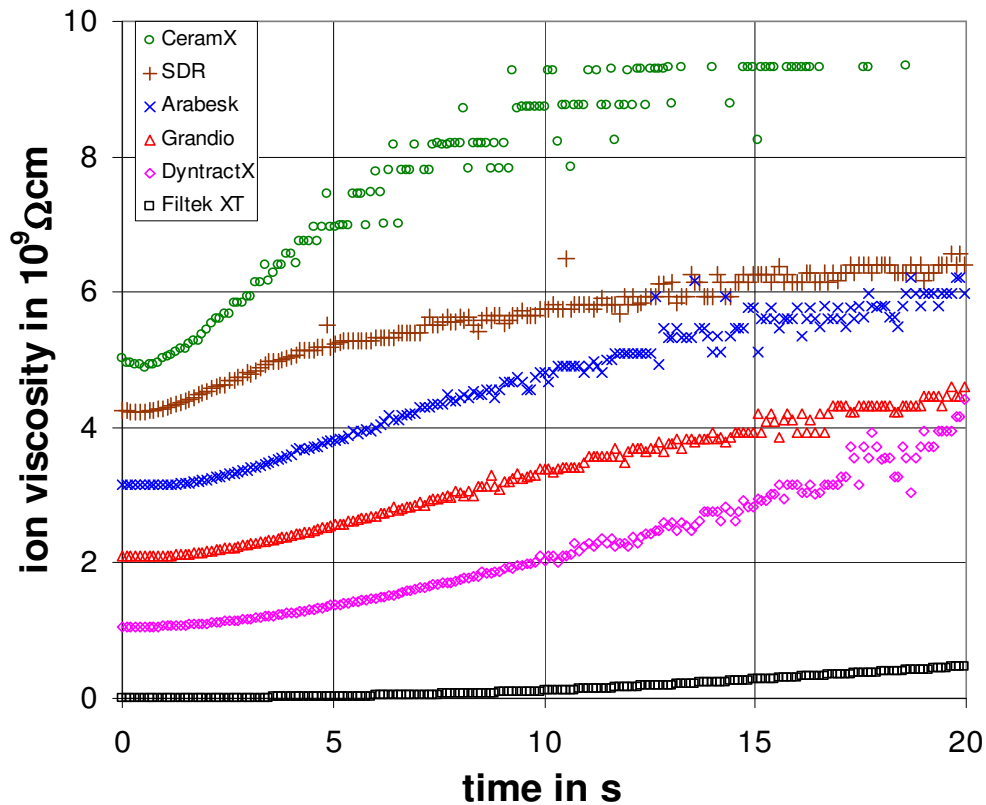


Fig. 3.15: Comparison of ion viscosity curves of all materials – for clarity reasons curves #3 to #6 are shifted in the vertical direction by $10^9 \Omega \cdot \text{cm}$ each, curve #1 is Filtek XT [P-II].

The linear increase of ion viscosity after starting the irradiation depends on the concentration of activated CQ molecules. This is affected by the light intensity, the concentration of CQ molecules in the resin and the filler content. This linear increase comes to an end if a certain ion viscosity is achieved indicating that the mobility of the DMA molecules is significantly reduced due to gel effects or passing the glass transition region indicating that the resin is transferred from the liquid state to the solid glassy state.

The subsequent degressive time dependency of the ion viscosity shows that the mobility in the material is significantly reduced due to diffusion controlled chain growth and cross-linking. If this reaction phase is reached, the molecules in the resin become more and more immobilized. The ion mobility goes to zero, while the ion viscosity reaches values close to the resolution limit of the measuring device being in the order of 10^{10} to $10^{11} \Omega \cdot \text{cm}$. The ion viscosity is the inverse of the ion mobility μ and is related to dielectric loss ϵ'' , dielectric susceptibility ϵ_0 and frequency f according to Eq. (19) [45]. This means that digitizing effects are seen in the measured curves if the ion mobility becomes very small - close to the resolution limit. This seems to be the case for ion viscosities exceeding $2 \cdot 10^9 \Omega \cdot \text{cm}$ (Fig. 3.16). The scatter of the ion viscosity in the long term range is much more pronounced for the highly filled materials than for pure resins. This may be due to the relaxation of internal stresses, filler matrix debonding, and local materials debonding from the

sensor. In spite of the scatter of the ion viscosity data one may assume the slow down of the curing process as shown by the dashed line.

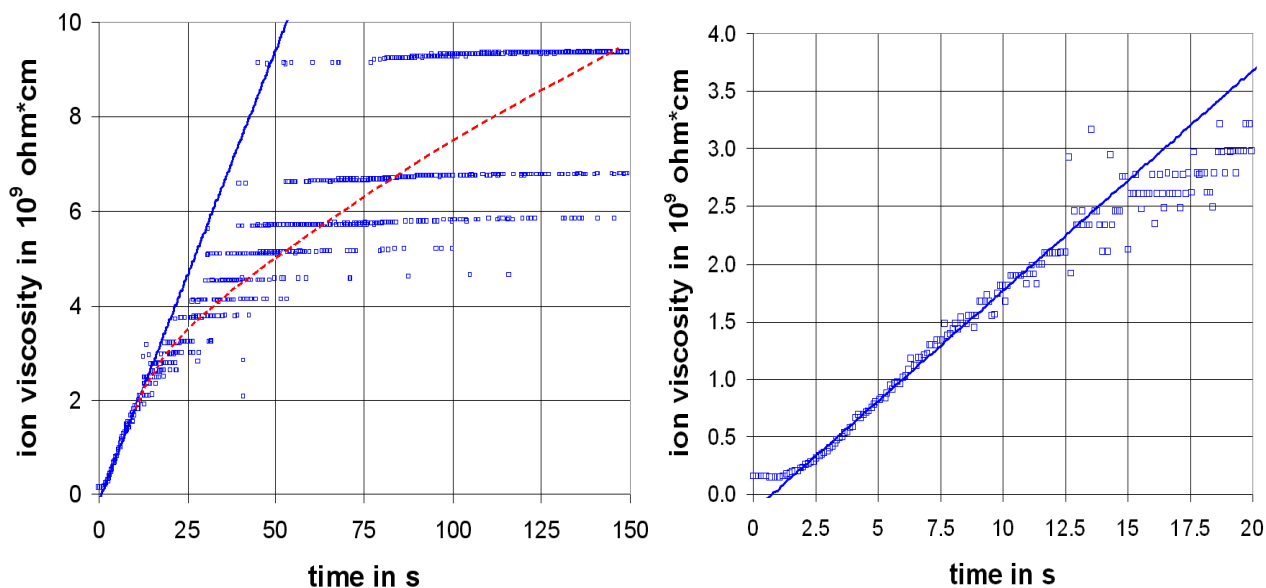


Fig. 3.16: Scatter of ion viscosity of Arabesk Top at large curing times (data points), straight line is the short time fit according to Eq. (32), dashed line shows the deviation from the linear behaviour beyond vitrification (left side); zoom to the time range of linear curing behaviour (right side) [P-II].

As the curing kinetics, in particular the kinetics of the undisturbed chain growth, is of interest, the data is evaluated with respect to the slopes in the linear time range B , the initiation time t_{init} and the reaction time constant τ_{reac} using Eq. (32) (Table 3.6 and Fig. 3.16).

Table 3.6: Evaluation of DEA curve according to Eq. (32)

Material	Fit range	Slope B	t_{init}	τ_{reac}
	[s]	[10 ⁶ Ω*cms ⁻¹]	[s]	[s]
Filtek Supreme XT	13 to 20	29.1 ± 9.3	7.35 ± 1.0	41.7 ± 12.4
Ceram X	1 to 5	559 ± 20	1.38 ± 0.13	17.6 ± 1.0
Dyract Xtra	5 to 15	138 ± 21	2.46 ± 0.66	83.6 ± 66.4
SDR	1 to 5	333 ± 192	0.91 ± 0.25	24.0 ± 8.1
Arabesk Top	2 to 10	204 ± 12	1.62 ± 0.5	56.1 ± 9.1
Grandio	3 to 13	143 ± 16	2.18 ± 0.42	73.7 ± 20.5

3.2.3 Extended model with time dependent initiator concentration (unpublished data, not included in Papers I-V)

During the light-curing reaction the ongoing chain growth increases the molecular mass and as a consequence the viscosity. Thus, the curing reaction slows down and the reaction time constant τ_{reac} being a time dependent measure increases rapidly. This can be described assuming an exponential time dependency of τ_{reac} .

$$\tau_{reac}(t) = \tau_{reac}^0 + T * e^{\frac{t}{t_{glass}}} \quad (33)$$

with

- τ_{reac}^0 reaction time constant in the liquid phase
- t_{glass} time to reach glass transition
- T pre-exponential coefficient

Introduction to Eq. (28) yields:

$$\frac{dc^{DMA}(t)}{dt} = - \frac{c^{DMA}(t)}{\left\{ \tau_{reac}^0 + T * e^{\frac{t}{t_{glass}}} \right\}} \quad (34)$$

This differential equation is of the type „seperated variables” and leads to the integral:

$$\int_{c(t=0)}^{c(t)} \frac{dc^{DMA}}{c^{DMA}} = - \int_0^t \frac{dt'}{\left\{ \tau_{reac}^0 + T * e^{\frac{t'}{t_{glass}}} \right\}} \quad (35)$$

Solving yields:

$$\frac{c^{DMA}(t)}{c_0^{DMA}} = e^{-\frac{t}{\tau_{reac}^0}} * \left(\frac{\tau_{reac}^0 + T * e^{\frac{t}{t_{glass}}}}{\left(\tau_{reac}^0 + T \right)} \right)^{\frac{t_{glass}}{\tau_{reac}^0}} \quad (36)$$

For the time dependent degree of conversion $DC(t)$ we get:

$$DC(t) = 1 - \frac{c^{DMA}(t)}{c_0^{DMA}} = 1 - e^{-\frac{t}{\tau_{react}^0}} * \underbrace{\left(\frac{\tau_{react}^0 + T * e^{\frac{t}{t_{glass}}}}{(\tau_{react}^0 + T)} \right)^{\frac{t_{glass}}{\tau_{react}^0}}}_{\text{correction term}} \quad (37)$$

The correction term takes into account the changing reaction time constant during the curing process. The DC is decreased by the correction term to an asymptotic value smaller than 1; Fig. 3.17 shows the effect of the correction term on DC curing curve of the dental composite Arabesk Top with 40 s light-curing time measured by FT-IR (with golden gate ATR). The fit yielded the parameter values given in Table 3.7. To achieve a reasonable fitting result with the solver, the measured DC curve was fitted first with the two parameters t_0 and τ_{react}^0 in the linear region (5-9 s) without the correction term. Then these parameters were held fixed and the other two fitting parameters T and t_{glass} are determined solving Eq. (37) including the correction term.

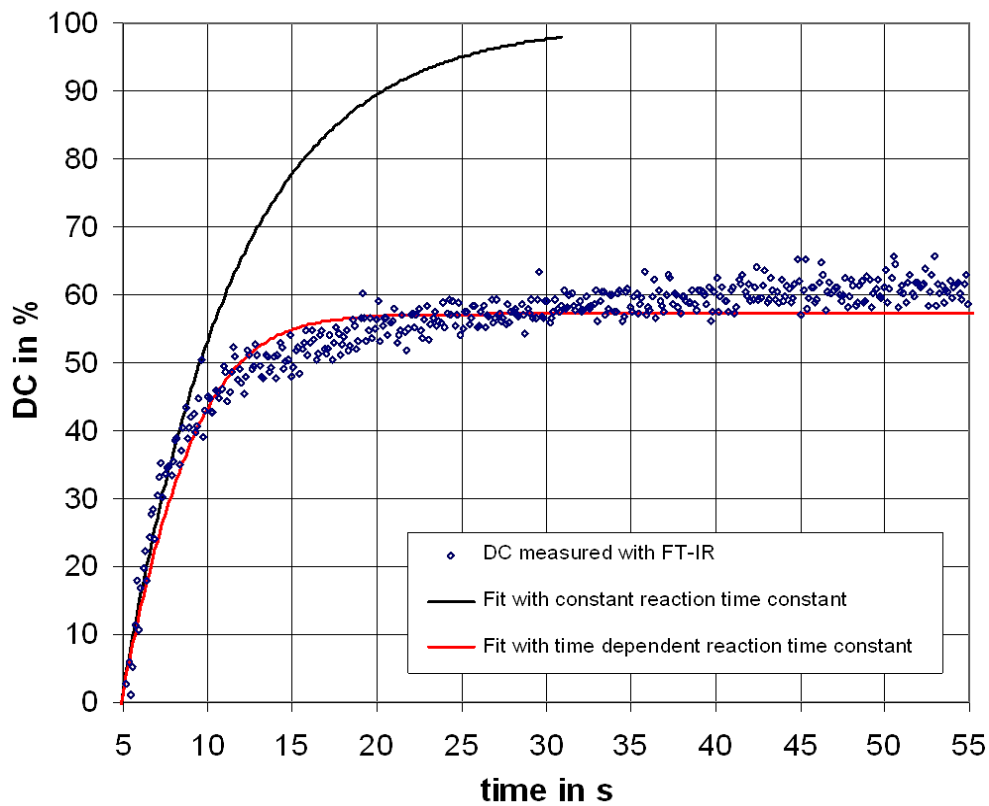


Fig. 3.17: DC curve of Arabesk Top irradiated for 40 s and measured with FT-IR, irradiation is started 5 s after the measurement. Fits with constant (upper line) and exponentially increasing (lower line) reaction time constant).

Table 3.7: Parameters determined acc. to Eq. (37) with the corresponding time fit intervals

Fitting parameter acc. to Eq. (37)	Unit	Time fit interval 5-9 s without correction term	Time fit interval 5-45 s
Starting time of light curing t_0	s	4.9	4.9
Reaction time constant τ_{reac}^0	s	6.7	6.7
Pre-exponential coefficient T	s	-	0.76
Time to reach glass transition t_{glass}	s	-	2.48

Transferring this new $DC(t)$ behaviour to ion viscosity measurements yields:

$$\eta^{\text{ion}}(t) = \eta_{\infty}^{\text{ion}} * \left(1 - \frac{\eta_{\infty}^{\text{ion}} - \eta_{0,\text{init}}^{\text{ion}}}{\eta_{\infty}^{\text{ion}}} * e^{-\frac{t-t_{\text{init}}}{\tau_{\text{reac}}^0}} * \left(\frac{\tau_{\text{reac}}^0 + T * e^{\frac{t-t_{\text{init}}}{t_{\text{glass}}}}}{\tau_{\text{reac}}^0 + T} \right)^{\frac{t_{\text{glass}}}{\tau_{\text{reac}}^0}} \right) \quad (38)$$

Fig. 3.18 shows fits of ion viscosity curves of the pure resin and the composite of Arabesk Top acc. to Eq. (38). Similarly to DC , the ion viscosity was fitted with the parameters given in Table 3.8.; first in the linear region (5-9 s) without the correction term to determine the two parameters t_{init} and τ_{reac}^0 , then keeping these parameters constant the other two fitting parameters T and t_{glass} were obtained. Two effects can be seen in Fig. 3.18. Firstly the ion viscosity curve of the composite seems to be horizontally shifted towards higher values in comparison to the pure resin curve. This can be explained by Eq. (19). The composite only contains about 40 vol.-% pure resin and thus, due to the fact that the glass filler do not contain any mobile ions, ca. 60% lower ion concentration. Secondly the curve characteristics are different with respect to the ion viscosity change $\Delta\eta^{\text{ion}} = (\eta_{\infty}^{\text{ion}} - \eta_{0,\text{init}}^{\text{ion}})$ as well as its kinetics parameters (t_{init} , τ_{reac}^0 , t_{glass}). One possible explanation is the different ratio of available light intensity and the number of CQ initiator molecules for pure and filled resins. Furthermore, the filler absorbs and scatters light, and thus reduces the radical concentration.

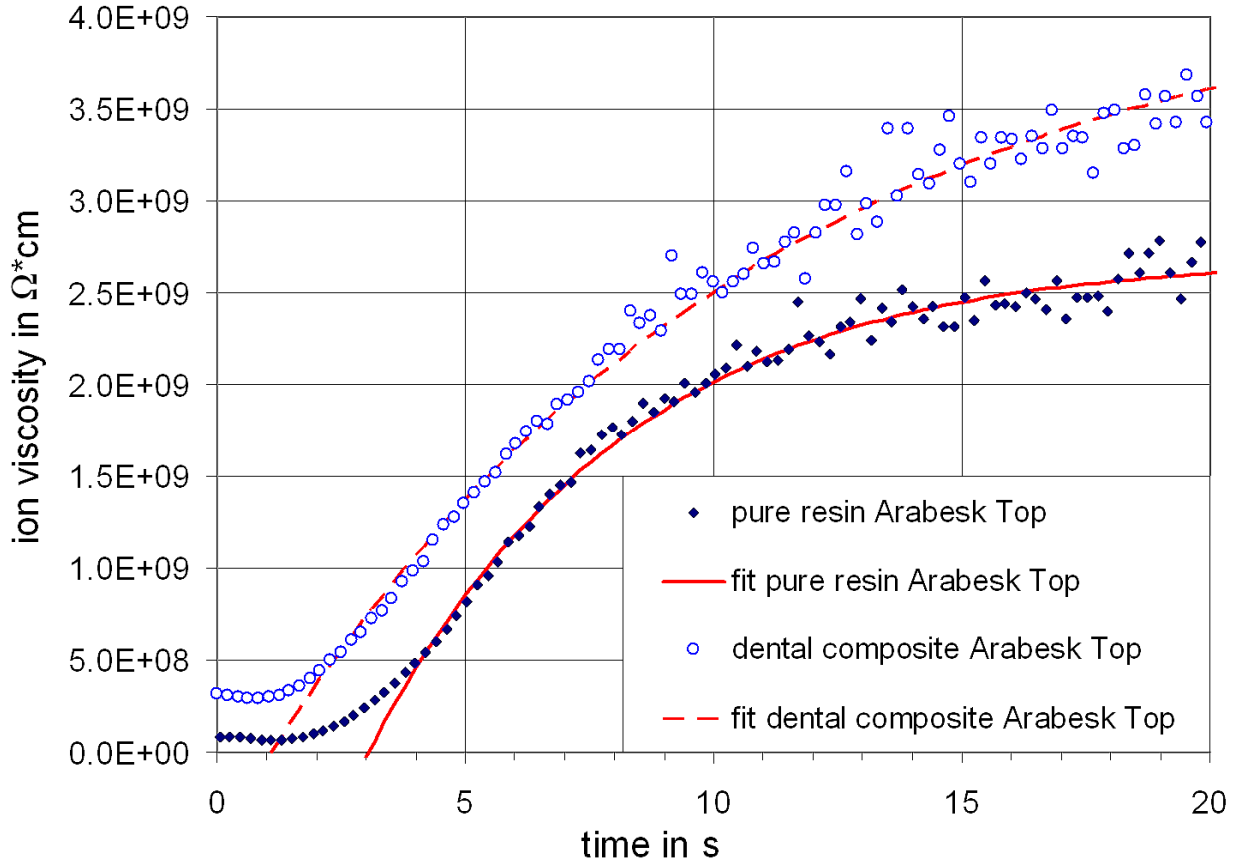


Fig. 3.18: DEA curing curves of Arabesk Top dental composite and pure resin fitted acc. to Eq. (38).

Table 3.8: Determined parameter values of Arabesk Top dental composite and pure resin acc. to Eq. (38).

	Unit	Pure resin	Commercial composite
Filler content	wt-%	0	75
Time fit interval	s	4 to 20	3 to 20
Initial ion viscosity $\eta_{0,init}^{ion}$	$10^7 \Omega^*cm$	8.4	31.5
True final ion viscosity $\eta_{\infty}^{ion,true}$	$10^9 \Omega^*cm$	3.8	5.0
Reaction time constant τ_{reac}^0	s	5.7	8.8
Time to reach glass transition t_{glass}	s	4.7	6.9
Pre-exponential coefficient T	s	1.7	1.7
Initiation time t_{init}	s	3.2	2.3

3.3 DEA kinetics evaluation of 3DP RP-resins

(unpublished data, not included in Papers I-V)

3.3.1 Reaction kinetics based Modeling of the 3DP RP-resin curing

The curing reaction of the investigated VXP1 3DP-RP-resin is a copolymerization of HEMA and styrene. Thus, the approach for the kinetic equation was chosen to be:

$$\frac{dc_M(t)}{dt} = -k_{ucg} * c_0^{radical}(t; x) * c_M^n(t) \quad (39)$$

with the time dependent monomer concentration $c_M(t)$, the reaction kinetics constant k_{ucg} of undisturbed chain grows (ucg), the time dependent initial radical concentration $c_0^{radical}(t;x)$ and monomer concentration $c_M^n(t)$. When an equilibrium between radical generation and termination is reached, $c_0^{radical}(t;x)$ becomes time independent and the variables can be seperated.

$$\frac{dc_M(t)}{c_M^n(t)} = -k_{ucg} * c_0^{radical}(x) * dt \quad (40)$$

Integration over equivalent limits yields:

$$\int_{c_{0,M}}^{c(t)} \frac{dc'_M}{c_M'^n} = \frac{1}{1-n} c_M'^{-n+1} \Big|_{c_{0,M}}^{c(t)} = -k_{ucg} * c_0^{radical}(x) * \int_0^t dt'$$

$$c_M^{-n+1}(t) - c_{0,M}^{-n+1} = -(1-n) * k_{ucg} * c_0^{radical}(x) * t \quad (41)$$

Solving for $c(t)$ yields:

$$c_M(t) = \left(c_{0,M}^{-n+1} - (1-n) * \frac{t}{\tau_{reac}} \right)^{\frac{1}{1-n}} \quad (42)$$

and the time dependent degree of cure $DC(t)$ is given by:

$$DC(t) = 1 - \frac{c_M(t)}{c_{0,M}} = 1 - \frac{1}{c_{0,M}} * \left(c_{0,M}^{-n+1} - (1-n) * \frac{t}{\tau_{reac}} \right)^{\frac{1}{1-n}} \quad (43)$$

$$DC(t) = 1 - \frac{1}{c_{0,M}} * \left(c_{0,M}^{1-n} * \left(1 - \frac{(1-n)}{c_{0,M}^{1-n}} * \frac{t}{\tau_{reac}} \right) \right)^{\frac{1}{1-n}} = 1 - \left(1 - \frac{(1-n)}{c_{0,M}^{1-n}} * \frac{t}{\tau_{reac}} \right)^{\frac{1}{1-n}} \quad (44)$$

Finally mathematical conversion yields:

$$DC(t) = 1 - \sqrt[1-n]{1 - \frac{(1-n)}{c_{0,M}^{1-n}} * \frac{t}{\tau_{reac}}} \quad (45)$$

Rewritten as a fit function one gets:

$$DC(t) = 1 - \sqrt[B]{1 - \frac{B*b}{C^B} * t} \quad (46)$$

with $b = \frac{1}{\tau_{reac}}$, $B = 1 - n$ and $C = c_{0,M}$

Assuming that the ion viscosity behaves analogously and that the reaction starts only after the initiation time yields:

$$\eta^{ion}(t) = \eta_0^{ion} + (\eta_{\infty}^{ion} - \eta_0^{ion}) * \left(1 - \sqrt[B]{1 - \frac{B*b}{C^B} * (t - t_{init})} \right) \quad (47)$$

With the short time approximation:

$$1 - \sqrt[B]{1 - \frac{B*b}{C^B} * t} = 1 - \left(1 - \frac{1}{B} * \frac{B*b}{C^B} * t \right) = \frac{b}{C^B} * t \quad (48)$$

and the condition $B > 0$ one ends up with:

$$\begin{aligned} \eta^{ion}(t) &= \eta_0^{ion} + (\eta_{\infty}^{ion} - \eta_0^{ion}) * \frac{b}{C^B} * (t - t_{init}) \\ &= \eta_0^{ion} + (\eta_{\infty}^{ion} - \eta_0^{ion}) * S * (t - t_{init}) \end{aligned} \quad (49)$$

The ratio b/C^B represents the slope S of the normalized ion viscosity curve at $t = t_{init}$. Thus, one can rewrite equation (47) as:

$$\eta_{rel}^{ion}(t) = \frac{\eta^{ion}(t) - \eta_0^{ion}}{\eta_{\infty}^{ion} - \eta_0^{ion}} = 1 - \left(1 - B * S * t\right)^{\frac{1}{B}} \quad (50)$$

The slope S is used as the start value for the first step of the fit procedure to determine the start value of B . In the second step both values are fitted. Fig. 3.19 shows the measured relative ion viscosity curve of a 3DP-RP-material (symbols) with the fit to determine the slope S (dotted line) and the fitted relative ion viscosity (full line). The parameters are:

$$B = (1-n) = -0.2376 \quad \Leftrightarrow \quad n = 1.2376$$

maximum slope $S = 0.0957/\text{min}$

initiation time $t_{init} = 35.9 \text{ min}$.

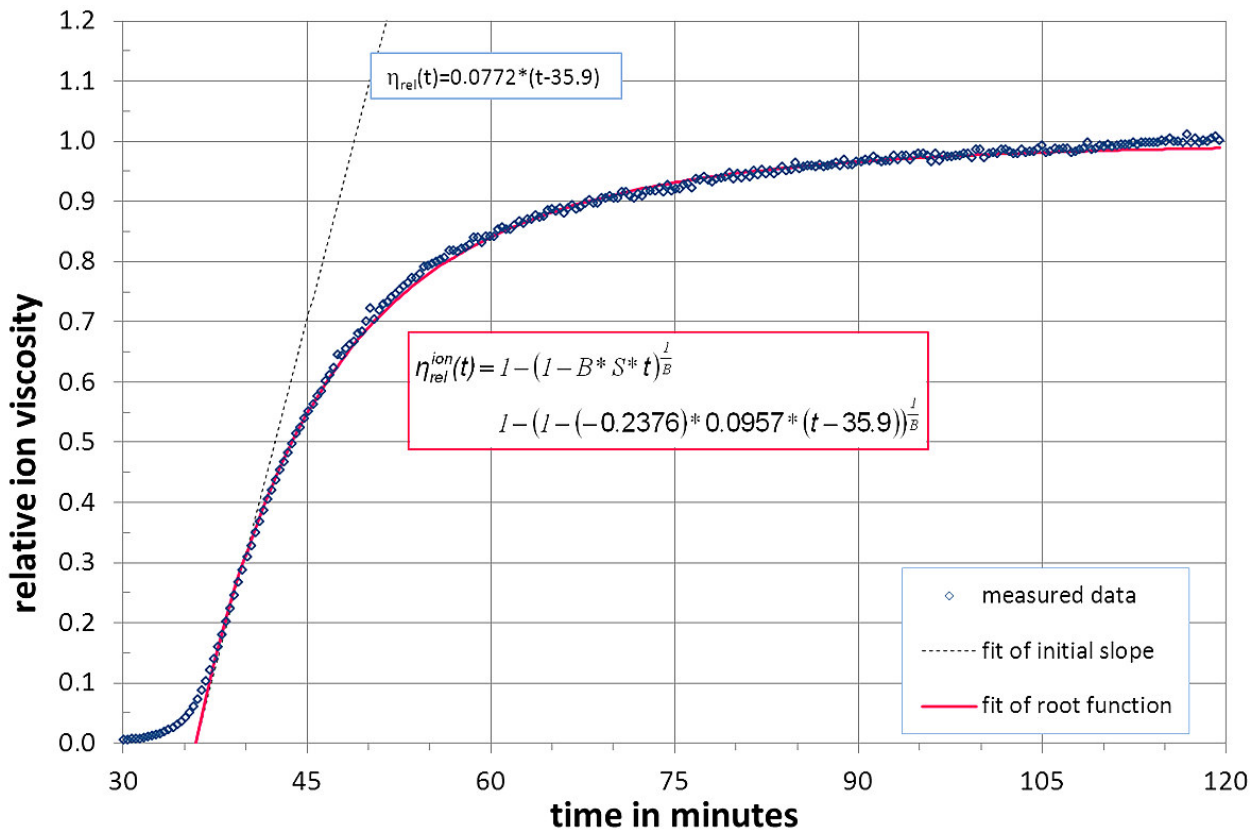


Fig. 3.19: Measured relative ion viscosity curve of the 3DP-RP-material (PMMA-powder with VXP1-binder) (symbols) with the fitted slope (dotted line) and the fitted relative ion viscosity (full line)

3.4 Correlation of ion viscosity (DEA) with shear viscosity (Rheometer) [P-V]

3.4.1 Investigations of pure dental resins

The resins behave in a Newtonian manner within the investigated shear rate range, thus the zero-shear viscosity η_0 (referred as shear viscosity in the following) has been evaluated and compared with initial ion viscosities. Shear viscosity η_0 of Bis-GMA resin is almost 5 orders of magnitude higher than that obtained for TEGDMA (Fig. 3.20). The effect of resin composition (ratio of Bis-GMA/TEGDMA) can be well described with the relation:

$$\lg \eta_0(w_{TEGDMA}) = A * e^{-B * w_{TEGDMA}} \quad (51)$$

with parameter A corresponding to the logarithm of the shear viscosity of pure Bis-GMA decreasing from about 600 to 500 Pa*s if the temperature is increased from 23 °C to 36 °C, and parameter B of 1.8 being characteristic for the chosen resin mixture.

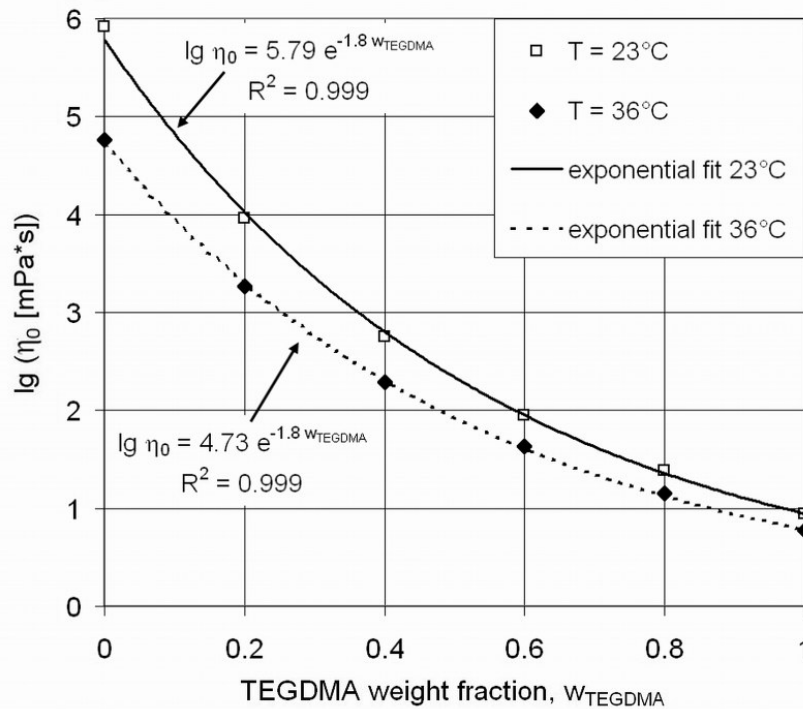


Fig. 3.20: Shear viscosity at room and body temperature with respect to mixing ratio of the pure resins Bis-GMA/TEGDMA [P-V].

Except of pure TEGDMA, ion viscosities depend on the resin composition qualitatively in a similar manner. The commercial resin Arabesk Top shows viscosity values close to 80/20 Bis-GMA/TEGDMA model resin, while Grandio can be related the best to 60/40 Bis-GMA/TEGDMA model resin. In such a

consideration it has to be taken into account that Arabesk Top contains UDMA as a third resin component, having shear viscosity of about 10 Pa*s at 23 °C. The ion viscosity of the pure UDMA (2032.5 MΩ*cm) resin is much higher than those of Bis-GMA (549.5 MΩ*cm) and TEGDMA (74.1 MΩ*cm). Although the ion viscosities of all model and commercial resins show a consistent trend with respect to the corresponding viscosities of the mixtures they are below the ion viscosity values of both 100 % Bis-GMA and 100 % TEGDMA, (Fig. 3.21).

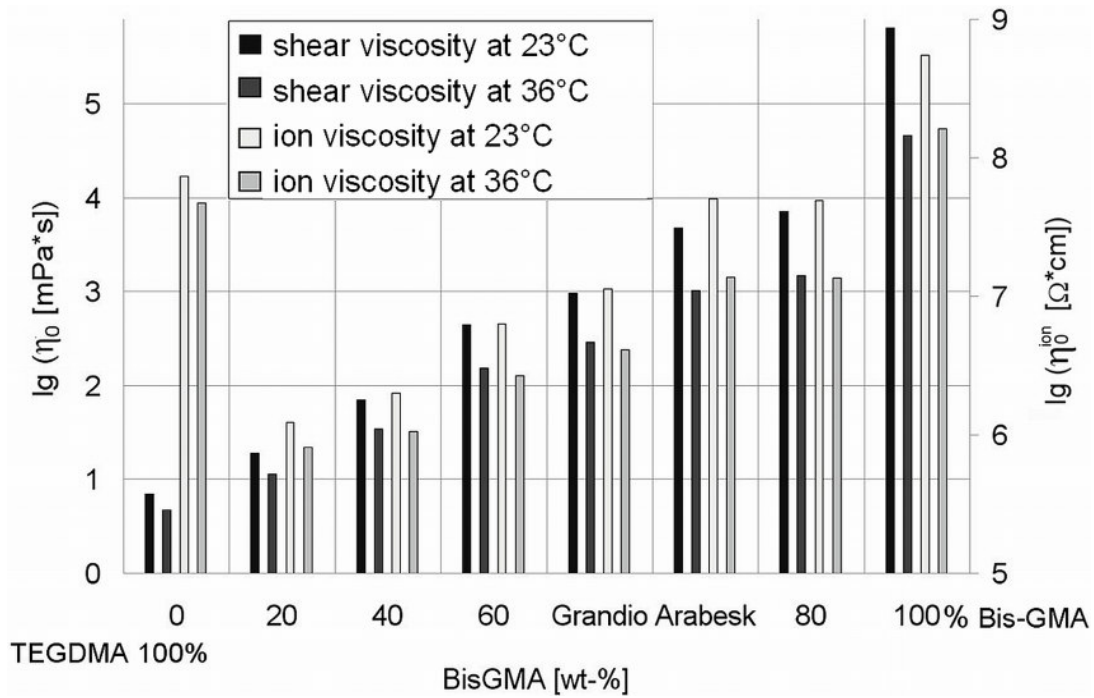


Fig. 3.21: Comparison of shear and ion viscosities at 23 and 36°C with respect to the composition of Bis-GMA/TEGDMA resins as well as the Grandio and Arabesk Top pure resins [P-V].

Predicting the ion viscosity of resin mixtures requires a model which takes into account the changes of both shear viscosity and ion concentration. The shear and ion viscosity of the uncured pure resin of Arabesk Top decrease exponentially in the temperature range from 20 to 50°C (Fig. 3.22). The shear viscosity drops from 7,295 to 304 mPa*s and the ion viscosity from 84.1 to 4.2 MΩ*cm. The shear and ion viscosity with respect to temperature T were evaluated according to Fig. 3.22 using the following equations:

$$\text{Ion viscosity: } \lg \eta_0^{\text{ion}}(T, v_F) = a^{\text{ion}} * T + b^{\text{ion}} \quad (52)$$

$$\text{Shear viscosity: } \lg \eta_0(T, v_F) = a^{\text{rheo}} * T + b^{\text{rheo}} \quad (53)$$

The parameters b^{ion} and b^{rheo} represent the ion viscosity and viscosity at 0°C and are due to their nature very different. The parameters a^{ion} and a^{rheo} describe the change of ion viscosity and viscosity with temperature being very similar for each composite. The mean values of $\langle a^{ion} \rangle$ and $\langle a^{rheo} \rangle$ were found to be -0.041/K and 0.046/K, respectively.

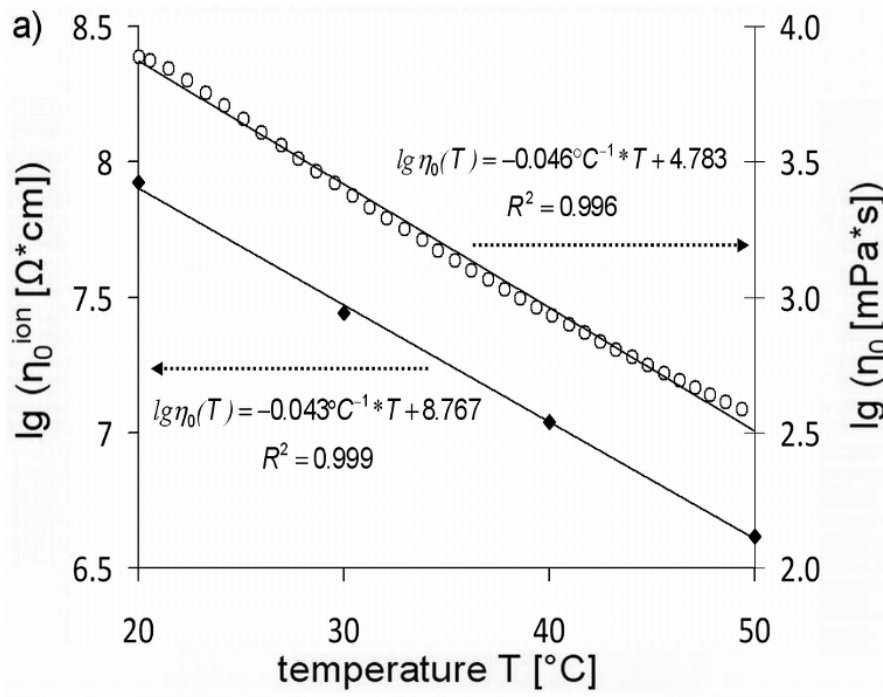


Fig. 3.22: Temperature dependent initial ion viscosity η_0^{ion} (open symbols) and shear viscosity η_0 (full symbols) of Arabesk Top pure resin in the uncured state [P-V].

3.4.2 Investigations of filled dental composites

Filler content increases the viscosity substantially. In some cases it may change more than a factor of 1,000 within the considered range of filler content [75, 76]. The ion viscosity also depends on the filler content but not in such a pronounced way. In paper V the following relation is introduced to calculate the dependency of the ion viscosity η_0^{ion} on the filler volume fraction v_F :

$$\lg(\eta_0^{ion}(v_F)) = \lg(\eta_{0,resin}^{ion}) + v_F + \frac{v_F^2}{2} + \frac{v_F^3}{3} \quad (54)$$

providing ion viscosities being in the same range as the measured values (Fig. 3.23). As expected the ion viscosities increase with filler content (Fig. 3.23 a and d). All initial ion viscosities of Arabesk Top and Grandio with respect to filler content for 20, 30, 40 and 50 °C are presented in Table 3.9. The Arabesk Top composite with 60

vol. % filler has an ion viscosity about 3 times higher than the pure resin, while in case of Grandio material (71 vol.-% filler) this factor is more than 7.

The calculated dependency of the ion viscosity on the filler content according to Eq. (54) provides values being in the same range as the measured values (Fig. 3.23 a and d). The idea of Eq. (54) is that according to the inverse mixing rule filler addition mainly reduces the ion concentration due to the dilution effect which in turn leads to an increase of the ion viscosity acc. to Eq. (19) [77]. But there are systematic deviations – too high ion viscosities for low filler contents and too low ion viscosities for high filler contents (Fig. 3.23 a and d) indicating that more processes affect the measured values of the ion viscosity. In order to further investigate the correlation of ion viscosity with shear viscosity the filler and temperature dependent data of Table 3.9 was evaluated using an exponential fit:

$$\eta_{0,r}^{ion} = \frac{\eta_0^{ion}(v_F)}{\eta_{0,resin}^{ion}} = 10^{\frac{v_F}{A}} \quad (55)$$

and a common viscosity model based on the frequently employed Maron-Pierce equation in the revised empirical form proposed by Kitano et al. [78]:

$$\eta_{0,r}^{ion} = \frac{\eta_0^{ion}(v_F)}{\eta_{0,resin}^{ion}} = \left(1 - \frac{v_F}{A}\right)^{-2} \quad (56)$$

Table 3.9: Filler content dependent initial ion viscosity of Arabesk Top and Grandio for different temperatures (n=5) [P-V].

Filler volume fraction v_F	Initial ion viscosity η_0^{ion} [M Ω *cm]							
	at 20°C	STD	at 30°C	STD	at 40°C	STD	at 50°C	STD
Arabesk Top								
0	84.1	1.4	27.7	0.9	11.0	0.2	4.1	0.3
0.15	136.1	1.6	45.6	0.4	19.8	1.0	9.0	0.1
0.3	269.8	12.4	84.9	4.9	41.0	1.1	14.6	0.6
0.6	313.3	10.8	97.9	8.1	42.8	0.8	17.3	1.7
Grandio								
0	17.2	0.9	7.0	0.2	3.2	0.1	1.7	0.1
0.15	27.8	1.5	10.5	0.7	4.5	0.1	2.8	0.2
0.3	52.6	0.5	17.4	2.1	7.9	0.1	4.2	0.4
0.6	68.2	0.6	26.7	0.7	13.2	0.4	6.4	0.5
0.71	112.5	3.1	51.2	1.9	23.0	1.8	10.6	0.6

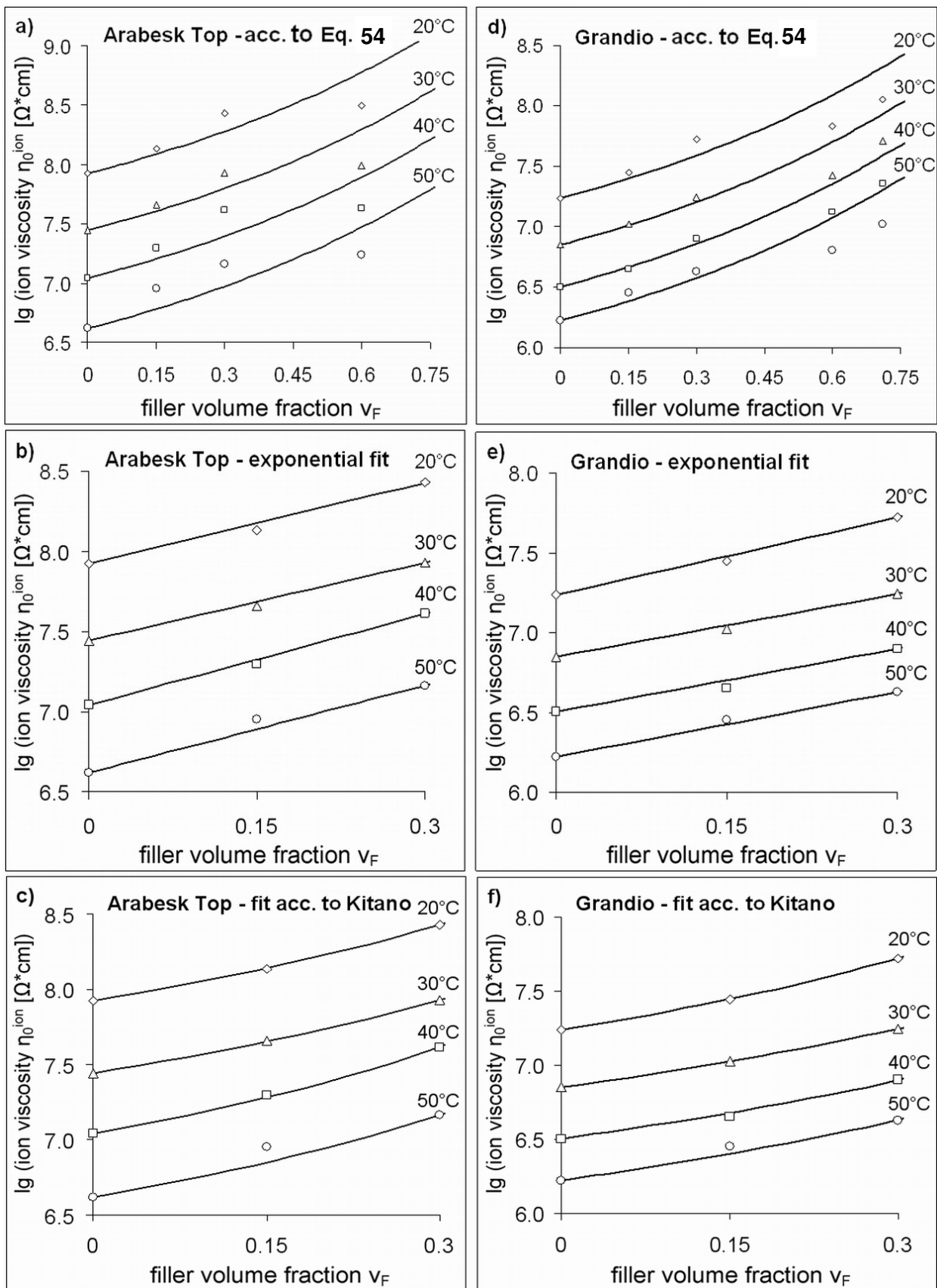


Fig. 3.23: Initial ion viscosity η_0^{ion} of Arabesk Top and Grandio in the uncured state with respect to filler content v_F at various temperatures. Straight lines represent fits of $\eta_0^{ion}(v_F)$ acc. to Eq.54 (a, d), exponential trendline acc. to Eq. 55 (b, e) and Kitano model acc. to Eq. 56 (c, f) [P-V].

For this purpose the relative shear viscosity η_r in the Kitano model is replaced by relative initial ion viscosity $\eta^{ion}_{0,r}$. In the original models fitting parameter A is typically related to the packing geometry of the filler [78]. Fig. 3.23 (b, c, e, f) shows the models application for a filler content up to 30 vol.-%. The fit acc. to the Kitano model shows the smallest relative sum of deviation [P-V], but still fails to predict the initial ion viscosity at higher filler contents > 30 vol.-% overestimating the measured values by far.

The ion viscosity changes substantially also with temperature. Linear fitting according to Eq. (52) yields resin characteristic slope values a^{ion} which are very similar for all filler contents (Table 3.10). This means that the temperature dependency of the ion viscosity is governed by the resin composition regardless of the filler content. This interpretation is supported by shear viscosity measurements of Arabesk Top and Grandio pure resins as well as Arabesk Top and Grandio composites having a filler content of 15 vol.-%. Linear fitting according to Eq. (53) yields also resin characteristic slope values a^{rheo} being only slightly higher than the slope values a^{ion} , but unaffected by the filler content (Table 3.10).

Table 3.10: Temperature dependency parameters of ion and shear viscosities (slopes and R²) of Arabesk Top and Grandio for different filler contents [P-V].

volume fraction v_F	ion viscosity (n=5)		shear viscosity (n=3)	
	a^{ion} [K-1]	R ²	a^{rheo} [K-1]	R ²
Arabesk Top				
0	-0.043	0.99	-0.046	0.99
0.15	-0.039	0.99	-0.046	0.99
0.30	-0.041	0.99		
0.60	-0.041	0.99		
Grandio				
0	-0.033	0.99	-0.039	0.99
0.15	-0.034	0.98	-0.039	0.99
0.30	-0.036	0.98		
0.60	-0.034	0.99		
0.71	-0.034	0.99		

4. CONCLUSIONS

In this thesis the curing reaction of light-curing medical dental filling materials as well as auto-curing 3D printing rapid prototyping materials was investigated with dielectric analysis (DEA). The time dependent ion viscosity was evaluated as a material property similar to the shear viscosity characterizing the curing evolution and serving as an input data for kinetic models. For this purpose the following project steps were carried out:

- 1) The curing reactions of both material classes were characterized with respect to basic curve shape, reproducibility, scattering, discrimination of different curing stages, material composition and in the case of light-curing dental materials also depth dependent light intensity.
- 2) Material models were developed and their accuracy was tested with fitted kinetic parameters extracted from the DEA-curves.
- 3) The correlation of ion and shear viscosity of pure resins and filled composites with various contents was investigated in order to identify limitations of the DEA curing characterization compared to rheometric methods.

It was found that generally the three curing stages - initiation, primary curing and post-curing - can be precisely distinguished with the DEA-method allowing for the investigation of the influence of the basic reaction process parameters as resin composition, viscosity, processing temperature and light absorption and scattering phenomena.

The developed material models integrating the kinetic parameters extracted from the DEA curves were capable of predicting the curing behavior. .

Generally the ion viscosity depends on the resin composition in a more complicated way than shear viscosity as it is affected by both ion concentration and mixture viscosity. But, the fact that a pure resin with a low ion concentration has a very high ion viscosity inspite of low shear viscosity shows that DEA can be used to control the purity of organic liquids also for quality control applications.

Fig. 4.1 visualizes how the papers I-V address the aims defined in the Thesis.

DEA curing characterization of thermoset resins

VLC dental composites

P-I Dielectric analysis of depth dependent curing behavior of dental resin composites

Sub-goals:

- How does the curing kinetics of VLC RBC change with depth?
- Does the light intensity decrease with depth according to Lambert-Beer in spite of multi-scattering processes?
- Does the curing kinetics correspond to the light absorption behavior?

P-III Time-Resolved Study of the Photo-Curing Process of Dental Resins with the NMR-MOUSE.

Sub-goals:

- Is the NMR a supplement method to measure the curing behavior of VLC RBC under the condition of low light intensity?
- How do temperature changes due to the reaction affect the curing process and the reaction kinetics?

3DP rapid prototyping materials

P-IV Characterizing the Auto-curing Behavior of Rapid Prototyping Materials for 3D-Printing via DEA.

Sub-goals:

- How has the measuring and evaluation method to be changed if 3DP RP materials are investigated?
- Is it possible to identify changes of the binder system due to composition and aging state?
- How do changes of the binder system affect the curing reaction?

DEA curing kinetics evaluation

P-II Curing kinetics of visible light curing dental resin composites investigated by dielectric analysis (DEA)

Sub-goals:

- How can the curing behavior of VLC RBC under the condition of high light intensity be described in terms of reaction kinetics?
- How can this reaction kinetics be transferred to ion viscosity measurements?
- Which differences concerning the curing behavior can be seen between different VLC RBC?

Correlation of ion viscosity (DEA) with shear viscosity (Rheometer)

P-V Correlation of shear viscosity and dielectric ion viscosity of dental resins – Effects of composition, temperature and filler content.

Sub-goals:

- How is the ion viscosity linked to the shear viscosity? Where are similarities? And where are differences?
- How do the ion viscosity and shear viscosity change with temperature?
- How do the ion viscosity and shear viscosity change with filler content?

Fig. 4.1: Correspondence of the papers I-V to sub-goals of the thesis: “Real-time Investigation of Curing Mechanisms of Thermoset Resins for Medical and Technical Applications”

5. CONTRIBUTION TO THE SCIENCE AND PRACTICE

As material properties of thermosets, and thus their beneficial use in later applications are set during the curing process, real-time investigation and characterization of the curing process is the key to successful thermoset product development. Each class of thermoset material has specific application requirements. As a consequence, in thermoset and composite science real-time curing monitoring is a key issue of interest.

This PhD study focused on investigating the curing mechanisms of thermoset resins for medical and technical applications in real-time with dielectric analysis (DEA). The curing behavior of these materials was precisely characterized with respect to various curing parameters. Furthermore, kinetics parameters were extracted from the DEA-curves allowing for the development and evaluation of material models predicting the curing process. Finally, the ion viscosity measured with the DEA method was compared and correlated with shear viscosity. The following topics can be considered as the most important contributions of this PhD study to both science and practice:

- 1) The ion viscosity is an appropriate quantity to measure the depth dependent curing behavior of dental composite resins. The time dependent increase of the ion viscosity is directly linked to the reaction rate. The depth dependent reaction rates determined by DEA measurements lead to the assumption that the structure formation of the resin changes with depth from a highly cross-linked thermoset in the surface near layer to a rather uncured material in the bottom layer [P-I].
- 2) For the investigated 3DP materials a concept was developed which describes the curing steps until the post-curing phase. The crucial role of styrene in the binder determining the curing kinetics in the printing process was demonstrated. Furthermore, it has been shown that the approach presented can be an important tool in the development and tailoring of powder-binder systems, especially as it is applicable under plant conditions [P-IV].
- 3) Kinetic models capable of predicting the curing behavior by fitting kinetic parameters extracted from the DEA curves were developed for the 3DP and VLC RBC materials. . For VLC RBCs a model assuming a constant light initiator concentration is presented and evaluated in paper P-II. The findings concerning more complex material models capable of describing the complete curing process (see chapter 3.2 and 3.3) are in preparation for publication.
- 4) Comparison of ion viscosity to shear viscosity shows a pronounced but almost identical temperature dependency. Both methods intercept the same physical phenomenon - motion of molecules; ion viscosity might be used for quality assurance purposes as a fast alternative to shear viscosity measurements.

ACKNOWLEDGEMENT

First of all I would like to thank my thesis advisor Bernhard Möglinger for his great support during my studies, his patience and his motivating words whenever the all too many tricky details obscured my view for the grater course of the project. His willingness to share his knowledge and experience were absolutely crucial in making my Ph.D. project become a reality. Thank you so much for showing me how to do research and getting a look for the big picture! Whenever I lost faith in my abilities, it was your competent advice coupled with your ever present humor that cheered me up and brought me back on track.

Next, I would like to thank my wonderful supervisor Berenika Hausnerová for her enthusiasm for my research topics, her unlimited and prompt support in all scientific and educational questions and last but not least for her helping getting all my examinations at TBU organized. Thank you for always being open both to discussion and to my worries, and for giving me so much precious advice!

Then I would like to say a big thank you to my parents, my family and friends for being there whenever I needed them, for listening to my worries, keeping their fingers crossed during my exams, understanding – sometimes even sharing – my excitement for material science, helping me to raise my children and for believing that I will finally successfully finish this thesis. I love you all!

Never will I forget all the nice, enthusiastic and funny scientific and non-scientific colleagues and research assistants at the Bonn-Rhein-Sieg University of Applied Science, far too many to mention, supporting me in my research projects and making this place of research, education and work a second home for me. Without you I probably wouldn't have made it. Thank you so much!

I also like to thank the friendly and supportive staff of Tomas Bata University in Zlin. LadaVojáčková, Renata Polepilová and Michaela Blahová always took my inquiries seriously and supported me in a most professional and kind manner. Mnohokrát děkujeme!

Then I would like to thank Matthias Frentzen of the Clinic for Periodontology, Operative and Preventive Dentistry at the University of Bonn and Martin Rosentritt of the Department of Prosthetic Dentistry of the University Medical Center in Regensburg for their kind support and for bringing the research issue of dental materials into my focus.

Furthermore, I would like to thank Andréé Barg and VOCO GmbH for providing the dental materials and light curing units, Florian Mögele and Voxeljet AG for providing the 3DP materials and Stephan Knappe from Netzsch Gerätebau GmbH for experimental support.

Last but not least the financial support due to the FHProfUnt project (grant no. 17081X10) of the Ministry of Education and Research of the Federal Republic of Germany is gratefully acknowledged.

REFERENCES

- [1] Mount G, Hume W. A revised classification of carious lesions by site and size. *Quintessence Int*, 1997; 28(5):301-303.
- [2] Ivoclar Vivadent AG: R&D Report Nr.18, *The Secrets of Composites*, 08-2007.
- [3] Rueggeberg FA. State-of-the-art: Dental photocuring – A review. *Dent Mater*, 2011; 27(1):39-52.
- [4] Moszner N, Salz U. Recent developments of new components for dental adhesives and composites. *Mocromol Mater Eng*, 2007; 292(3):245-271.
- [5] Watts DC. Dental restorative materials. In: Cahn RW, Haasen P, Kramer EJ, editors. *Materials science and technology: a comprehensive treatment. Dental and medical materials*, vol. 14. Weinheim, FRG: VCH Verlagsgesellschaft mbH, 1992; p. 224, ISBN 3527268278.
- [6] Goncalves F, Azevedo CLN, Ferracane JL, Braga RR. BisGMA/TEGDMA ratio and filler content effects on shrinkage stress. *Dent Mater*, 2011; 27(6):520-526.
- [7] Stansbury JW. Dimethacrylate network formation and polymer property evolution as determined by the selection of monomers and curing conditions. *Dent Mater*, 2012; 28(1):13-22.
- [8] Moszner N, Salz U. New developments of polymeric dental composites. *Prog Polym Sci*, 2001; 26(4):535-576.
- [9] Floyd CJE, Dickens SH. Network structure of Bis-GMA- and UDMA-based resin systems. *Dent Mater*, 2006; 22(12):1143-1149.
- [10] Stansbury JW. Curing Dental Resins and Composites by Photopolymerization. *J Esthet Dent*, 2000; 12(6):300-308.
- [11] Fouassier JP. *Photoinitiation, Photopolymerization and Photocuring – Fundamentals and Applications*. Carl Hanser Verlag, 1995; p. 36, ISBN 3446170693.
- [12] Ferracane JL, Aday P, Matsumoto H, Marker VA. Relationship between shade and depth of cure for light-activated dental composite resins. *Dent Mater*, 1986; 2(2):80-84.
- [13] Heintze SD, Forjanic M, Ohmiti K, Rousson V. Surface deterioration of dental materials after simulated toothbrushing in relation to brushing time and load. *Dent Mater*, 2010; 26(4):306-319.
- [14] Gebhardt A. *Rapid Prototyping*. 2nd Ed. Carl Hanser Verlag, 2000; p. 77, ISBN 3446212426.
- [15] Chua CK, Chou M, Wong TS. A Study of the State-of-the-Art Rapid Prototyping Technologies. *Int J Adv Manuf Technol*, 1998; 14(2):146-152.
- [16] Dimitrov D, Schreve K, de Beer N. Advances in three dimensional printing. *Rapid Prototyping J*, 2006; 12(3):136-147.
- [17] Azari A, Nikzad S. The evolution of rapid prototyping in dentistry: a review. *Rapid Prototyping J*, 2009; 15(3):216-225.
- [18] Ferracane JL. Resin composite – state of the art. *Dent Mater*, 2011; 27(1):29-38.
- [19] Aravamudhan K, Rakowski D, Fan PL. Variation of depth of cure and intensity with distance using LED curing lights. *Dent Mater*, 2006; 22(11):988-994.

- [20] Suwanprateeb J. Improvement in mechanical properties of three-dimensional printing parts made from natural polymers reinforced by acrylate resin for biomedical applications: a double infiltration approach. *Polym Int*, 2006; 55(1):57-62.
- [21] Patirupanusara P, Suwanpreuk W, Rubkumintara T, Suwanprateeb J. Effect of binder on the material properties of polymethyl methacrylate fabricated by three dimensional printing technique. *J Mater Process Tech*, 2008; 207(1-3):40-45.
- [22] Pham DT, Gault RS. A comparison of rapid prototyping technologies. *Int J Mach Tool Manufact*, 1998, 38(10-11):1257-1287.
- [23] Elias HG. *Makromoleküle – Chemische Struktur und Synthesen*. 6th Ed. Wiley-VCH, 1999; p. 355, ISBN 352729872X.
- [24] Cook WD. Photopolymerization kinetics of dimethacrylates using the camphorquinone/ amine initiator system. *Polymer*, 1992; 33(3):600-609.
- [25] Watts DC. Reaction kinetics and mechanics in photo-polymerized networks. *Dent Mater*, 2005; 21(1):27-35.
- [26] Jakubiak J, Wrzyszczyński A, Linden LA, Rabek JF. The Role of Amines in the Camphorquinone Photoinitiated Polymerization of Multifunctional Monomer. *J Macromol Sci Pure*, 2007; 44(2):239-242.
- [27] Vazquez B, San Roman J, Deb S, Bonfield W. Application of Long Chain Amine Activator in Conventional Acrylic Bone Cement. *J Biomed Mater Res-A*, 1998; 43(2):131-139.
- [28] Qui K, Shui L, Feng X. Studies on radical polymerization of methyl methacrylate initiated with organic peroxide-amine systems. *Chinese J Polym Sci*, 1984; 2(1):64-70.
- [29] Tieke B. *Makromolekulare Chemie – Eine Einführung*. 2nd Ed. Wiley-VCH, 2005; p. 65, ISBN 3527313796.
- [30] Feng X. Role of Aminum Radical in the initiation of Vinyl Polymerization. *Chinese J Polym Sci*, 1986; 2(1):109-118.
- [31] Odian G. *Principles of Polymerization*. 4. Ed. John Wiley & Sons, 2004; p. 465, ISBN 0471274003.
- [32] Guvendiren M, Purcell B, Burdick JA. Photopolimerizable Systems. In: Langer RS, Tirrell DA, editors. *Polymer Science: A Comprehensive Reference*. vol. 9, *Polymers in Biology and Medicine*. Elsevier B.V., 2012; p. 415, ISBN 9780444533494.
- [33] Millmyer MA. Polymer Synthesis. In: Langer RS, Tirrell DA, editors. *Polymer Science: A Comprehensive Reference*. vol. 1, *Basic Concepts and Polymer Properties*. Elsevier B.V., 2012; p. 35, ISBN 9780444533494.
- [34] Andrzejewska E. Photopolymerization kinetics of multifunctional monomers. *Prog Polym Sci*, 2001; 26(4):605-665.
- [35] Lovell LG, Berchtold KA, Elliott JE, Lu H, Bowman CN. Understanding the Kinetics and Network Formation of Dimethacrylate Dental Resins. *Polym Adv Technol*, 2001; 12(6):335-345.
- [36] Vaidyanathan J, Vaidyanathan TK, Wang Y, Viswanadhan T. Thermo analytical characterization of visible light cure dental composites. *J Oral Rehabil*, 1992; 19(1):49-64.
- [37] Maffezzoli A, Della Pietra A, Rengo S, Nicolais L, Valetta G. Photopolymerization of dental composite matrices. *Biomaterials*, 1994; 15(15):1221-1228.

- [38] Rosentritt M, Behr M, Leibrock A, Handel G. Veneering composites – a thermoanalytical examination. *J Mater Sci*, 1999; 10(2):91-98.
- [39] Atai M, Watts DC. A new kinetic model for the photopolymerization shrinkage-strain of dental composites and resin-monomers. *Dent Mater*, 2006; 22(8):785-791.
- [40] Watts DC, Cash AJ. Determination of polymerization shrinkage kinetics in visible-light-cured materials: methods development. *Dent Mater*, 1991; 7(4):281-287.
- [41] Watts DC, Marouf AS. Optimal specimen geometry in bonded-disk shrinkage-strain measurements on light-cured biomaterials. *Dent Mater*, 2000; 16(6):447-451.
- [42] DeWald JP, Ferracane JL. A Comparison of four modes of evaluating depth of cure of light-activated composites. *J Dent Res*, 1987; 66(3):727-730.
- [43] Steinhaus J, Frentzen M, Rosentritt M, Moeginger B. Dielectric analysis of short-term and long-term curing of novel photo-curing dental filling materials. *Macromol Symp*, 2010; 296(1):622-625.
- [44] Steinhaus J, Moeginger B, Grossgarten M, Hausnerova B. Evaluation of dielectric curing monitoring investigating light-curing dental filling composites. *Mater Eng*, 2011; 18(1):28-33.
- [45] Zahouily K, Decker C., Kaisersberger E, Gruener M. Real-time UV cure monitoring. *Eur Coating J*, 2003; 11(1):245-249.
- [46] Pethrick RA, Hayward D. Real time dielectric relaxation studies of dynamic polymeric systems. *Prog Polym Sci*, 2002; 27(9):1983-2017.
- [47] DEA Epsilon product information brochure, Netzsch Gerätebau GmbH, Selb, Germany, 2008.
- [48] Rosentritt M, Behr M. Dielectric Analysis of light-curing dental restorative materials – a pilot study. *J Mater Sci*. 2006; 41(10):2805-2810.
- [49] Rosentritt M, Shortall AC, Palin WM. Dynamic monitoring of curing photoactive resins: a methods comparison. *Dent Mater*, 2010; 26(6):565-570.
- [50] Henkel M. Dissertation: Untersuchung des Aushärtungsverhaltens lichthärtender Füllungskomposite mittels DEA (Investigation of the curing behavior of VLC composites with DEA). Medical Faculty of the Friedrich-Alexander University of Erlangen-Nürnberg, 2012.
- [51] Lairez D, Emery JR, Durrand D, Hayward D, Pethrick RA. Dielectric study of epoxy vitrification: does a percolation model apply? *Macromolecules*, 1992; 25(26):7208-7210.
- [52] Maistros GM, Partridge IK. Dielectric Monitoring of Cure in a Commercial Carbon-Fiber Composite. *Compos Sci Technol*, 1995; 53(1):355-359.
- [53] Maistros GM, Partridge IK. Monitoring autoclave cure in commercial carbon fibre/epoxy composites. *Composites Part B*, 1998; 29(3):245-250.
- [54] Silikas N, Watts DC. Rheology of urethane dimethacrylate and diluent formulations. *Dent Mater*, 1999; 15(4):257-261.
- [55] Lee JH, Um CM, Lee IB. Rheological properties of resin composites according to variations in monomer and filler composition. *Dent Mater*, 2005; 22(6):515-526.
- [56] Beun S, Bailly C, Dabin A. Rheological properties of experimental Bis-GMA/TEGDMA flowable resin composites with various macrofiller/microfiller ratio. *Dent Mater*, 2009; 25(2):198-205.

- [57] Ellakawa A, Cho N, Lee IB. The effect of resin matrix composition on the polymerization shrinkage and rheological properties of experimental dental composites. *Dent Mater*, 2007; 23(10):1229-35.
- [58] Shenoy AV. *Rheology of Filled Polymer Systems*. Kluwer Academic Publishers, 1999; p.321, ISBN 0412831007.
- [59] Moszner N, Hirt T. New Polymer-Chemical Developments in Clinical Dental Polymer Materials: Enamel-Dentin Adhesives and Restorative Composites. *J Polym Sci Part A*, 2012; 50(21):4369-4402.
- [60] Rubbi E, Baffa O, Vinha D, de Camargo Thomé LH. Rheological studies of photopolymerized dental composites. *Dent Mater*, 1993; 9(6):361-364.
- [61] Ferracane JL, Moser JB, Greener EH. Rheology of Composite Restoratives. *J Dent Res*, 1981; 60(9):1678-1685.
- [62] Nahm SH. Use of Dielectric Spectroscopy for Real-Time In-situ Reaction Monitoring. *J Coating Technol Res*, 2006; 3(3):257-265.
- [63] Mackinnon AJ, Jenkins SD, Mcgrail PT, Pethrick RA. A Dielectric, Mechanical, Rheological, and Electron-Microscopy Study of Cure and Properties of a Thermoplastic-Modified Epoxy Resin. *Macromolecules*, 1992; 25(13):3492-3499.
- [64] Lindberg A, Peutzfeld A, van Dijken JWV. Effect of power density of curing unit, exposure duration, and light guide distance on composite depth of cure. *Clin Oral Invest*, 2005; 9(2):71-76.
- [65] Musanje L, Darvell BW. Polymerization of resin composite restorative materials: exposure reciprocity. *Dent Mater*, 2003; 19(6):531-541.
- [66] De la Rie ER. Polymer stabilizers: A survey with reference to possible applications in the conservation field. *Studies in Conservation*, 1988; 33:9-22.
- [67] Hongkyeong K, Kookheon C. Dielectric changes during the curing of epoxy resin. *Bull Kroean Chem Soc*, 1999; 20:1329-1334.
- [68] Angiolini L, Caretti D, Salatelli E. Synthesis and photoinitiation activity of radical polymeric photoinitiators bearing side-chain camphorquinone moieties. *Macromol Chem Phys*, 2000; 201:2646-2653.
- [69] Ferry JD. *Viscoelastic properties of polymers*. 3rd Edition, John Wiley & Sons Inc.;1980. p. 271 Chapter A5.
- [70] Lange J, Altmann N, Kelly CT, Halley PJ. Understanding vitrification during cure of epoxy resins using dynamic scanning calorimetry and rheological techniques. *Polymer*, 2000;41:594.
- [71] Fukushima E, Roeder S.B.W. *Experimental Pulse NMR: A Nuts and Bolts Approach*. Addison-Wesley, MA, 1981.
- [72] Carr H.Y, Purcell E.M. Effects of Diffusion on Free Precession in Nuclear Magnetic Resonance Experiments. *Physical Review*, 1954; 94:630–638.
- [73] Meiboom S, Gill D. Modified Spin - Echo Method for Measuring Nuclear Relaxation Times. *Rev. Sci. Instrum.*, 1958; 29:688–691.
- [74] Kohlrausch F. For experimental data. *Pogg. Ann. Phys.*, 1854; 167:56–82.

- [75] Honek T, Hausnerova B, Saha P. Relative Viscosity Models and Their Application to Capillary Flow Data of Highly Filled Hard-Metal Carbide Powder Compounds. *Polymer Composites*, 2005;26:29-36.
- [76] Hausnerova B, Honek T, Saha P, Kitano T. Viscoelastic Properties of Powder Injection Molding Compounds. *J Polym Mater*, 2004; 21(1):1-10.
- [77] Lee HL, *The Handbook of Dielectric Analysis and Curing Monitoring*, Lambert Technologies, 2014.
- [78] Kitano T, Kataoka T, Shirota T. An empirical equation of the relative viscosity of polymer melts filled with various inorganic fillers. *Rheol Acta*, 1981;20:207-9.
- [P-I] Steinhaus J, Moeginger B, Grossgarten M, Rosentritt M, Hausnerova B. Dielectric analysis of depth dependent curing behaviour of dental resin composites. *Dent Mater*, 2014; 30(6):679-687.
- [P-II] Steinhaus J, Hausnerova B, Haenel T, Grossgarten M, Moeginger B. Curing kinetics of visible light curing dental resin composites investigated by dielectric analysis (DEA). *Dent Mater*, 2014; 30(3):372-380.
- [P-III] Netto A M, Steinhaus J, Hausnerova B, Moeginger B, Blümich B. Time-Resolved Study of the Photo-Curing Process of Dental Resins with the NMR-MOUSE. *Appl Magn Reson*, 2013; 44(9):1027-1039.
- [P-IV] Steinhaus J, Moeginger B, Harrach M, Guenther D, Moegele F, Hausnerova B. Characterizing the Auto-curing Behaviour of Rapid Prototyping Materials for 3D-Printing via DEA. *Polym Eng Sci*, accepted 03/2015.
- [P-V] Steinhaus J, Haenel T, Selig D, Duvenbeck F, Moeginger B, Hausnerova B. Correlation of Shear and Dielectric Ion Viscosity of Dental Resins – Influence of composition, temperature and filler content. Submitted to *Dent Mater*, 03/2015.

ABBREVIATIONS

3D	three dimensional
3DP	three dimensional printing
acc.	According
APO	acylphosphine oxide
ATR	attenuated total reflection
Bis-EMA	ethoxylated bisphenol A dimethacrylate
Bis-GMA	bisphenol A glycidyl methacrylate
BHT	butylated hydroxytoluene
BPO	dibenzoyl peroxide
CAD	computer aided design
CPMG	NMR relaxation acc. to Carr Purcell Meiboom Gill
CQ	camphorquinone
DABE	ethyl 4-(dimethylamino)benzoate
DC	degree of cure
DCG	disturbed chain growth
DEA	dielectric analysis
DMA	dimethacrylate monomer
DMT	N,N-dimethyl-p-toluidine
DoC	depth of cure
DSC	differential scanning calorimetry
FT-IR	fourier transform infrared spectroscopy
HEMA	2 hydroxy methylacrylate
HQ	hydroquinone
IDEX	interdigitated electrode film sensor (DEA, 115 μ m electrode distance, NETZSCH)
KHN	Knoop hardness
LCU	light curing unit
NMR	nuclear magnetic resonance
PMMA	poly methyl methacrylate
RBC	resin based composite

rf	radio frequency
RP	rapid prototyping
SEM	scanning electron microscopy
TCB resin	carboxylic acid modified dimethacrylate
TDP	three dimensional printing
TEGDMA	triethylene glycol dimethacrylate
TMS	tool mount sensor (DEA, 1 mm electrode distance, NETZSCH Gerätebau GmbH)
UCG	undisturbed chain growth
UDMA	urethane dimethacrylate
VLC	visible light curing
vol.-%	volume-%
VXP1	3DP binder containing HEMA and styrene (voxeljet AG)
VXP1-new	fresh VXP1-binder
VXP-old	6 month old VXP1-binder (styrene mainly volatilized)
VLC	visible light curing
wt-%	weight-%

SYMBOLS

a	slope of $\lg \eta_0$ with respect to temperature and filler content (VLC)
a_{ion}	slope of $\lg \eta_0^{ion}$ with respect to temperature and filler content (VLC)
A	amine monomer (3DP kinetics) or fitting parameter of Eq. 51, 55 or 56 (VLC)
A^\bullet	amine radical
$A^{+\bullet}$	amine ion radical
b	reciprocal reaction time constant (VLC kinetics) or n-1 (3DP kinetics) or shear viscosity at 0°C (VLC)
b_{ion}	ion viscosity at 0°C (VLC)
B	slope of linear region of DEA curing curve (VLC kinetics) or fitting parameter of Eq. 51
B_0	static magnetic field (NMR)
B_1	magnetic field pulse perpendicular to B_0 (NMR)
c^{DMA}	concentration of DMA monomers
$c_M(t)$	time dependent monomer concentration (3DP kinetics)
$c_M^n(t)$	time dependent initial monomer concentration (3DP kinetics)
c_0^{DMA}	initial concentration of DMA monomers
$c_0^{initiator}$	initial initiator concentration
c_0^{rad}	initial radical concentration (VLC kinetics)
$c_0^{radical}$	initial radical concentration (3DP kinetics)
C or $c_{0,M}$	initial monomer concentration (3DP kinetics)
d	penetration depth of light in a specimen
D	self-diffusion coefficient (NMR)
$d_a = 1/\gamma$	light absorption depth in VLC RBCs
$d_0 = 3*d_a$	maximum curing depth
DC_∞	final possible DC
DMA^\bullet	dimethacrylate radical
f	frequency
G	magnetic field gradient (NMR)
$h\nu$	quantum radiation energy
I	initiator molecule

$I\bullet$	initiator radical
$I\dot{-}$	initiator ion radical
$[I]$	initiator concentration
I_0	incident light intensity
$I(d)$	light intensity in penetration depth d
$[ion]$	concentration of ions
k_i	initiation rate constant
k_p	propagation rate constant
k_{start}	rate constant of start reaction
k_t	termination rate constant
k_{ucg}	rate constant of undisturbed chain growth
l	layer thickness of specimen
M	molecular mass
M_{crit}	critical molecular mass to be exceeded to account for entanglements
$M(t)$	time dependent decay of magnetization (NMR)
M_0	initial maximum magnetization (NMR)
$M^n(t)$	molecular mass with curing time and exponent n changing from 1 to 3.4 at M_{crit}
$M(M_1, M_2)$	monomer (type 1, type 2)
$M\bullet(M_1\dot{-})$	monomer radical (type 1, type 2)
$[M]$	monomer concentration
n	reaction order, number of multiple experimental determinations or exponent
p_v	vapor pressure
q	charge of an ion
Q	heat
R^2	correlation coefficient
$R\bullet$	radical
R_i	rate of initiation
$RM_{1,n,m}\bullet$	radical reacted with 1, n or m times of monomers
$[RM_{1,n,m}\bullet]$	concentration of radical reacted with 1, n or m times of monomers
R_p	rate of propagation

R_t	rate of termination
R_{poly}	rate of polymerization
S	slope of the normalized ion viscosity curve at t_{init} (3DP kinetics)
t	time
t_0	start time of light curing (VLC) or initial time (NMR)
t_{end}	end time of primary curing in DEA-curve (3DP)
t_E	time of spin echo of rf pulse
t_{min}	time of DEA curve minimum
t_{MAX}	time of maximum of CMPG-curve (NMR)
t_{glass}	curing time to reach glass transition (VLC kinetics)
t_{init}	time of curing initiation
t_{start}	time of starting ion viscosity after initiation phase (3DP)
T	temperature or pre-exponential coefficient in time dependent reaction time constant (VLC kinetics)
T_1	longitudinal relaxation time (NMR)
T_2	transverse relaxation time (NMR)
T_{2eff}	relaxation time of inhomogeneous impulse response decay acc. to CPMG (NMR)
T_b	boiling temperature
T_g	glass transition temperature
T_m	melting temperature
T_{sample}	sample temperature
v_F	filler volume fraction
w_{TEGDMA}	weight fraction of TEGDMA

GREEK SYMBOLS

$\alpha(t)$	time dependent degree of conversion
ε_0	dielectric constant
ε''	dielectric loss
Φ	quantum yield for initiation
γ	extinction coefficient
δ	solubility parameter
$\Delta\eta$	drop of initial ion viscosity to minimum value (VLC kinetics)
$\Delta\eta^{ion}$	difference between minimum and final ion viscosity
$\Delta\eta^{ion}_{max}$	difference between ion viscosity of curing initiation and final ion viscosity
$\Delta\eta^{ion}_0$	scattering of initial ion viscosity after binder addition (3DP)
$\Delta\eta^{ion}_{100}$	scattering of end ion viscosity 100s after addition of binder (3DP)
$\Delta\eta^{ion}_{end}$	scattering of ion viscosity at the end of primary curing in DEA-curve (3DP)
$\Delta\eta^{ion}_{min}$	scattering of DEA-curve minimum (3DP)
$\Delta\eta^{ion}_{start}$	scattering of starting ion viscosity after initiation phase (3DP)
Δt_{end}	scattering of end time of primary curing in DEA-curve (3DP)
Δt_{min}	scattering of time of DEA-curve minimum (3DP)
Δt_{start}	scattering of time of starting ion viscosity after initiation phase (3DP)
$\Delta V/V$	relative change in volume
η	shear viscosity
η^{ion}	ion viscosity
η^{ion}_{100}	end ion viscosity 100s after addition of binder (3DP)
η^{ion}_{end}	ion viscosity at the end of primary curing in DEA-curve (3DP)
$\eta^{ion}_{rel}(t)$	relative ion viscosity (3DP)
η^{ion}_{start}	starting ion viscosity after initiation phase (3DP)
η^{ion}_0	initial ion viscosity after binder addition (3DP)
η^{ion}_{min}	DEA-curve minimum
η_0^{ion}	initial ion viscosity of non-irradiated (VLC) / non-initiated (3DP) material
$\eta_{0,init}^{ion}$	ion viscosity of curing initiation
$\eta_{0,r}^{ion}$	initial relative ion viscosity (VLC)

$\eta_{0,resin}^{ion}$	initial ion viscosity of of non-irradiated pure resin (VLC)
$\eta_0^{ion}(V_F)$	initial ion viscosity of of non-irradiated VLC RBC with respect to filler content
η^{rheo}	shear viscosity (VLC kinetics)
η_{τ}^{ion}	ion viscosity at τ
η_{∞}^{ion}	final ion viscosity of fully cured material
$\eta_{\infty}^{ion,measured}$	measured final ion viscosity of fully cured material with DEA (VLC kinetics)
$\eta_{\infty}^{ion,true}$	true final ion viscosity of fully cured material (VLC kinetics)
$\dot{\eta}_0^{ion}$	extrapolated slope of the linear range in the DEA curing curve for zero thickness
$\dot{\eta}_{lin}^{ion}$	slope of linear range in DEA curing curve
$\bar{\eta}_{37-40}^{ion}$	average ion viscosity of DEA curing curve between 37-40s of irradiation
μ	ion mobility
ρ	density
σ	ion conductivity
τ	reaction time constant or time when the measured value reaches $(1-e^{-1})$ or 63% of the final value
τ_{reac}	reaction time constant evaluated acc. to Eq. (31) (VLC kinetics)
$\tau_{reac}(t)$	time dependent reaction time constant (VLC kinetics)
τ^0	fit parameter $\tau_{reac}^0 * c_{rad}^0$ (VLC kinetics)
τ_{reac}^0	reaction time constant in the uncured state (VLC kinetics)

PUBLICATIONS, POSTERS AND PRESENTATIONS

Publications in the context of this doctoral work:

- Netto AM, Steinhaus J, Hausnerova B, Moeginger B, Blümich B. Time-Resolved Study of the Photo-Curing Process of Dental Resins with the NMR-MOUSE. *Appl Magn Reson*, 2013;44:1027-1039.
- Steinhaus J, Hausnerová B, Haenel T, Grossgarten M, Moeginger B. Curing kinetics of visible light curing dental resin composites investigated by dielectric analysis (DEA). *Dent Mater*, 2014; 30(3):372-380.
- Steinhaus J, Moeginger B, Grossgarten M, Rosentritt M, Hausnerová B. Dielectric analysis of depth dependent curing behavior of dental resin composites. *Dent Mater*, 2014; 30(6):679-687.
- Steinhaus J, Moeginger B, Harrach M, Guenther D, Moegele F, Hausnerova B. Characterizing the Auto-curing Behaviour of Rapid Prototyping Materials for 3D-Printing via DEA. *Polym Eng Sci*, accepted 03/2015.
- Steinhaus J, Haenel T, Selig D, Duvenbeck F, Moeginger B, Hausnerova B. Correlation of Shear and Dielectric Ion Viscosity of Dental Resins – Influence of composition, temperature and filler content. Submitted to *Dent Mater*, 03/2015.

Other Publications in English language:

- Steinhaus J, Frentzen M, Rosentritt M, Moeginger B. Dielectric analysis of short-term and long-term curing of novel photo-curing dental filling materials. *Macromol Symp*, 2010; 296:622-5.
- Steinhaus J, Moeginger B, Grossgarten M, Hausnerová B. Evaluation of dielectric curing monitoring investigating light-curing dental filling composites. *Mater Eng*, 2011; 18:28-33.
- Kusch P, Obst V, Schroeder-Obst D, Fink W, Knupp G, Steinhaus J. Application of pyrolysis-gas chromatography/mass spectrometry for the identification of polymeric materials in failure analysis in the automotive industry. *Engin Fail Anal*, 2013; 35:114-124.
- Kusch P, Knupp G, Fink W, Schroeder-Obst D, Obst V, Steinhaus J. Application of Pyrolysis–Gas Chromatography–Mass Spectrometry for the Identification of Polymeric Materials. Published in: *Lc Gc North America*, 2014; 32(3):210-217 / *LC GC Europe*, 2014; 27(6):296-303 and *LCGC Asia Pacific*, 2014; 17(4):18-21.
- Haenel T, Hausnerová B, Steinhaus J, Price RBT, Sullivan B, Moeginger B. Effect of the irradiance distribution from light curing units on the local micro-hardness of the surface of dental resins. *Dent Mater*, 2015; 31(2):93-104.

Conference Presentations:

- Investigations of curing kinetics of composites. AfG conference 2004 (Committee for Dental Fundamental Research), Mainz, Germany, oral poster presentation
- Methods for online-monitoring of curing kinetics of photo-cured composites. DGZ conference 2005 (German Society for Dental Preservation), Wuppertal, Germany, oral presentation
- Cross-linking behavior of photo-cured dental composites, NETZSCH Application Seminar at Achema 2009, Frankfurt, Germany, oral presentation
- Steinhaus J., Möglinger B., Frentzen M., Rosentritt M. Dielectric real-time analysis of the photo-curing and post-curing behavior of dental composite fillings. Transcom Meeting 2009, Zilina, Slovakia, oral presentation
- Dielectric analysis of short-term and long-term curing of novel photo-curing dental filling materials. European Polymer Conference 2009, Graz, Austria, oral presentation
- Evaluation of a Dielectric Real-Time Curing Monitoring Method by Investigating the Curing Behavior of Light-Curing Dental Filling Composites. SEMDOK PhD students seminar 2011, Zilina-Terchová, Slovakia, oral presentation
- Post-Curing of Photo-Polymeric Dental Composites - Effects on Mechanical and Dielectrical Performance. European Polymer Conference 2011, Granada, Spain, poster presentation
- Dielectric Monitoring of Light Curing Composites – Effects of Light Intensity. ECD-IADR Conference 2011, European Continental Division of the International Association of Dental Research, Budapest, Hungary, oral poster presentation
- Characterizing the curing behavior of thermosets with dielectric analysis (DEA). GEFTA STK Joint Meeting 2012 (German Society for Thermal Analysis), Saarbrücken, Germany, oral presentation
- Correlation of dynamic viscosity and dielectric ion viscosity of resins used for nano-hybrid dental composites and the effects of resin composition, temperature and filler content, 9th AERC 2014 (Annual European Rheology Conference), Karlsruhe, Germany, oral presentation

CURRICULUM VITAE

Date and place of birth: April 16, 1979, Bonn, Germany
Permanent Address: von-Liebig Str. 20, 53359 Rheinbach, Germany
tel.: (+49) 2241 865 458
e-mail: johannes.steinhaus@h-brs.de

EDUCATION

since 09/2009: PhD studies at: Thomas Bata University in Zlín, Faculty of Technology, Department of Production Engineering
10/2003: Diploma Thesis: „Investigation of reaction kinetics of dental photopolymers“, in cooperation with Dental University Hospital, Bonn
10/1999 – 10/2003: Materials Technology, Bonn-Rhein-Sieg University of Applied Sciences, Rheinbach, Germany (10/1999 – 10/2003)

WORK EXPERIENCE

since 09/2013: German Society of Material Science (DGM), trainer for polymer testing and failure analysis
since 09/2010: Technical Academy of Wuppertal, trainer for polymer applications
since 01/2008: Bonn-Rhein-Sieg University of Applied Sciences, Rheinbach, Germany
Dept. of Natural Sciences, deputy head of the polymer research group
since 10/2008: Part-time assistant lecturer at the Bonn-Rhein-Sieg University of Applied Sciences
06/2006 – 12/2007: igus GmbH, Cologne, Germany, junior product manager automotive
04/2005 – 06/2006: Dotherm Isolierwerkstoffe GmbH, Dortmund, Germany, sales engineer
01/2004 – 04/2005: Bonn-Rhein-Sieg University of Applied Sciences, Rheinbach, Germany
Dept. of Natural Sciences, project engineer

OTHER ACTIVITIES

since 01/2004: co-author of scientific publications as well as author of posters and presentations on national and international conferences
10/2011 – 10/2013: Member of the Faculty Council

FIELDS OF INTEREST

Characterization and modification of polymers, material failure analysis

PAPER I

PAPER II

PAPER III

PAPER IV

PAPER V